Geochemical Characterization and Longevity Estimates of a Permeable Reactive Barrier System Remediating a ^{90}Sr Plume

by

Jutta Hoppe

A thesis
presented to the University of Waterloo
in fulfillment of the
thesis requirement for the degree of
Master of Science
in
Earth Sciences

Waterloo, Ontario, Canada, 2012

AUTHOR'S DECLARATION

I hereby declare that I am the sole author of this thesis. This is a true copy of the thesis, including any required final revisions, as accepted by my examiners.

I understand that my thesis may be made electronically available to the public.

Abstract

In 1998, a permeable reactive barrier system was installed at the Atomic Energy of Canada Ltd. (AECL) Chalk River Laboratories in Chalk River, Ontario, to prevent the discharge of a ^{90}Sr plume into a nearby swamp. The system known as the "Wall and Curtain" contains clinoptilolite, a zeolite, as a reactive material to sorb ^{90}Sr. The overall objective of this study was to provide refined estimates of the efficiency and longevity of the system. To better understand the flow in the aquifer and through the Wall and Curtain, a detailed physical field characterization of the site was performed. Borehole-dilution tests were performed in 19 mm (¾ inch) drive-point piezometers. The reproducibility of this method was tested in a sandbox experiment and in the field on two different drive-point versions. The results indicate that the Wall and Curtain system intercepted deeper, contaminated groundwater as intended. Hydraulic conductivities (K) determined through slug tests indicate that the aquifer was relatively homogeneous. Average linear groundwater velocities determined through borehole dilution compared well with velocities determined through the Darcy equation based on slug-test K estimates. The modified version of the drive-point, which included a finer, continuous screen, seemed to produce more closely correlated results in borehole-dilution tests than the original drive-point. Results indicate that the borehole dilution method was more reproducible in determining groundwater velocities than the Darcy equation with incorporated field data. The measurements of groundwater velocities and hydraulic conductivities from the field study were combined with previous characterization of the hydrogeology of the site to develop a three dimensional physical flow model. The numerical computer code HydroGeoSphere was used to provide an approximate representation of groundwater flow in the aquifer and through the Wall and Curtain. The model was calibrated by comparing simulated and observed hydraulic head values across the site. The results from the field tests were compared with groundwater velocities simulated by the numerical model. The model showed good agreement with the observed heads and acceptable agreement with the field estimates of groundwater velocities.

A detailed geochemical characterization of the aquifer and the reactive material, clinoptilolite, was performed through field and laboratory work. Pore-water samples were taken from multiple locations in the aquifer, as well as from the outflow drains of the system. Solid and pore-water samples from the reactive material were used to determine distribution coefficients for ^{90}Sr and competing cations. Sequential leach tests were performed on small amounts of the radioactive solid samples to investigate the main sorption mechanisms and preferential conditions for ^{90}Sr desorption from the clinoptilolite. Results indicate that the system was highly efficient in treating an average mass flux of > 17,000 Bq/m^2day^{-1}. The leading edge of the plume was found to have only reached 40 cm into the 2 m thick Curtain of clinoptilolite after nearly 14 years of operation. The reactive material readily sorbed ^{90}Sr, with a distribution coefficient of > 76,000 mL/g for beta activity. Kinetically controlled ion exchange was the main mechanism of sorption onto the clinoptilolite for most cations. High ionic strength and low pH were conditions under which Sr desorption is favourable, which are not expected on the site. The results indicate that the system was highly efficient and will probably remain so for another 50 years.

Reactive transport models of the site using two different numerical codes, HydroGeoSphere and MIN3P, were constructed to provide refined estimates of the longevity of the system. The model constructed in HydroGeoSphere included five solutes, including radioactive strontium and the daughter products of Sr, yttrium and zirconium. Zoned distribution coefficients were specified for the transported solutes. In MIN3P, only the reactive material was used as a model domain. Typical concentrations of the uncontaminated groundwater and the plume were specified for major components in the system. Ion exchange was considered in the simulation, as well as radioactive decay of Sr. An updated version of MIN3P was used which also considers kinetic sorption of Sr. Longevity estimates of the different simulations ranged between 30 years and over 200 years for the Wall and Curtain system. Based on field and laboratory experiments, longevity estimates of 80 years to 100 years seemed more reasonable. Results of the numerical simulation indicate that by that time, the system would have remediated 1200 MBq of ^{90}Sr. Continuous monitoring of the outflow will ensure that the time-to-replacement of the system will be met. Future field and laboratory work as well

as the incorporation of kinetically controlled ion exchange into the code MIN3P will be helpful in providing more refined longevity estimates.

Acknowledgements

I would like to thank my co-supervisors David Lee and David Blowes for giving me the unique opportunity to work on this project and all their support on the way. I would also like to thank my committee members Sung-Wook Jeen for his support and help in the field and Carol Ptacek for her ideas and input for the project. My thanks also go to AECL and NSERC for funding this project. As this project is a collaboration between the University of Waterloo and AECL`s Chalk River Laboratories, people at both locations were involved and helped me immensely.

At the Chalk River Laboratories, I would like to thank Doug Killey for his help by sharing his lab space and equipment, his ideas and his experience. My thanks also go to Lee Bellan and Dan Festarini for their help in the field and in the lab. My work would not have gone half as smoothly and organized without their help. Thanks also to Todd Chaput and Patricia Robinson for the efficient analysis of the many samples at the Chalk River Laboratories.

At the University of Waterloo, I am grateful to Rob McLaren for the introduction to HydroGeoSphere and Jeff Bain for his help in the setup of the flow model in HydroGeoSphere and his experience on the organization and preparation of field work. I would like to thank Paul Johnson for saving my field work several times by machining and lending equipment; Laura Groza for her help in the lab and Julia Jamieson-Hanes for the analysis of samples in Waterloo, as well as Stanley Pak Hung Yung for the setup of the column experiment. My thanks also go to the co-op students Brandon O'Leary and especially to Ellie Owens for their help in the field and lab. It was a pleasure to work with them. Thanks also go to Rich Amos, Uli Mayer and Jun Yin for their help with MIN3P.

I thank all my friends abroad and in Waterloo, especially the two other amigos, for all the support in and especially distractions from my work over the last 2 years. I did not expect to meet so many good hearted and fun people here and I would not have made it without them. Last, and most importantly, I thank my family who have always supported me and believed in me and everything I have done.

Table of Contents

List of Figures

List of Tables

Chapter 1
Hydrological Characterization of the Wall and Curtain Site

1.1 Introduction

Single-point dilution tests (commonly known as borehole-dilution tests) were established in the 1960's as an *in situ* method of determining average linear groundwater velocities (e. g. Drost et al., 1968, Ogilvi, 1958). A solution containing a tracer is injected into a packed off volume of a well screen. The concentration decline of the tracer over time is proportional to the groundwater flow through the interval (Lee and Forsyth, 1983). Until the 1960's, radioactive tracers were widely used for borehole dilution due to their low detection limit. Later, other conservative tracers like bromide (Lee and Forsyth, 1983) and fluoride (Grisak et al., 1977) have been used. This study used electrical conductivity (EC) as a tracer by injecting a sodium chloride solution with high EC. This is the first study known to the authors that uses the borehole dilution method in a small pipe diameter (19 mm) in the field.

Permeable reactive barriers (PRBs) are *in situ* remediation systems that are installed in the flow path of a contaminant plume. A reactive material is used to either adsorb the contaminant or promote chemical reactions that lead to reaction products that are not considered to cause health concerns. Permeable reactive barriers have been applied for remediation of a variety of contaminants, including inorganic and organic contaminants, as well as radionuclides (e.g. Blowes et al., 2000). Although extensive studies are executed before and shortly after the installation, fewer studies exist that focus on the long-term performance of PRBs (Wilkin et al., 2002). Usually no control exists of the capture zone of the permeable reactive barrier. However, the permeable reactive barrier system installed at the Chalk River Laboratories, known as the Wall and Curtain (Lee and Hartwig, 2005), provides control over the gradient across site and thus the capture zone of the system. The overall objective of this project was to estimate the efficiency and longevity of this system. This study focused on better understanding the flow through a PRB system through field

characterization and testing the reproducibility of the borehole dilution method when using a small pipe diameter.

1.2 Site description

The study site is located at the Atomic Energy of Canada Ltd. Chalk River Laboratories in Chalk River, Ontario, approximately 193 km northwest of Ottawa. In 1954, a treatment plant was operated to decompose ammonium nitrate solutions containing mixed fission products. Some of these solutions, which contained ^{90}Sr and tritium, were released in pits lined with crushed limestone and subsequently moved into the predominantly sandy aquifer. The aquifer has a saturated thickness of 5-13 m. A stony till unit overlies the irregular Precambrian gneiss bedrock surface (Killey and Munch, 1987). In some places, the till is overlain by a thin gravel layer, in other locations it is in direct contact with fluvial fine to medium sand. Fine sands and, in most locations, a silty very fine sand unit are next in sequence, with gradational contacts between those units (Killey and Munch, 1987). The silty very fine sand unit defines the transition from fluvial deposits to overlying aeolian deposits, which consist predominantly of fine sand with interstratified sand and silt units (Killey and Munch, 1987). Hydraulic conductivities on site determined through permeameter tests and grain size analyses range from 3.5×10^{-6} m/s to 1.2×10^{-4} m/s (Killey and Munch, 1987). Groundwater velocities in the aquifer range from 100 m/a to 150 m/a (Klukas and Moltyaner, 1995). Recharge of the shallow aquifer (at depths of 0 to 5 m) comes from infiltration of precipitation, whereas the lower has a more distant recharge area, Lake 233, some 500 m upgradient of Duke Swamp (Killey and Munch, 1987). As Lake 233 is labelled with road salt, the lower aquifer shows high values of electrical conductivity and high concentrations of Na and Cl. The source area of the ^{90}Sr plume is directly downgradient of Lake 233, resulting in a thin, discrete plume in the transition zone between Lake 233 recharge and direct infiltration (Killey and Munch, 1987). The transport of ^{90}Sr is retarded due to geochemical interactions with the aquifer, resulting in a ^{90}Sr travel time of over forty years from the source area to Duke Swamp (Lee and Hartwig, 2005).

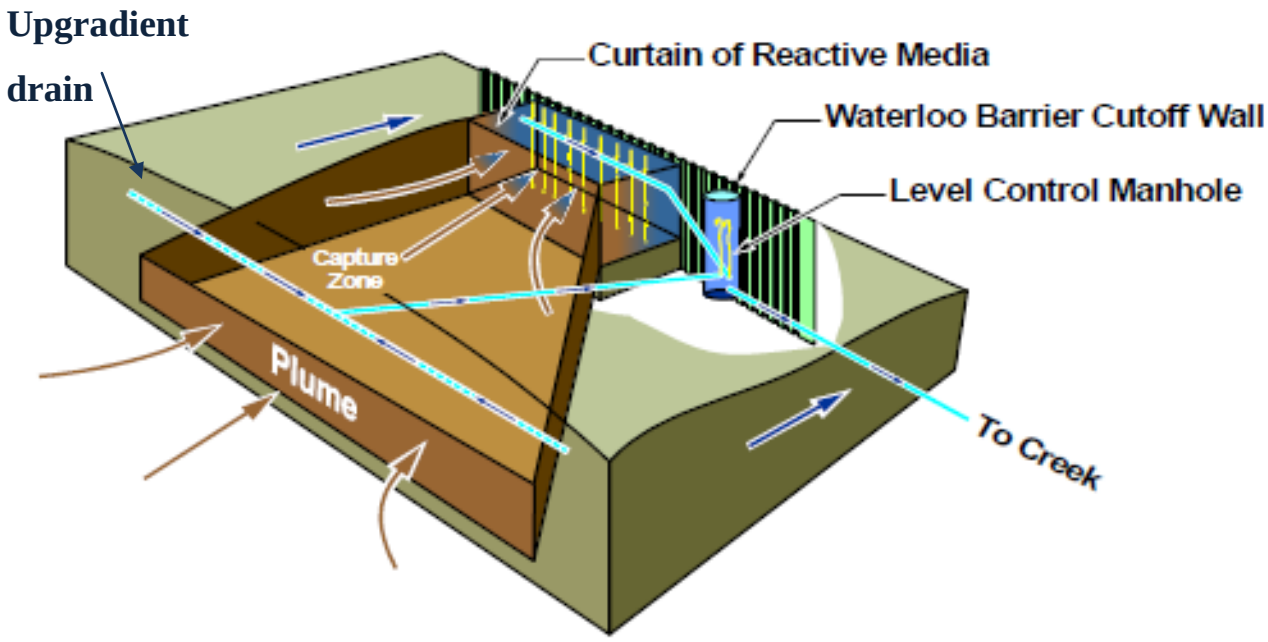

Figure 1.1: Schematic of the Wall and Curtain PRB (modified from Lee and Hartwig, 2005).

In December 1998, a PRB system known as the Wall and Curtain (Figure 1.1) was installed to prevent ^{90}Sr from discharging into Duke Swamp. The system consists of a 30 m wide sealed-joint, steel-sheet pile cut-off wall (Waterloo Barrier®) that is locked into the bedrock or the till above bedrock. In front of the wall an 11 m wide, 2 m thick and 6 m deep curtain of clinoptilolite, a zeolite, acts as the reactive material to sorb ^{90}Sr. Clinoptilolite was suggested as a reactive material due to a high sorption capacity and the affinity to both Sr and Ca (Cantrell et al., 1994; Fuhrmann et al., 1996). Calcium concentrations are low across site, making it an ideal setting for the employment of clinoptilolite for the sorption of strontium. The hydraulic conductivity of clinoptilolite is estimated to be 3×10^{-4} m/s (Sale, 2003). Groundwater velocities previously determined through borehole dilution in the clinoptilolite range from 200 m/a to 1070 m/a, and predominant velocities are between 400 m/a to 600 m/a (Sale, 2003). The Wall and Curtain system is the first PRB known to employ clinoptilolite as a reactive material. It was constructed as a "hanging wall" PRB, as the clinoptilolite is not in contact with bedrock and does not reach the lower half of the aquifer, where the ^{90}Sr plume is located.

Two wings of sheet-piling perpendicular to the cut-off wall help direct groundwater flow through the reactive material and are in contact with bedrock as well. Ten 5.1 cm (2 inch), 6 m deep, fully penetrating Polyvinyl chloride (PVC) wells are located at the back of the curtain directly in front of the sheet-piling wall, which are connected to a manhole by a horizontal drain. A second horizontal drain installed 60 m upgradient of the Wall and Curtain (Figure 1.1) intercepts shallow, uncontaminated groundwater, ensuring less loading of the reactive material with species other than ^{90}Sr and thus prolonging the time to replacement of the system. The upgradient drain also discharges into the manhole, where the outflow height of both horizontal drains can be adjusted. This system design has a unique advantage in that the gradient and thus the capture zone of the system can be adjusted. The effluents of the Wall and Curtain and the upgradient drain can be sampled, which is another advantage of the design of the system. As a road salt label coincides with the plume location in the lower half of the aquifer, the effluents of the system are consistently monitored for EC. These advantages make the site an ideal setting to estimate the reproducibility of the borehole dilution method by testing the response of the method to different hydraulic gradients across site caused by a change in the flow rate of the Wall and Curtain.

1.3 Methods

1.3.1 Field tests for characterization of the site

In summer 2012, a detailed elevation survey in combination with water table measurements was conducted at the Wall and Curtain site. In addition to water table measurements from wells across the site, water-table measurements from every piezometer close to the Wall and Curtain were taken, which were used to estimate the variability in the vertical hydraulic gradient in the proximity of the reactive barrier (see Figure 1.2).

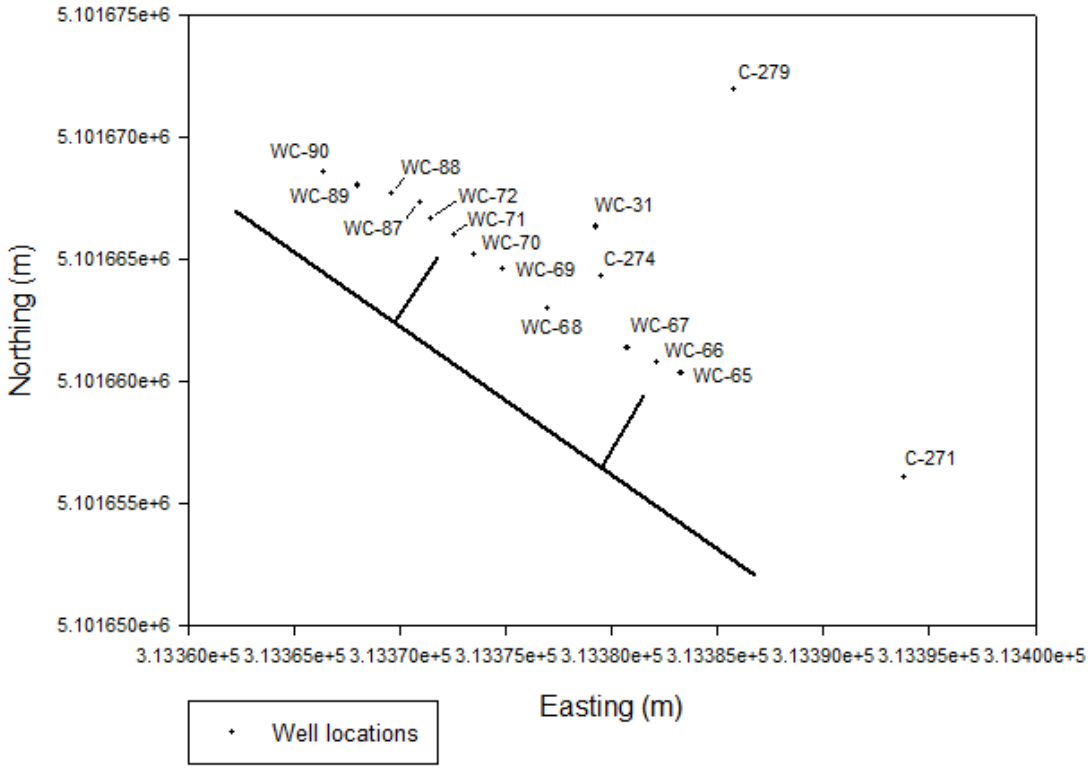

Figure 1.2: Location of wells, of which water levels in every piezometer were measured to determine the vertical component of the hydraulic gradient.

In 2011 and 2012, six 19 mm (¾ inch, ID) stainless steel Solinst® (model number 615) drive-points were driven vertically into the ground using 1.52 m (5 foot) long, 19 mm (¾ inch, ID) sections of stainless steel pipe, long shoulder couplings and pounded into the subsurface using a Bosch 11316EVS manual electric hammer. Figure 1.3 shows a map view of the Wall and Curtain site including the location of the installed drive-point piezometers. Because the purchased drive-points were not continuously slotted and had a slot size that was too coarse for the prevalent grain sizes at site, modifications to the drive-points were performed at the beginning of 2012. The modifications were achieved by removing the 297 micron (50 mesh) screen; removing ¼ of the thickness of the wall, continuously grooving the wall and tack welding of a 149 micron (100 mesh) stainless steel screen onto the drive-point (see Figure 1.4). The modified version of the drive-points was used in locations DP-4 to DP-

6 (see Figure 1.3). After reaching their maximum depth of 9 m, the drive-point piezometers were pulled out of the subsurface using a truck jack with a crank and chain.

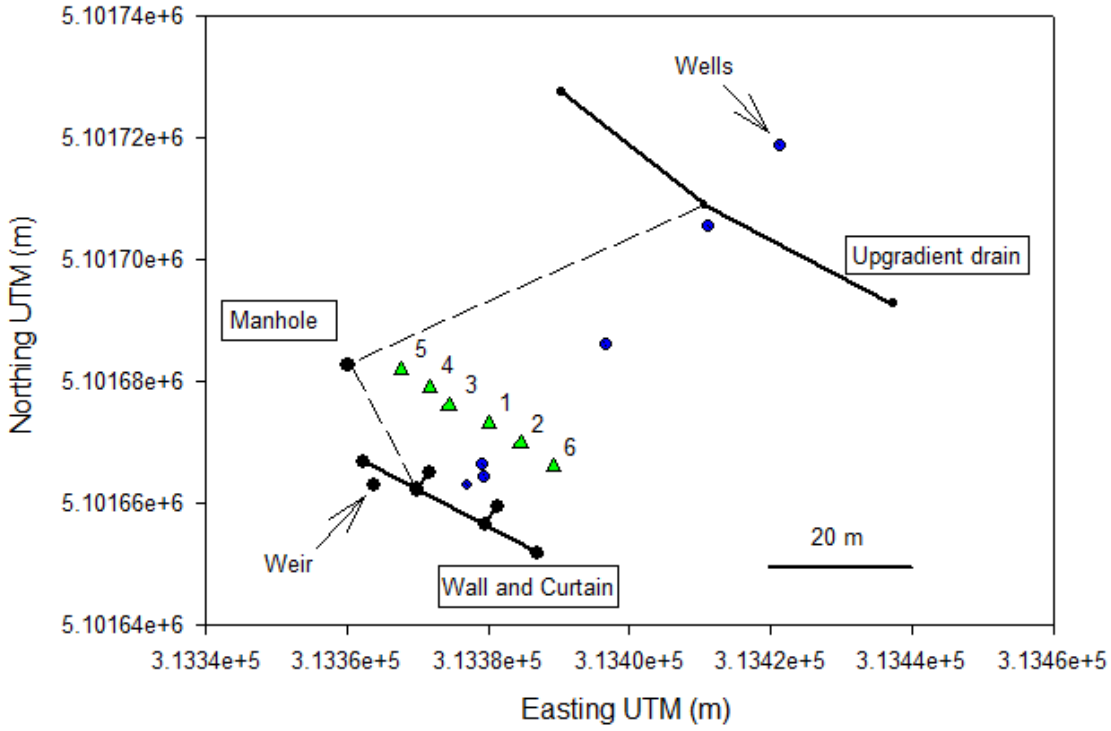

Figure 1.3: Site schematic with locations of the Wall and Curtain sheet-piling wall, selected wells and the upgradient drain. Drive-point piezometers DP-1 to DP-6 are depicted by green triangles and numbered accordingly.

Figure 1.4: The two drive-points used on site. The original drive-point is shown on the bottom (used in locations DP-1 to DP-3), the modified version on top (used in locations DP-4 to DP-6).

Single-well response tests (slug tests) were performed in 1 m vertical intervals in the drive-point piezometers starting at a depth of approximately 1.5 m below ground surface (bgs) (1 m below the water table). In drive-point piezometer locations 4 to 6, the vertical spacing was reduced to every 30.48 cm (1foot) at depths > 4.5 m, where the plume is located. Between 14 and 21 intervals were tested at each drive-point location. A 60.96 cm (2 feet) long, 0.95 cm (3/8 inch) stainless steel slug connected to a string was introduced in the drive-point piezometer (falling-head test). Water-level responses were recorded manually with a water-level meter and a stopwatch and tabulated. The slug was then removed and the water-level recovery recorded in the same manner (rising-head test). At least one falling-head test and one rising-head test were performed for each slug test location. The manual approach was necessary as the 19 mm (¾ inch) pipes were too narrow to automate the procedure with leveloggers. The collected data were analyzed manually and with the software AquiferTest using the Hvorslev method (Hvorslev, 1951).

Borehole-dilution tests were performed in the same drive-point locations and 1 m vertical intervals. A single inflatable packer was lowered into the 19 mm (¾ inch) stainless steel pipe and inflated just above the drive-point screen to isolate this interval from the remaining pipe.

The packer consisted of two brass tubes that act as inflow and outflow tube and pierce through two brass plates. Bicycle-tire tubing that could be inflated was attached to the two brass plates. The packer was specifically manufactured for this purpose and these were the first borehole-dilution tests known to be performed in small diameter drive-points. Before the tracer solution was injected, air bubbles were removed from the circulation tubing to avoid interferences from air with EC readings. 1 to 5 mL of a NaCl solution with a high EC of ca. 25 mS/cm were injected with a syringe through a rubber stopper. The solution was pumped into the isolated interval through the inflow pipe of the packer, and pumped out of the outflow pipe. The EC was measured over time with a HACH IntelliCAL™ CDC401 EC probe and meter in a flow cell isolated from the atmosphere and recorded automatically every 10 s on a USB key. Circulation was run for at least 4 hours, and overnight if possible.

1.3.2 Testing the borehole dilution method

Sandbox experiments were conducted at the Chalk River Laboratories to evaluate the applicability of using small diameter drive-point piezometers prior to use in the field. A 55 cm long, 34 cm wide and 20 cm high sandbox was built using plywood. The box was then lined with a plastic sheet to make it impermeable. A Nitex (Sefar America Inc.) mesh (236 micron) was set against a 0.64 cm (¼ inch) slotted Plexiglas® plate which was held in place by slotted wooden spacers on both ends of the box to establish a consistent inflow and avoid clogging of the outflow. The box was packed with a medium to coarse grained sandblasting sand for the first experiments, which was later replaced by fine sand (<420 µm) from the Wall and Curtain site for the second experiments. When saturated conditions were established and maintained through pumping, drops of rhodamine dye were placed on washers on the surface of the sand to determine if dyed flow lines showed laminar flow. Afterwards, the shape factor α was determined experimentally for both, the original and modified Solinst® drive-points, by measuring the asymptotic width of the rhodamine dye flow lines that still converged into the drive-points (see Figure 1.5).

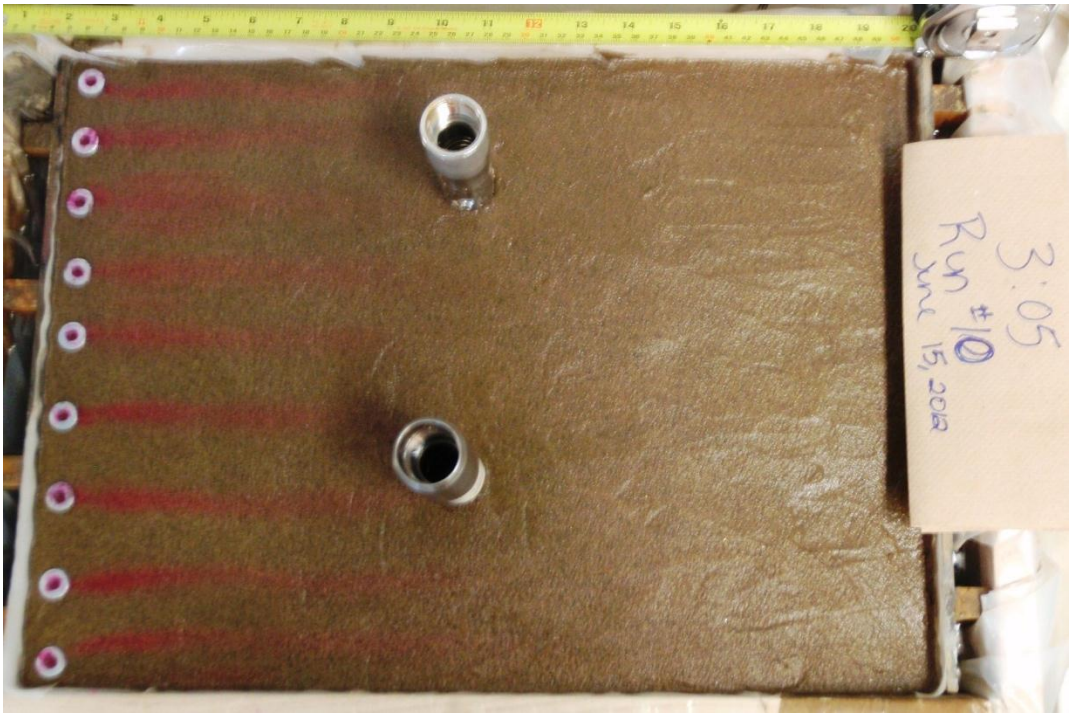

Figure 1.5: Determination of the shape factor for both drive-points in the sandbox experiment, using rhodamine dye.

After the determination of the shape factor, borehole-dilution tests were performed at two different known flow rates in both drive-points. The first flow rate was a high flow of 25.5 mL/min (6.6 x 10^{-6} m/s), which was higher than velocities expected on site. The second scenario tested the borehole dilution method with both drive-points at a flow rate of 3 mL/min (7.7 x 10^{-7} m/s), which corresponded to groundwater velocities expected in the field. The last test scenario was repeated with both drive-points in fine grained sand (< 420 µm) from the site.

One of the problems encountered with the original drive-point in the field was that it clogged with sediment when pulled up with a jack, due to the coarse screen of the drive-point. To test if the volume inside the original drive-point was reduced by sediment clogging in the field, a comparison of velocity estimates determined through borehole dilution with the two different drive-points in the same location was conducted. Borehole-dilution tests were

performed with the modified drive-point in DP-3 at depths of 4.5 m and 5.4 m. These locations were chosen as they include one location of good agreement between the velocity estimates from borehole dilution using the original drive-point and the Darcy equation with slug test hydraulic conductivity values, and one location in which agreement between the two estimates is poor. As the Wall and Curtain system has the unique advantage of an adjustable flow rate and hydraulic gradient across site, it is an ideal setting to test the response of the borehole dilution method to changing velocities. This response test was conducted in location DP-3 at a depth of 5.4 m with the modified drive-point version. The flow rate of the Wall and Curtain was changed from 0.50 L/s, which was used in borehole-dilution tests before, to a flow rate of 0.77 L/s. After the flow rate stabilized, a borehole-dilution test was run at this flow rate and compared to the velocity determined through the Darcy equation including slug test data and the newly established hydraulic gradient.

1.4 Results and Discussion

1.4.1 Results from field experiments

The water-table map and flow net created with elevation and water-level measurements in July 2012 can be seen in Figure 1.6. It can be clearly seen that the water-table contour curved in the proximity of the Wall and Curtain, which resulted in flow lines bending towards the Curtain. The capture zone of the Curtain 35 m upgradient of the system was approximately 15 m wide in July 2012.

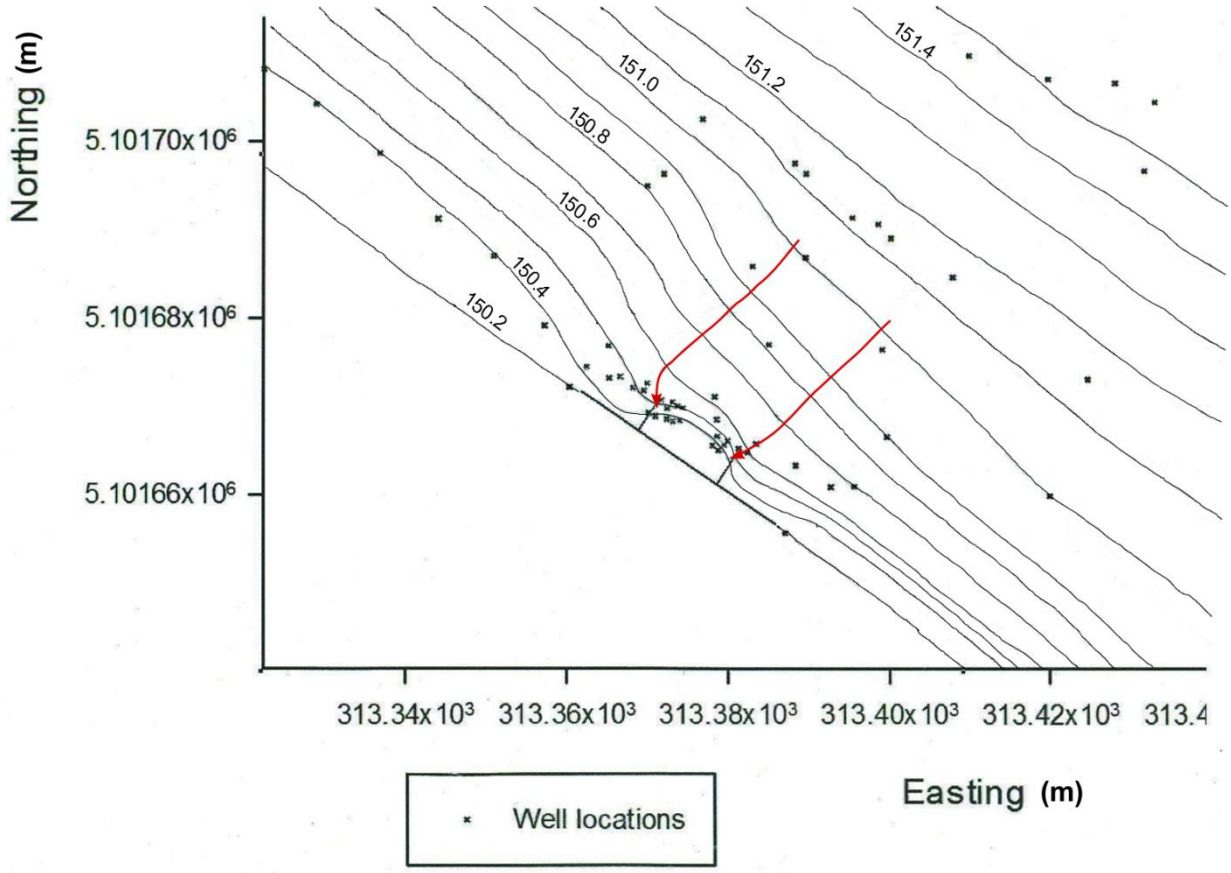

Figure 1.6: Water-table map of the Wall and Curtain Site. Black lines are water-table contours, labels are meters above sea level (masl). Flow lines are in red and form the boundary of the capture zone.

Hydraulic heads with depth from 16 locations in the Curtain and the proximity of the system are shown in Figure 1.7. The two upper graphs and the graph on the lower left show head measurements from wells just upgradient of the clinoptilolite. The wells included in these three graphs form a transect from just east of the eastern sheet-piling wing (WC-65) to west of the Curtain (WC-90). It can be clearly seen that there was a strong vertical component to the gradient in the immediate vicinity of the PRB. The gradient was upward, strongly increasing between depths of 4 m to 8 m and as stronger directly upgradient of the curtain (approximately 0.020, in wells WC- 67 to WC-71) than on either side of the sheet-

piling wings. Outside of the sheet-piling wings, the gradient was 0.010 to 0.016 higher on the eastern side (in wells WC-65 and WC-66, respectively) than in the west of the Curtain (≤ 0.01, in wells WC-72 and WC-87 to WC-90). The lower right graph includes wells that are 3 m to 13 m further upgradient from the curtain than the locations in the other three plots. Well C-271 is located further upgradient east of the Curtain, and showed a lower upward gradient of 0.0036. The other three wells shown in the graph are located upgradient along the centerline of the curtain. The vertical gradient decreased from C-274 (0.019) over WC-31 (0.0099) to C-279 (0.0014), which corresponded to increasing distance from the curtain. These results indicate that flow is generally horizontal until the groundwater approaches the PRB, where it becomes strongly vertical upward due to the relatively low hydraulic head within and the high hydraulic conductivity of the clinoptilolite. This means that flow through the lower half of the aquifer bent upwards close to the Wall and Curtain, which induces interception of the contaminant plume, as intended by design.

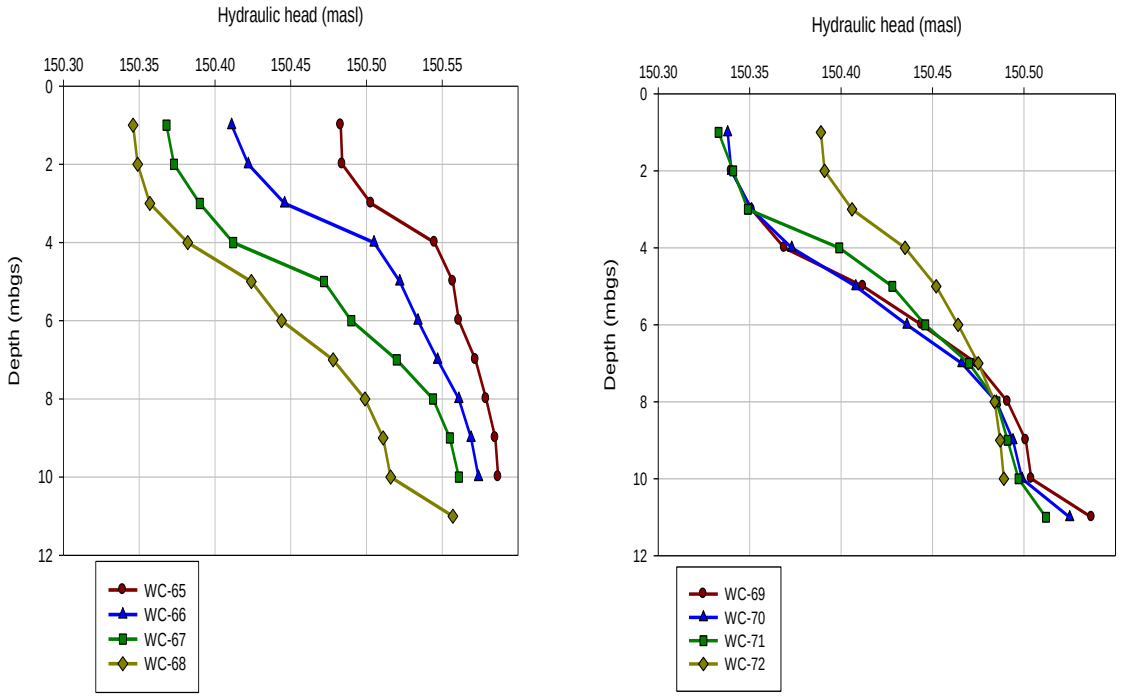

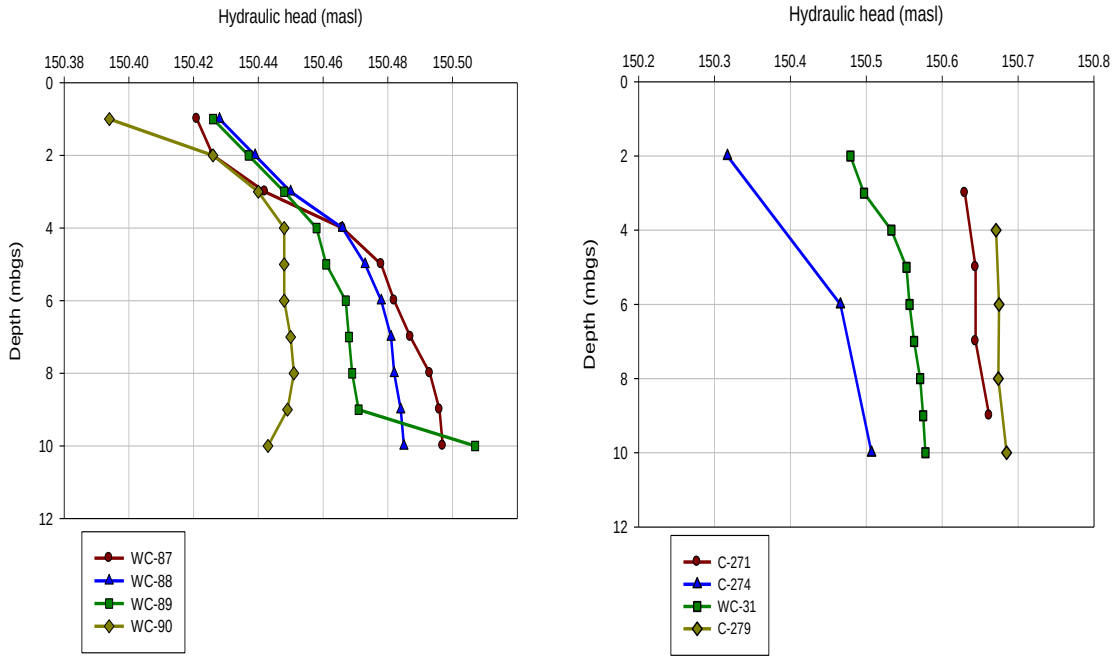

Figure 1.7: Plots of hydraulic head versus depth in the proximity of the Wall and Curtain.

The results of the single-well response tests are summarized in Table 1.1 and Figure 1.8. In general, the hydraulic conductivity estimates from the six drive-points were in good agreement with each other and could be correlated horizontally, indicating that the aquifer was rather homogeneous. However, some trends with depths and some horizontal differences between locations can be seen. The hydraulic conductivity at depths ≤ 3.5 m bgs for all locations was in the order of 10^{-6} m/s, indicating a dominant grain size of fine sand (Freeze and Cherry, 1979). At depths > 3.5 m and ≤ 8.0 m, K values were in the order of 10^{-5} m/s, which was in agreement with the reported fine to medium grained sand (Killey and Munch, 1987) at these depths. At depths > 8.0 m, hydraulic conductivity estimates generally decreased again, indicating predominantly finer grain sizes. However, some discrepancies can be seen in the transect. At depths between 4.8 m and 5.4 m bgs in DP-4, the hydraulic conductivity was lower than in the other drive-points at the same depths, indicating a lens of finer grain sizes. The hydraulic conductivity value in DP-5 at a depth of 5.2 m was in the same order as the lower values in DP-4, which could mean that the lens continued and

thinned out further to the West. DP-4 also showed lower hydraulic conductivity values at depths of 7.2 and 7.5 m, but higher K values in depths of 7.7 m and 8 m than the surrounding locations at similar depths. This difference could indicate that the layer of finer grain sizes at this depth was not completely horizontal, but showed a slight trend upwards close to DP-4. At the eastern end of the transect, lower hydraulic conductivity values in DP-2 at a depth of 7.3 m and in DP-6 at a depth of 7.1 m indicate a lens of finer grain sizes at this depth. The *in situ* values ranged from 2.2×10^{-6} m/s to 5.3×10^{-5} m/s, which was lower than the reported K values by Killey and Munch (1987), which are between 3.5×10^{-6} m/s to 1.2×10^{-4} m/s. However, the factor of comparison was < 2, which is considered a small difference considering the determination of hydraulic conductivity, indicating that hydraulic conductivities determined *in situ* through slug tests were in agreement with the K values determined by permeameter tests and grain size analyses by Killey and Munch (1987). The K values from the slug tests gave a better understanding of flow in the proximity of the Wall and Curtain, and were used to calculate the average linear groundwater velocity through the Darcy equation. Understanding the physical flow across site was necessary in order to develop a numerical flow model and give estimates of the longevity of the system.

Table 1.1: Hydraulic conductivity values determined from the slug tests.

DP-1		DP-2		DP-3	
depth (m)	K (m/s)	depth (m)	K (m/s)	depth (m)	K (m/s)
1.6	2.64×10^{-6}	1.9	9.68×10^{-6}	1.9	7.90×10^{-6}
2.5	3.86×10^{-6}	2.8	4.17×10^{-6}	2.7	4.77×10^{-6}
3.5	1.92×10^{-5}	3.5	1.31×10^{-5}	3.6	1.06×10^{-5}
4.5	7.00×10^{-6}	4.5	7.10×10^{-6}	4.6	2.53×10^{-5}
5.4	2.00×10^{-5}	5.4	2.35×10^{-5}	5.6	3.95×10^{-5}
6.2	5.32×10^{-5}	6.4	2.78×10^{-5}	6.5	1.98×10^{-5}
7.1	2.00×10^{-5}	7.3	2.38×10^{-6}	7.4	2.86×10^{-5}
8.1	2.40×10^{-5}	8.0	4.01×10^{-6}	8.3	6.30×10^{-6}

9.0	4.00×10^{-6}	8.9	8.44×10^{-6}	9.2	8.85×10^{-6}

DP-4		DP-5		DP-6	
depth(m)	K (m/s)	depth (m)	K(m/s)	depth (m)	K (m/s)
2.0	4.14×10^{-6}	2.0	4.20×10^{-6}	2.4	8.61×10^{-6}
3.0	4.26×10^{-6}	2.9	8.18×10^{-6}	3. 3	5.58×10^{-6}
4.0	2.89×10^{-6}	3.8	3.07×10^{-5}	4.3	2.32×10^{-5}
4.5	3.76×10^{-5}	4.9	2.29×10^{-5}	5.0	4.99×10^{-5}
4.8	2.16×10^{-6}	5.2	3.93×10^{-6}	5. 3	1.72×10^{-5}
5.1	6.65×10^{-6}	5.5	2.02×10^{-5}	5. 6	1.61×10^{-5}
5.4	2.56×10^{-6}	5.8	8.69×10^{-6}	5. 9	9.42×10^{-6}
5.7	3.71×10^{-5}	6.2	4.24×10^{-5}	6.2	4.57×10^{-5}
6.3	1.64×10^{-5}	6.5	2.93×10^{-5}	6.5	1.18×10^{-5}
6.6	1.81×10^{-5}	6.8	1.54×10^{-5}	6. 8	1.10×10^{-5}
6.9	2.32×10^{-5}	7.1	1.31×10^{-5}	7.1	2.20×10^{-6}
7.2	5.06×10^{-6}	7.4	1.32×10^{-5}	7.4	3.27×10^{-5}
7.5	8.05×10^{-6}	7.7	1.56×10^{-5}	7.6	1.84×10^{-5}
7.7	1.78×10^{-5}	8.0	4.67×10^{-6}	8.0	6.07×10^{-6}
8.0	2.44×10^{-5}	8.3	2.53×10^{-6}		
8.6	8.46×10^{-6}	8.6	2.65×10^{-5}		
8.9	1.26×10^{-5}	8.9	2.32×10^{-5}		

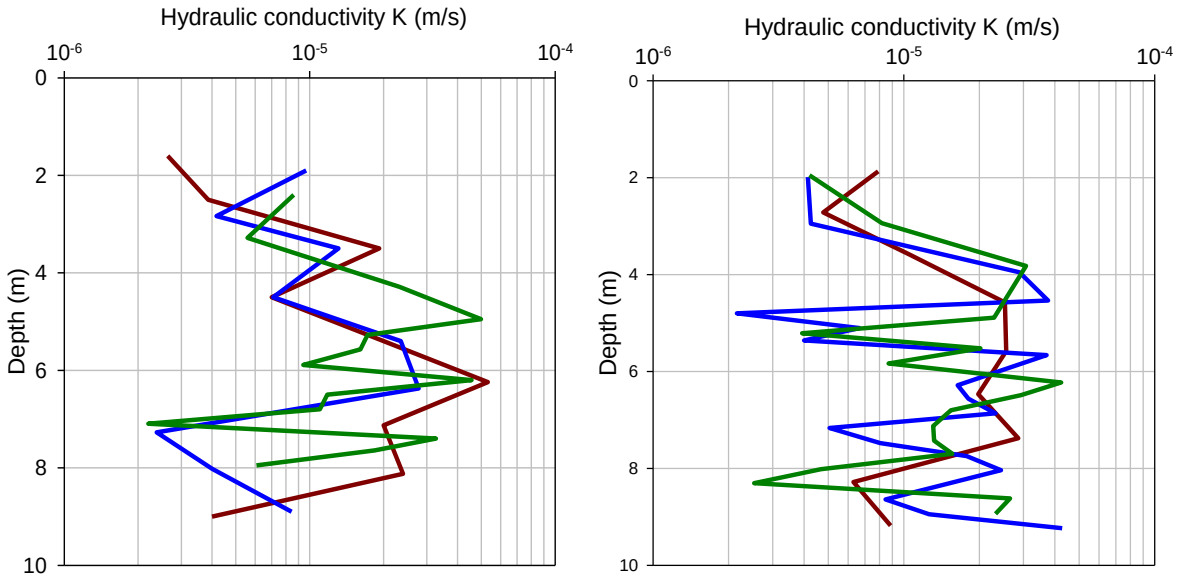

Figure 1.8: Left: Hydraulic conductivity profiles for drive-points 1 (red), drive-point 2 (blue) and drive-point 6 (green). Right: Hydraulic conductivity profiles for drive-points 3 (red), drive-point 4 (blue) and drive-point 5 (green).

1.4.2 Borehole dilution in comparison to slug tests

Collected EC data were analyzed using the method presented by Grisak et al (1977). When the EC values are plotted semi-logarithmically versus time, a linear regression line forms as:

$$\ln C = \ln C_0 + mt \quad \textbf{(1.1)}$$

where C is the measured EC at any time t, C_0 is the initial EC and m is the slope, is fitted to the data (Grisak et al., 1977). If a time corresponding to $C_0/2$ is selected, then:

$$v_f = 0.693V/\alpha At \quad \textbf{(1.2)}$$

(from Grisak et al., 1977) where v_f is the linear groundwater velocity, V is the packed off volume and A is the cross sectional area of the screen. The shape factor α accounts for the distortion of flow lines in the presence of a well screen and is defined as the asymptotic width of the tracer cloud over the inside diameter of the well screen (Drost et al., 1968). For a

borehole without gravel pack, it can be determined theoretically through Ogivli's equation (Ogilvi, 1958):

$$\alpha = \frac{4}{\left[1+\left(\frac{r_1}{r_2}\right)^2\right]+\frac{k_2}{k_1}\left[1-\left(\frac{r_1}{r_2}\right)^2\right]} \quad \textbf{(1.3)}$$

Where r_1 is the inside radius of the well screen, r_2 is the outside radius of the well screen, k_1 is the well screen permeability and k_2 is the permeability of the aquifer. The well screen permeability can be determined through calculations described in detail by Drost et al. (1968). The theoretical values for α were 2.45 and 2.80 for the original drive-point and the modified drive-point, respectively. The parameters used in the calculations are listed in Table 1.2. The values listed for the shape factors were experimentally determined and are explained in section 1.4.3.

Table 1.2: Parameters used in calculations of the average linear groundwater velocities from borehole-dilution tests.

Parameter (Unit)	**Value used in calculation**
Packed-off volume (m^3)	2.38×10^{-4}
Shape factor for original drive-point	2.36
Shape factor for modified drive-point	2.62
Cross-sectional area (m^2)	2.13×10^{-3}

By injecting a solution with a high salt concentration, one possible effect could be that due to the higher density of the salt solution compared to the groundwater, the injected solution could sink rapidly to the bottom of the drive-point. The measured EC would then show a rapid decrease, leading to an overestimate in groundwater velocity. Although the EC of the injected solution was with 25 mS/cm more than two orders of magnitude higher than the EC of the groundwater (generally between 30 µS/cm and 300 µS/cm), an injection of 1-5 mL resulted in mixing within the packed-off volume, and caused the EC within this volume (238 mL) to increase to 600 to 1000 µS/cm. If the tests were affected by density effects, a rapid

decrease would be seen in the beginning of circulation, shown by a steeper slope of the first part of plotted EC data over time. As no steeper slope in the first part of plotted data was observed, density effects were not considered to affect the results of the borehole-dilution tests.

Average linear groundwater velocities (v_f) were calculated with the Darcy equation from the slug test data. A porosity of 0.38 for fine to medium sand is reported for sediments on site (Killey and Munch, 1987) and used in the equation, as well as a hydraulic gradient of 0.0165 determined from the water-level measurements along the groundwater flow path during the field tests. The velocity estimates from the Darcy equation are compared to the average groundwater velocity values determined through borehole-dilution tests, as shown in Figure 1.9. Overall, the velocity values from the borehole dilution showed good agreement with values from slug tests and the Darcy equation, being generally within a factor of ≤ 3. Discrepancies were smaller at depths of 5.6 m (1.72×10^{-6} m/s from Darcy equation compared to 3.31×10^{-7} m/s from borehole dilution) and 7.4 m (5.82×10^{-7} m/s from Darcy equation compared to 1.2×10^{-7} m/s from borehole dilution) in DP-3 as well as at 9 m in DP-1 (8.95×10^{-7} m/s from borehole dilution compared to 1.74×10^{-7} m/s from the Darcy equation). Larger discrepancies were observed in DP-2 at depths of 1.9 m (2.04×10^{-6} m/s from borehole dilution compared to 4.2×10^{-7} m/s from Darcy equation), 6.4 m (7.14×10^{-6} m/s from borehole dilution compared to 1.21×10^{-6} m/s from Darcy equation) and 8 m (1.02×10^{-6} m/s from borehole dilution compared to 1.74×10^{-7} m/s from Darcy equation). The largest discrepancy of all values existed in DP-2 at a depth of 2.8 m. At this depth, the value from the borehole dilution (3.37×10^{-6} m/s) was more than an order of magnitude higher than the estimate from the Darcy equation (1.81×10^{-7} m/s). In the case of DP-2, the velocity estimate from the Darcy equation was in good agreement with other locations at the same depths, indicating that the borehole dilution method overestimated the velocity in the two shallowest depths, probably due to an insufficiently inflated packer. In the case of DP-3, especially at 7.4 m, the borehole dilution velocities were low compared to the values from the Darcy equation and borehole dilution for DP-1 and DP-2 at similar depths. This could be due to the non-continuous drive-point screen openings used for locations DP-1 to DP-3. If

the openings were not facing the direction of flow, groundwater flow and the amount of dilution that occurred in the monitored zone would be restricted. However, it must always be kept in mind that slug tests can only be seen as hydraulic conductivity estimates within a factor of 5-10. It is important to note that in locations DP-4 to DP-6, in which the modified drive-point was used, only one point comparison showed a difference of a factor larger than 4. At a depth of 7.4 m in DP-6, the velocity from the borehole dilution was 3.33 x 10^{-7} m/s, and the estimate from the Darcy equation was 1.42 x 10^{-6} m/s, resulting in the factor of difference between those values being 4.3. From these results, it can be concluded that the modified drive-point seemed to produce results that were more closely correlated to the slug test results from the borehole dilution, probably due to the finer, continuous screen.

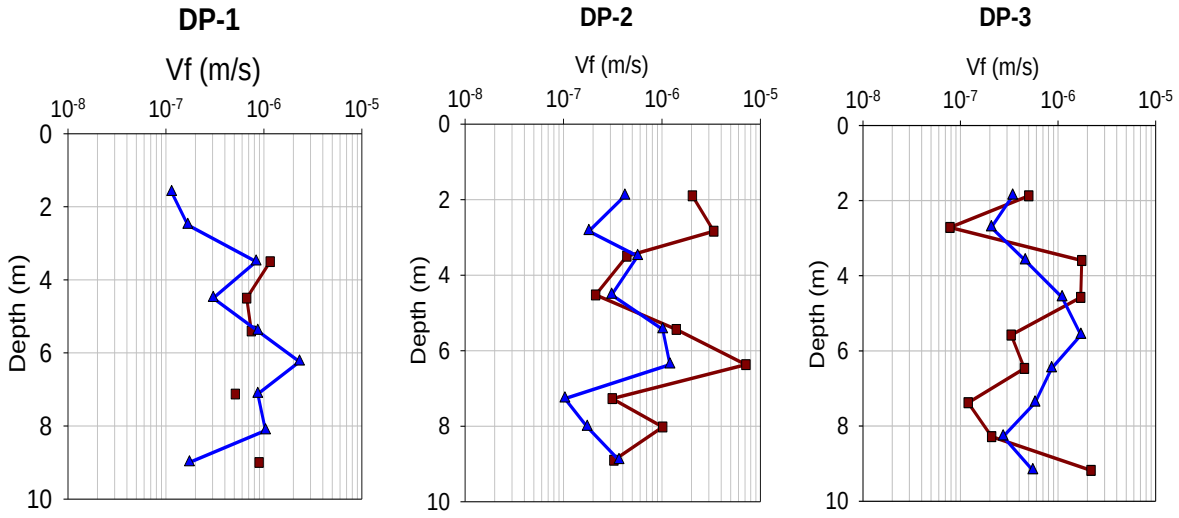

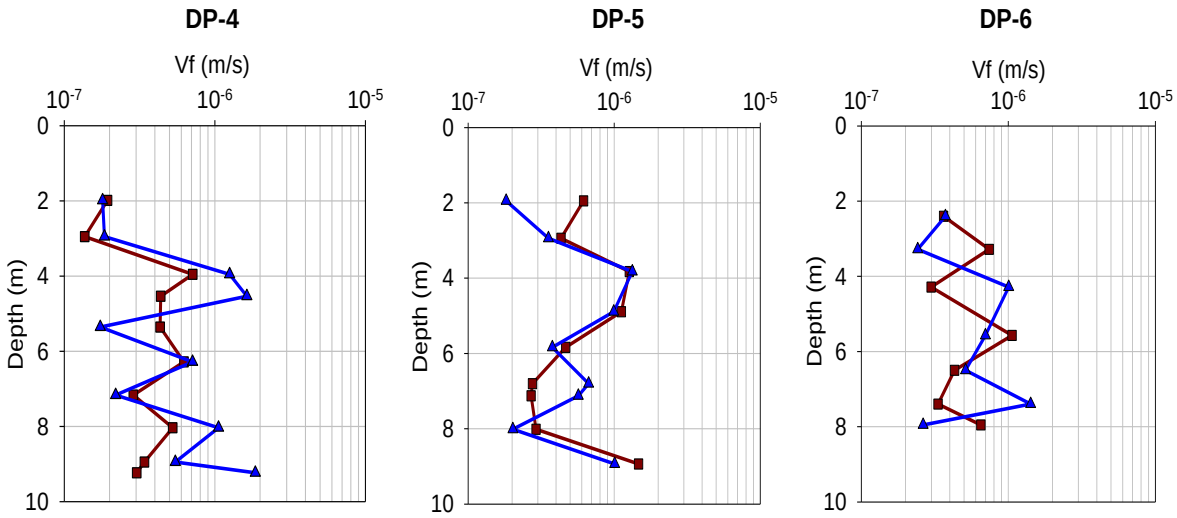

Figure 1.9: Average linear groundwater velocity profile for drive-point piezometers DP-1 to DP-6 determined through borehole-dilution tests (red) and calculated with Darcy's Law from slug tests (blue).

1.4.3 Sandbox experiment

The shape factor α was experimentally determined to be 1 for both drive-point modifications in the medium to coarse sandblasting sand. As the permeability of medium to coarse sand was high, flow lines did not converge into the drive-point screens of similar permeability, but went straight through them. In the less permeable fine sand from site, flow lines converged into both modifications of drive-points. The shape factor was determined to be 2.36 for the original Solinst® drive-point, which was in good agreement with the theoretically calculated value of 2.45. Convergence of flow into the modified drive-point was greater than into the original one due to a bigger intake area. The modified drive-point had an experimentally determined shape factor of 2.62, which was in close agreement with the theoretical value of 2.80. The shape factors determined from the sandbox experiments in the fine grained sand were used in calculations of the average linear groundwater velocity from borehole dilution data collected in the field.

The groundwater velocity estimates determined through borehole dilution are compared to the actual flow rate, as listed in Table 1.3. At a flow rate of 3.0 mL/min in coarse sand, the two velocities determined in the different drive-points were in good agreement, within a factor of 1.9 for the borehole dilution in the original drive-point and a factor of 1.4 for the borehole dilution in the modified drive-point. At a high flow rate of 25.5 mL/min, the velocity determined through borehole dilution in the modified drive-point was in very good agreement with the flow rate, within a factor of 1.2. The velocity value from the borehole dilution in the original drive-point considerably underestimated the actual flow rate by a factor of 4.5. A possible reason for this low estimate is the discontinuous open area of the original drive-point. The calculation of the average groundwater velocity incorporated the cross sectional area of the screen; however, it was not certain in this case that flow occurred through the entire cross sectional area of the screen. As the permeability of the coarse sand was high and the shape factor was 1, it is possible that flow only occurred through the cross sectional area of the distinct holes in the drive-point that are aligned in the direction of flow. If only this area was considered in the calculation, the velocities determined through the borehole dilution in the original drive-point for the high flow and the low flow rate scenarios would increase to 10.3 mL/min and 2.9 mL/min, respectively. This velocity would be in better agreement with the high flow rate (factor of 2.5).

The first test scenario, in which a high flow rate was applied, was not reproducible for the fine grain size because response times between inflow and outflow were too long, leading to flooding at the influent boundary. In the fine sand, velocity values from the borehole dilutions in both drive-point versions were in acceptable agreement with the actual flow rate, with factors of 2.7 for the original drive-point and 1.8 for the modified drive-point. However, it is important to note that the estimates from the borehole dilutions were in very close agreement with each other, within a factor of 1.5. This could indicate that the actual flow rate was not steady at 3 mL/min. The observed long response time between inflow and outflow of the sandbox with the fine grain size supported this explanation.

The results from the sandbox experiment indicate that the modified version of the drive-point produced results that were in better agreement with the actual flow rate than the

original version. Inconsequence, results from borehole-dilution tests in the modified drive-point in the field should be weighed higher than the results in the original drive-point. However, for low flow rates, both drive-points worked well and results were in close correlation.

Table 1.3: Comparison of actual flow rate and flow rate estimates determined through borehole dilution in the different drive-points.

Grain size	Actual flow rate from inflow (pump) and outflow	Flow rate from borehole dilution in original drive-point	Flow rate from borehole dilution in modified drive-point
Coarse Sand	3.0 mL/min	1.6 mL/min	4. 1 mL/min
Coarse sand	25.5 mL/min	5.7 mL/min	21.6 mL/min
Fine sand	3.0 mL/min	1.1 mL/min	1.7 mL/min

1.4.4 Comparison of original drive-point and modified drive-point in the field

The groundwater velocity estimates from the borehole-dilution tests performed with the two drive-point modifications in DP-3 at depths of 4.6 m and 5.6 m are compared to the velocity estimate from the slug test and Darcy equation in Table 1.4. The velocity estimate from the slug test and Darcy equation and the velocity estimate from the borehole dilution were in very close agreement at a depth of 4.5 m. At a depth 5.4 m, the original drive-point was suspected to clog with sediment, indicated by a poorer agreement (factor 5.2) of the velocity estimate from the borehole dilution and the value from the slug test and Darcy equation. It can be clearly seen that values from both drive-points were in very close agreement for both depths. At a depth of 4.6 m, the velocity from borehole dilution in the original drive-point was within a factor of 1.6 compared to the velocity determined through the Darcy equation. The factor between the velocity from the borehole dilution in the modified drive-point and the velocity from the Darcy equation was higher with 2.1. However, the factor between the velocities determined through borehole dilution in the different drive-points was only 1.4. At a depth of 5.6 m, the velocity values from borehole-dilution tests in the two different drive-

points were in even closer agreement, within a factor of 1.1. Compared to the velocity estimate determined with the Darcy equation, the agreement of both velocities from the borehole dilution was poorer, with a factor of 3.2 to 3.4. The results from this comparison suggest that average groundwater velocities determined through borehole-dilution tests were more closely correlated than the velocities determined through the incorporation of slug test data into the Darcy equation. Furthermore, the data obtained from borehole-dilution tests in the original drive-point could be used as velocity estimates, as the values from tests in the modified drive-point were in close agreement.

Table 1.4: Comparison of groundwater velocities determined through borehole dilution in the different drive-points and the estimate derived from the Darcy equation and slug test at the same location.

Depth (m)	Vf original DP (m/s)	Vf modified DP (m/s)	Vf from Slug test and Darcy equation (m/s)
4.5	1.71×10^{-6}	2.34×10^{-6}	1.10×10^{-6}
5.4	3.31×10^{-7}	3.46×10^{-7}	1.11×10^{-6}

1.4.5 Response Test

On October 12, 2012, the flow rate of the Wall and Curtain was increased from 0.50 L/s to 0.77 L/s to determine how well the borehole dilution method responded to the resulting change in groundwater velocity; therefore, the name response test was chosen for this experiment. The high flow rate of the Wall and Curtain caused the hydraulic gradient to increase from 0.0165 to 0.033. Using this value in the Darcy equation, the average linear velocity doubled from 1.11×10^{-6} m/s to 2.22×10^{-6} m/s. The velocity estimate from the borehole-dilution test during the increased flow rate of the Wall and Curtain was 9.40×10^{-7} m/s, which was 2.7 times higher than the velocity determined before (3.46×10^{-7} m/s). This means that between the velocity determined through borehole dilution and the estimate from the Darcy equation were within a factor of 2.4 in high flow rate conditions, which was a

better agreement than observed previously (factor 3.2). The results indicate that the borehole dilution method responded well to changes in average groundwater velocities due to an increased hydraulic gradient, especially considering the higher uncertainty of the slug test results and thus velocity estimates from the Darcy equation.

1.5 Summary and Conclusion

The Wall and Curtain site in Chalk River, Ontario, is a permeable reactive barrier system with the unique advantage of an adjustable hydraulic gradient and capture zone. To provide estimates of the longevity of the system, a detailed physical field characterization was conducted in 2011 and 2012. The water-table map created from a detailed elevation study and water-level measurements indicates that equipotential lines curved close to the Wall and Curtain and flow lines converged into the system, with a capture zone width of approximately 15 m. The vertical gradient in the proximity of the Wall and Curtain was upward, increasing strongly with decreasing distance from the system due to the high hydraulic conductivity of the clinoptilolite. This caused flow from the lower half of the aquifer to bend upwards. The Wall and Curtain thus intercepted deep, contaminated groundwater on site, which indicates that the system was working well from a physical flow perspective. Hydraulic conductivities determined *in situ* through slug tests showed that the aquifer was rather homogeneous and indicate that grain sizes were predominantly fine sand and fine to medium sand, although some lenses of finer material existed. Velocities from borehole-dilution tests compared approximately with velocity estimates from the Darcy equation with the slug test data. A detailed physical characterization of the site was necessary to develop a well calibrated flow model in order to meet the overall objective of providing refined estimates of the Wall and Curtain's longevity.

As this was the first study known to the authors that used the borehole dilution method in a small pipe diameter, the reproducibility of the method was evaluated in the laboratory and in the field. As the original drive-point filled up with sediment and was not continuously screened, modifications were performed in 2012 for use in locations DP-4 to DP-6. The

shape factor was determined for both drive-points in a sandbox experiment. In the field and in sandbox experiments, borehole-dilution tests with the modified version of the drive-point produced results in better agreement with the actual flow rate than tests in the original drive-point. In a low flow situation, both drive-points produced closely correlated results. In direct comparison in the field at the same locations, both drive-points produced results that were in very close agreement with each other. The results indicate that borehole dilution was a method producing more closely correlated results in the determination of the average linear groundwater velocity than the Darcy equation with incorporated field data.

Chapter 2

Combining field methods and numerical modeling to characterize the flow of a ^{90}Sr plume through a permeable reactive barrier

2.1 Introduction

Strontium-90 (^{90}Sr) is a mobile radioactive isotope which is present in the environment at low concentrations as a result of nuclear testing that occurred in the 1950's and 1960's, and in nuclear waste (Department of Health and Human Services, 2005). ^{90}Sr decays with a half-life of 28.8 years to yttrium 90 (^{90}Y) by emitting a beta particle. ^{90}Y in turn undergoes beta decay with a half-life of 64.4 hours to form zirconium 90 (^{90}Zr). Among a few methods to treat ^{90}Sr in groundwater, permeable reactive barriers (PRBs) have gained particular attention. PRBs are passive remediation systems which are installed in the flow path of a contaminant plume and have been applied for many contaminants, including organic compounds, inorganic substances, and radionuclides (e.g. Blowes et al., 2000). The reactive material used in reactive barriers either promotes chemical reactions with the contaminant which lead to a product that does not cause health concerns or adsorbs the contaminant. For example, PRBs using zero valent iron as reactive material have been used successfully in the treatment of Cr, U and Tc (Blowes et al., 2000), as well as halogenated hydrocarbons. Organic carbon, used as a reactive material in the form of sawdust or wood chips, has been used to treat constituents of acid-mine drainage, including SO_4, Fe, Ni, Co and Zn (Blowes et al., 2000). With regard to the treatment of radioclunides, zeolites, aluminosilicates with a high sorption capacity of heavy metals and radionuclides, have been used in PRBs (Lee and Hartwig, 2005). A permeable reactive barrier using clinoptilolite, a zeolite, as a reactive medium was installed at the Atomic Energy of Canada Limited Chalk River Laboratories in Chalk River, Ontario, to prevent the discharge of a ^{90}Sr plume into a nearby swamp. The PRB, known as the Wall and Curtain (Lee and Hartwig, 2005), is the first PRB that uses clinoptilolite for the treatment of ^{90}Sr in groundwater. Although flow rates and outflow

quality of the system are well monitored, data gaps exist in the physical properties of the groundwater flow system, especially regarding the variability of hydraulic conductivity and groundwater velocities across the site.

Numerical models have been used extensively over recent decades to characterize flow and transport properties at contaminated sites (e.g. Frind et al., 1999) and are a valuable tool for evaluating remediation strategies. However, errors arise in applying groundwater models to field problems, because of conceptual deficiencies, numerical errors and inappropriate parameter estimation (Konikow and Bredehoeft, 1992). HydroGeoSphere is a three-dimensional, finite element numerical computer code that offers fully integrated hydrologic, water quality and subsurface flow and transport simulation capabilities (Therrien et al., 2010). The fully-coupled numerical simulation approach allows the simultaneous solution of saturated and variably saturated zones at each time step, as water derived from rainwater is allowed to partition into a variety of components, e.g. overland flow, evaporation, infiltration and recharge (Therrien et al., 2010; Li et al., 2008). Solute concentrations are also solved simultaneously for each time step in subsurface and surface flow regimes. Features like wells, tile drains (e.g. Rozemeijer et al., 2010), streams (e.g. Doble et al., 2011) and fractures (e.g. Park et al., 2004) can be included, as well as external flow and transport stresses such as infiltration and evapotranspiration, seepage faces, specified mass flux and the dissolution of immiscible substances (Cai et al., 2007). All the components mentioned above make HydroGeoSphere an ideal tool to simulate water flow and solute transport within watersheds in a realistic, physically-based manner (Therrien et al., 2010).

In order to better understand the flow system at the Wall and Curtain site, a numerical model was constructed using HydroGeoSphere. Field data were collected in the summers of 2011 and 2012 to fill the data gaps mentioned above and make the simulation more representative of the flow regime on site. Thus, the objective of this study was to incorporate field data into a 3-D numerical model using HydroGeoSphere to describe the flow system that transports a ^{90}Sr plume through the aquifer and the PRB, to achieve a better understanding of the system. The flow model is later used as a basis of a reactive transport

model to make more refined estimates of the longevity of the permeable reactive barrier system.

2.2 The Wall and Curtain Site

The Wall and Curtain site is located on the property of Atomic Energy of Canada Limited (AECL) Chalk River Laboratories, Ontario, Canada, approximately 193 km northwest of Ottawa. In the early 1950s, solutions containing ^{90}Sr were stored in limestone lined pits. Leakage from these pits released ^{90}Sr into the underlying aquifer. The predominantly sandy aquifer has a saturated thickness of 5 m to 13 m. It consists of very fine sand, fine sand, fine to medium sand, minor interstratified silty-sand units and is underlain locally by a basal till unit (Killey and Munch, 1987). Hydraulic conductivities of the aquifer materials determined by permeameter experiments range from 6.6×10^{-6} m/s to 4.0×10^{-5} m/s. Groundwater velocities range from 100 to 150 m/a (Klukas and Montyaner, 1995). The transport of ^{90}Sr is retarded due to geochemical interactions with the aquifer material, resulting in a travel time of ^{90}Sr from the source to the Duke Swamp, located 440 m downgradient, which exceeds 40 years. In 1994, the plume approaching Duke Swamp was about 7 m wide and was located in the bottom half of the aquifer (Lee and Hartwig, 2005). The horizontal hydraulic gradient at the site ranges between 0.01 and 0.016.

In December 1998, a PRB system was installed in order to prevent the ^{90}Sr plume from discharging into the pond downstream. The PRB configuration is known as the Wall and Curtain (Fig.1.1) and uses clinoptilolite, a zeolite, as the reactive material. It consists of a 30 m long, sealed-joint, steel sheet pile cut-off wall (Waterloo Barrier®) on the downgradient side of the reactive barrier or "curtain". The cut-off wall contacts the till or bedrock at a depth of 9 to 12 m. In front of the cut-off wall, a 2 m thick, 6 m deep and 11 m wide curtain of granular clinoptilolite is placed. Whereas clinoptilolite has been suggested as a reactive material for PRBs due to a high sorption capacity and the affinity for both Sr and Ca (Cantrell et al., 1994; Fuhrmann et al., 1996), the Wall and Curtain site is the first to employ clinoptilolite as the reactive material in a PRB. Calcium concentrations in the groundwater

are low, thus limiting the saturation of sorption sites available for Sr and making it a suitable setting to use clinoptilolite. The hydraulic conductivity of the clinoptilolite is estimated to be 3.0×10^{-4} m/s (Sale, 2003). Two sheet-piling walls on either side of the curtain help to direct the groundwater flow through the curtain. Ten fully-penetrating wells behind the curtain are connected to each other by a horizontal drain that collects and directs outflow from the curtain to a manhole. At the manhole, the height of the outflow hose can be adjusted to control the hydraulic head and gradient near the Wall and Curtain. These adjustments, in turn, can control the capture zone of the Wall and Curtain, one of the major advantages of the design. A second adjustable horizontal drain located 60 m upgradient of the Wall and Curtain system intercepts clean, shallow groundwater and discharges it into the manhole. This diversion of clean water away from the Wall and Curtain reduces the loading of dissolved constituents to the Curtain, thus extending the operational life of the reactive material. The hydraulic head at the upgradient drain can also be controlled the same way as the Wall and Curtain using an adjustable outflow hose in the manhole. The outflow of both the Wall and Curtain and the upgradient drain are monitored regularly to ensure that all the contaminated groundwater is captured by the Wall and Curtain and that the outflow of the Wall and Curtain meets water quality guidelines.

Field investigations were conducted at the Chalk River Laboratory site in 2011 and 2012, to characterize the aquifer and the groundwater flow system in the vicinity of the Wall and Curtain. These investigations included hydraulic conductivity measurements made in 1.9 cm-diameter drive-point piezometers at six locations. The hydraulic conductivity values showed good horizontal correlation, indicating that the aquifer was relatively homogeneous. Horizontal hydraulic conductivities were in the order of 10^{-6} m/s at depths ≤ 3.5 m, indicating fine sand grain sizes. At depths between 3.5 m and 8 m, hydraulic conductivity values increased to the order of 10^{-5} m/s, indicating fine to medium sand. At depths > 8 m, hydraulic conductivity values decreased to the order of 10^{-6} m/s. Hydraulic heterogeneities at 7 m depth at the east end of the transect (DP-6 and DP-2) indicate finer grain sizes to the east.

Borehole-dilution tests were performed in the drive-point piezometers in 1 m vertical intervals between 1.5 m bgs and 9 m bgs. A NaCl solution with a high electrical conductivity

(EC) was injected into and circulated through the screened interval. The decrease in EC was recorded over time and analyzed with the method described by Grisak et al. (1977).

Average horizontal linear groundwater velocities (Vf) were calculated with the Darcy equation, using the hydraulic conductivities from the slug tests, assuming typical porosity of fine-medium sand on site of 0.38 (Killey and Munch, 1987) and a horizontal hydraulic gradient of 0.0165, based on water-level measurements made during the field data collection. These values were compared to the velocities determined with borehole-dilution tests. Overall, the agreement between the Darcy equation and borehole dilution velocities was good, with a difference of a factor of ≤ 3 for most measurement points. Some larger discrepancies existed at the two shallowest depths and at 8 m bgs in DP-2, in which velocities from borehole-dilution tests were much higher than the estimates from the Darcy equation. These discrepancies might have been due to an insufficiently inflated packer, which led to faster dilution and a falsely high borehole dilution velocity. A detailed description of the results from field experiments is provided in chapter 1.

2.3 Set up of a numerical flow model

A physical flow model of the Wall and Curtain site was constructed using the three-dimensional finite-element numerical computer code HydroGeoSphere (Therrien et al., 2010). The model domain was set up as a 200 m long (x-direction), 150 m wide (y-direction) and 12 m high (z-direction) rectangular block. The size of the domain in the direction of groundwater flow (x-direction) and across the direction of flow (y-direction) was chosen to be approximately10 times larger than the capture zone to decrease effects on the flow system by the model domain boundaries. As bedrock topography only changes minimally at the Wall and Curtain site, a fully saturated aquifer thickness of 12 m was assigned to the entire model domain.

The finite element grid spacing ranged from 1-3 m far away from the Wall and Curtain. Close to the Wall and Curtain, a more detailed view was anticipated with a spacing of 0.25 to 0.5 m (see Figure 2.1). For the sheet-piling walls, a spacing of 0.005 m was used. The model

domain consisted of a total of 378,480 nodes and 353,430 elements. The inflow (x = 0 m) and outflow boundaries (x = 200 m) were constant head boundaries. The lateral (y = 0 and 150 m) and bottom boundaries were considered no flow boundaries. A uniform precipitation recharge flux of 0.3 m/yr (Klukas and Moltyaner, 1995) was applied to the top surface of the model domain.

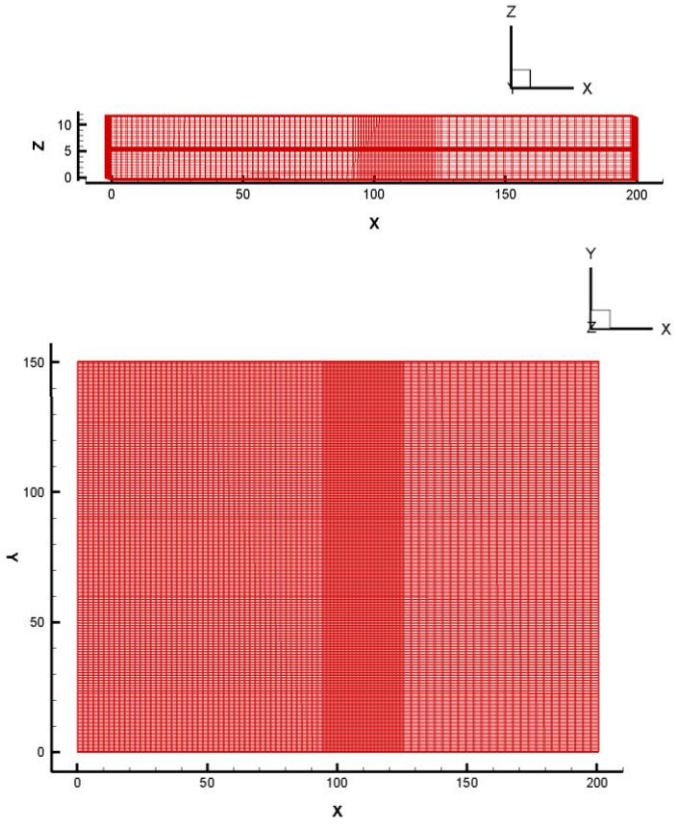

Figure 2.1: Grid of the model domain in HydroGeoSphere. Longitudinal cross section along the centerline on the top, map view on the bottom.

Hydraulic conductivity (K) values determined through the slug tests were incorporated in the model to describe the flow more accurately. The top of the aquifer was assigned a hydraulic conductivity value of 5.4 x 10^{-6} m/s, which represents the average of slug test values for depths < 3.5 m. The hydraulic conductivity values assigned to the central and lower aquifer were 2.2 x 10^{-5} m/s and 1.3 x 10^{-5} m/s, respectively, and were the average

values for depths from 3.5 m to 6.5 m and from 7.5 m to 9 m, respectively. A thin gravel layer at the top of the till layer has a hydraulic conductivity of 1.3 x 10^{-4} m/s, determined through permeameter tests. It was included in the model as part of a 0.5 m thick unit consisting of 0.49 m sand (K = 4.0 x 10^{-5} m/s) and 0.01 m gravel (K = 1.3 x 10^{-4} m/s), leading to a hydraulic conductivity of 4.2 x 10^{-5} m/s for the unit using the weighted average of K data. This approach was preferred over the specification of an additional 1 cm thin gravel layer to facilitate computation. The stony till layer was represented by a 1 m thick unit at the base of the domain with a hydraulic conductivity of 1.4 x 10^{-6} m/s. Hydraulic conductivities were assumed to be isotropic. Table 2.1 shows the input parameters of the numerical model.

The sheet-piling wall was represented in the model by a 30 m long (y-direction), 1 cm thick unit that extends from the surface to 1.5 m above bedrock, equivalent to the top of the gravel containing layer. It was situated perpendicular to the direction of flow at x = 115 m. The side walls of the curtain were 2 m long in the x-direction and had the same vertical extent. The hydraulic conductivity of the sheet-piling walls was set to 1 x 10^{-10} m/s, to make it virtually impermeable. The clinoptilolite curtain was 11 m wide and 2 m thick and was placed on the upgradient side of the sheet-piling wall. It extended from the surface to a depth of 6 m. A hydraulic conductivity value of 2 x 10^{-4} m/s was assigned to the clinoptilolite. A 2 x 11 m x 0.2 m (x, y, z) low K layer with the same hydraulic conductivity as the sheet-piling was included at the bottom of the curtain to represent the clay and plastic liner at the base of the curtain.

The ten vertical discharge wells in the curtain were included in the model with a diameter of 0.054 m and spaced 1 m apart from each other. They were situated 0.2 m upgradient of the sheet-piling wall and were screened continuously from the surface to a depth of 6 m. Each well was assigned a discharge corresponding to a tenth of the total measured Wall and Curtain discharge. An average of measurements was used for the specification of discharge rates of the Wall and Curtain and upgradient drain, as flow rates were adjusted during the field experiments. Moreover, an average of discharge rates will give longer-term estimates of the longevity of the Wall and Curtain in a reactive transport model.

The horizontal upgradient drain was represented in the model by a 0.15 m diameter, 60 m long horizontal tile drain, which was situated 64 m upgradient of the Wall and Curtain (x = 51 m). It acted as a horizontal well 0.5 m below the top surface of the domain and was permeable to groundwater along the full length. Discharged water from the horizontal drain and the ten vertical discharge wells was removed from the simulation. Seepage flux recorded at a weir in the southwest downgradient of the Wall and Curtain was represented in the model by a 20 m long (x-direction) and 15 m wide (y-direction) area on the surface with an assigned averaged specified discharge.

The model was calibrated by comparing observed and simulated heads across the modeling domain, using an influent boundary head of 10.9 m and an effluent boundary head of 8.3 m, which resulted in an average a hydraulic gradient of 0.013 across the domain in the x-direction. Water-level data from July 2012 were adjusted with an arbitrary datum to fit the model domain and used as observed heads.

Table 2.1: Model input parameters.

Parameter (Unit)	Input value in model
Influent boundary head (m)	10.9
Effluent boundary head (m)	8.3
K1 (m/s), upper third of aquifer (z = 8 – 12)	5.5×10^{-6}
K2 (m/s), central aquifer (z = 4.5 – 8)	2.2×10^{-5}
K3 (m/s), lower aquifer (z = 1.5 – 4.5)	1.2×10^{-5}
K4 (m/s) gravel above till (z = 1 – 1.5)	3.8×10^{-5}
K5 (m/s) till above bedrock (z = 0 – 1)	1.4×10^{-6}
K6 (m/s) curtain	2.0×10^{-4}
K7 (m/s) wall and base of curtain	1.0×10^{-10}
Curtain discharge (m^3/s)	3.5×10^{-4}

Upgradient drain discharge (m^3/s)	1.5×10^{-4}
Seepage area discharge (m^3/s)	7.0×10^{-5}
Area of downgradient seepage (m^2)	300
Seepage area specific discharge (m/s)	2.3×10^{-7}

2.4 Simulation results

Figure 2.2 plots observed hydraulic heads versus simulated heads for the July 2012 data set. The overall fit was good, as data points showed a linear trend, the regression line having a slope of 1.01, and an R^2 value of 0.85 indicates small scatter. Close to the Wall and Curtain, the fit was acceptable. The regression line had a slope of 1.01; the R^2 value was lower with 0.67, indicating higher scatter from the regression line. However, the data still followed a linear trend and were scattered evenly above and below the 1:1-line, indicating that simulated heads generally corresponded with observed heads and that the simulation neither over- nor underestimated heads close to the Curtain, making the comparison reasonable. A reason for the poorer agreement close to the Curtain could be the representation of flow through the Curtain by 10 extraction wells. In the field, flow through the Wall and Curtain is not forced by pumping, but occurs along the hydraulic gradient. However, the closest representation of the system was achieved by including 10 extraction wells instead. Cones of depression were developed on the upgradient side of the wells in the simulation, which affected simulated heads and the comparison to observed heads in this area. Another factor that could affect the comparison of observed and simulated heads is the fact that hydraulic head measurements are snap shots in time, whereas the simulation represents average flow. The heterogeneity of the hydraulic conductivity distribution was simplified in the simulation, which could also affect the comparison of observed and simulated hydraulic heads.

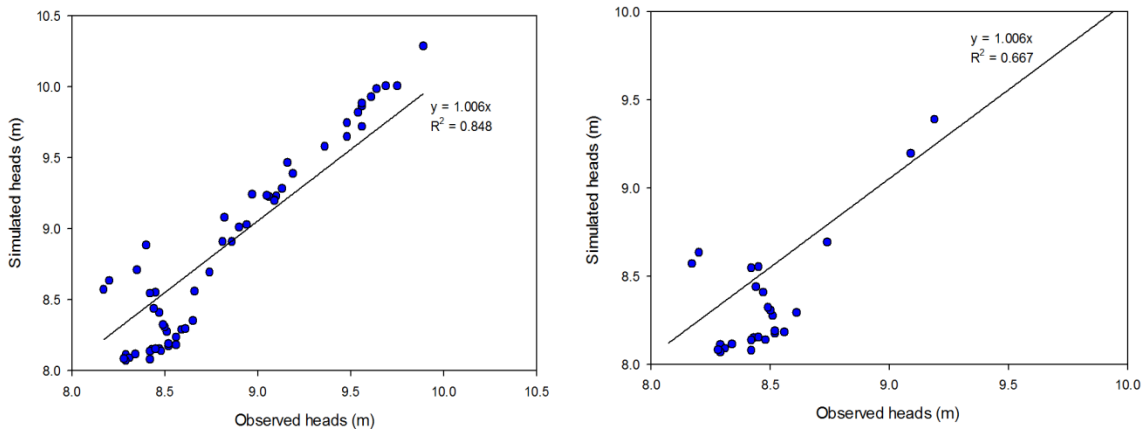

Figure 2.2: Comparison of observed and simulated heads of the numerical model. The left plot shows all observed heads compared to simulated heads, the plot on the right only shows locations close to the Wall and Curtain (< 10 m distance).

The simulated hydraulic gradient increased strongly on the upgradient side of the Wall and Curtain and decreased on the downgradient side of the system. Streamlines converged to the Curtain, with a zone of influence width of 100 m on the influent boundary. Figures 2.3 and 2.4 indicate that the upgradient drain intercepted shallow groundwater and drew deeper groundwater to shallower depths. Streamlines deep in the aquifer bent upwards near the Wall and Curtain, indicating that the Wall and Curtain intercepted groundwater flow in deep portions of the aquifer, where the plume is located, as intended by design and observed in the field from water-level measurements. The low head condition in the Wall and Curtain also prevented groundwater deep in the aquifer from passing beneath it through the gravel layer.

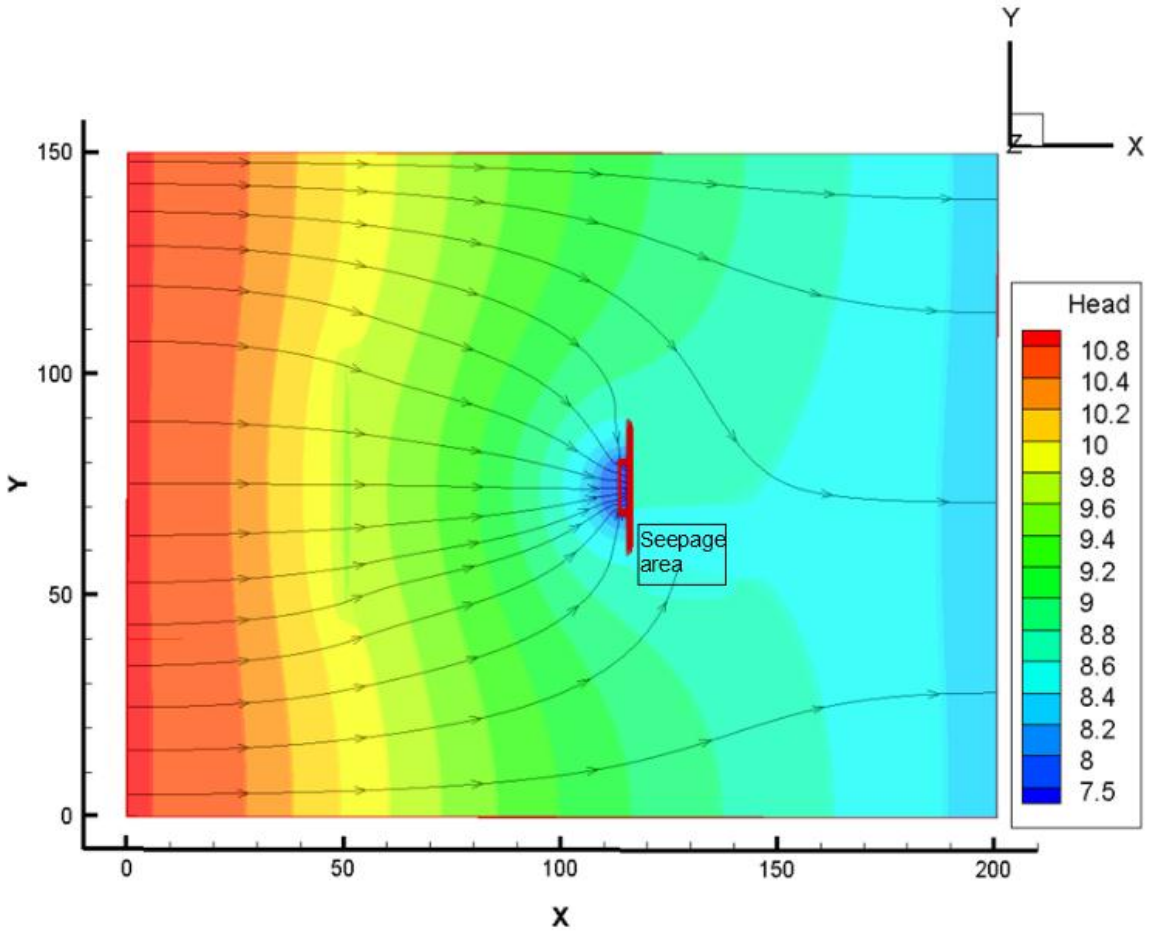

Figure 2.3: Hydraulic head distribution for the July 2012 simulation. The streamlines shown originate on the influent boundary at 5 m above bedrock. The horizontal drain is located at 51 m in the X-direction and from 46 m to 104 m in the Y-direction.

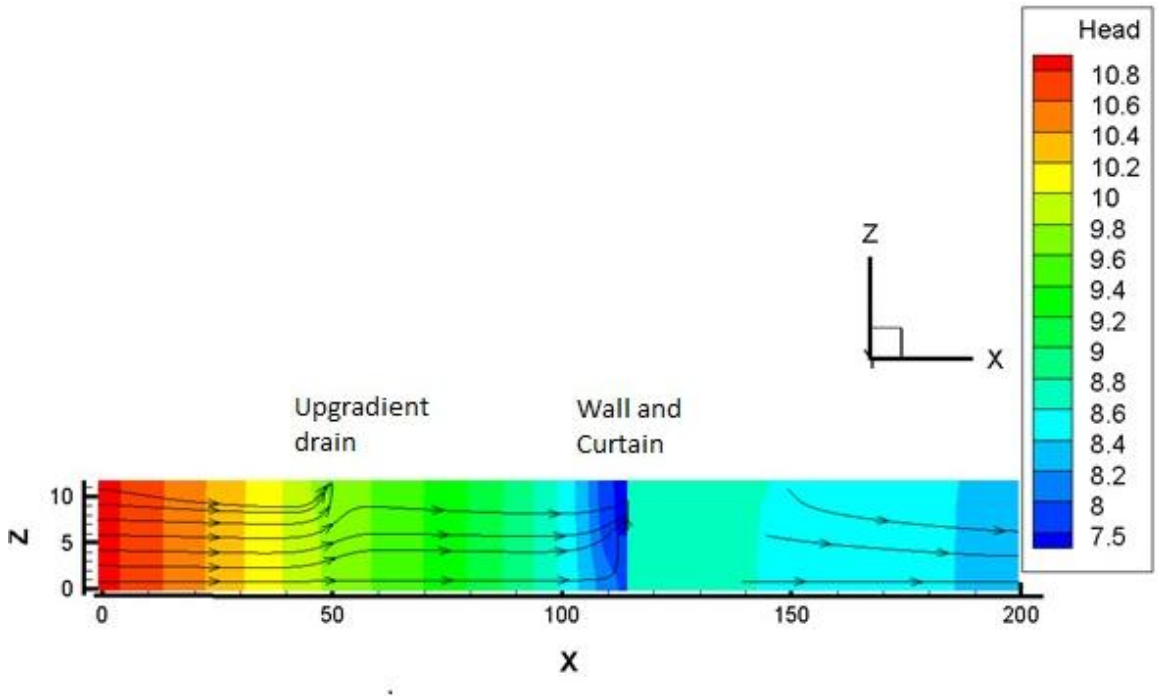

Figure 2.4: Cross section of the model along the centerline (y =75) of the domain.

Simulated groundwater velocities are compared with velocities calculated from field data (Table 2.2 and Figure 2.5). The simulated velocity (Vx) is the velocity in the direction of flow (x-direction), and is thus comparable to the average linear groundwater velocity determined through borehole-dilution tests and Darcy calculations with slug test K values. Simulated velocities were generally higher than velocities calculated from the field data, possibly due to the using average values of hydraulic conductivities and a uniform porosity of 0.38 (from Killey and Munch, 1987); however, some good matches were observed, especially at a depth of 4 m to 5 m (Figure 2.5). A point to point comparison with field data seemed unreasonable as the velocities determined through field tests themselves are not direct observations and can only be deemed estimates within a factor of ≥ 2. Thus, as simulated velocities followed the same trend as velocities determined through field tests overall, the incorporation of field data into the model seemed reasonable and acceptable to describe the system realistically.

Table 2.2: Comparison of groundwater velocity values determined through Borehole dilution, Darcy calculation with slug test K values, and as simulated by the numerical model.

Drive-point	Depth (m)	Vf from borehole dilution (m/s)	Vf from slug test and Darcy equation (m/s)	Vx from model (m/s)
DP-1	1.6		1.15×10^{-7}	7.24×10^{-7}
	2.5		1.68×10^{-7}	1.56×10^{-6}
	3.5	1.16×10^{-6}	8.34×10^{-7}	2.49×10^{-6}
	4.5	6.68×10^{-7}	3.04×10^{-7}	2.48×10^{-6}
	5.4	7.46×10^{-7}	8.68×10^{-7}	2.46×10^{-6}
	6.2		2.31×10^{-6}	2.32×10^{-6}
	7.1	5.11×10^{-7}	8.68×10^{-7}	1.86×10^{-6}
	8.1		1.04×10^{-6}	1.39×10^{-6}
	9.0	8.95×10^{-7}	1.74×10^{-7}	1.38×10^{-6}
DP-2	1.9	2.04×10^{-6}	4.20×10^{-7}	1.07×10^{-6}
	2.8	3.37×10^{-6}	1.81×10^{-7}	1.99×10^{-6}
	3.5	4.41×10^{-7}	5.69×10^{-7}	2.64×10^{-6}
	4.5	2.12×10^{-7}	3.08×10^{-7}	2.62×10^{-6}
	5.4	1.40×10^{-6}	1.02×10^{-6}	2.60×10^{-6}
	6.4	7.14×10^{-6}	1.21×10^{-6}	2.37×10^{-6}
	7.3	3.13×10^{-7}	1.03×10^{-7}	1.87×10^{-6}
	8.0	1.02×10^{-6}	1.74×10^{-7}	1.46×10^{-6}
	8.9	3.25×10^{-7}	3.66×10^{-7}	1.44×10^{-6}
DP-3	1.9	5.01×10^{-7}	3.43×10^{-7}	8.18×10^{-7}
	2.7	7.82×10^{-8}	2.07×10^{-7}	1.48×10^{-6}
	3.6	1.75×10^{-6}	4.60×10^{-7}	2.08×10^{-6}
	4.6	1.71×10^{-6}	1.10×10^{-6}	2.07×10^{-6}
	5.6	3.31×10^{-7}	1.72×10^{-6}	2.06×10^{-6}

	6.5	4.53×10^{-7}	8.60×10^{-7}	1.85×10^{-6}
	7.4	1.20×10^{-7}	5.82×10^{-7}	1.45×10^{-6}
	8.3	2.09×10^{-7}	2.74×10^{-7}	1.17×10^{-6}
	9.2	2.18×10^{-6}	5.51×10^{-7}	1.41×10^{-6}
DP-4	2.0	1.94×10^{-7}	1.80×10^{-7}	6.96×10^{-7}
	3.0	1.37×10^{-7}	1.85×10^{-7}	1.27×10^{-6}
	4.0	7.13×10^{-7}	1.25×10^{-6}	1.60×10^{-6}
	4.5	4.37×10^{-7}	1.63×10^{-6}	1.60×10^{-6}
	5.4	4.33×10^{-7}	1.74×10^{-7}	1.59×10^{-6}
	6.3	6.24×10^{-7}	7.12×10^{-7}	1.50×10^{-6}
	7.2	2.88×10^{-7}	2.20×10^{-7}	1.20×10^{-6}
	8.0	5.26×10^{-7}	1.06×10^{-6}	9.20×10^{-7}
	8.9	3.41×10^{-7}	5.47×10^{-7}	9.17×10^{-7}
DP-5	2.0	6.17×10^{-7}	1.82×10^{-7}	5.29×10^{-7}
	2.9	4.33×10^{-7}	3.55×10^{-7}	9.98×10^{-7}
	3.8	1.27×10^{-6}	1.33×10^{-6}	1.26×10^{-6}
	4.9	1.12×10^{-6}	9.94×10^{-7}	1.26×10^{-6}
	5.8	4.65×10^{-7}	3.77×10^{-7}	1.26×10^{-6}
	6.8	2.76×10^{-7}	6.69×10^{-7}	1.05×10^{-6}
	7.1	2.70×10^{-7}	5.69×10^{-7}	9.64×10^{-7}
	8.0	2.92×10^{-7}	2.03×10^{-7}	7.32×10^{-7}
	8.9	1.47×10^{-6}	1.01×10^{-6}	7.32×10^{-7}
DP-6	2.4	3.63×10^{-7}	3.74×10^{-7}	1.20×10^{-6}
	3.3	7.41×10^{-7}	2.42×10^{-7}	1.87×10^{-6}
	4.3	2.99×10^{-7}	1.01×10^{-6}	2.02×10^{-6}
	5.6	1.06×10^{-6}	6.99×10^{-7}	2.01×10^{-6}
	6.5	4.31×10^{-7}	5.12×10^{-7}	1.78×10^{-6}
	7.4	3.33×10^{-7}	1.42×10^{-6}	1.40×10^{-6}

	8.0	6.52×10^{-7}	2.64×10^{-7}	1.16×10^{-6}

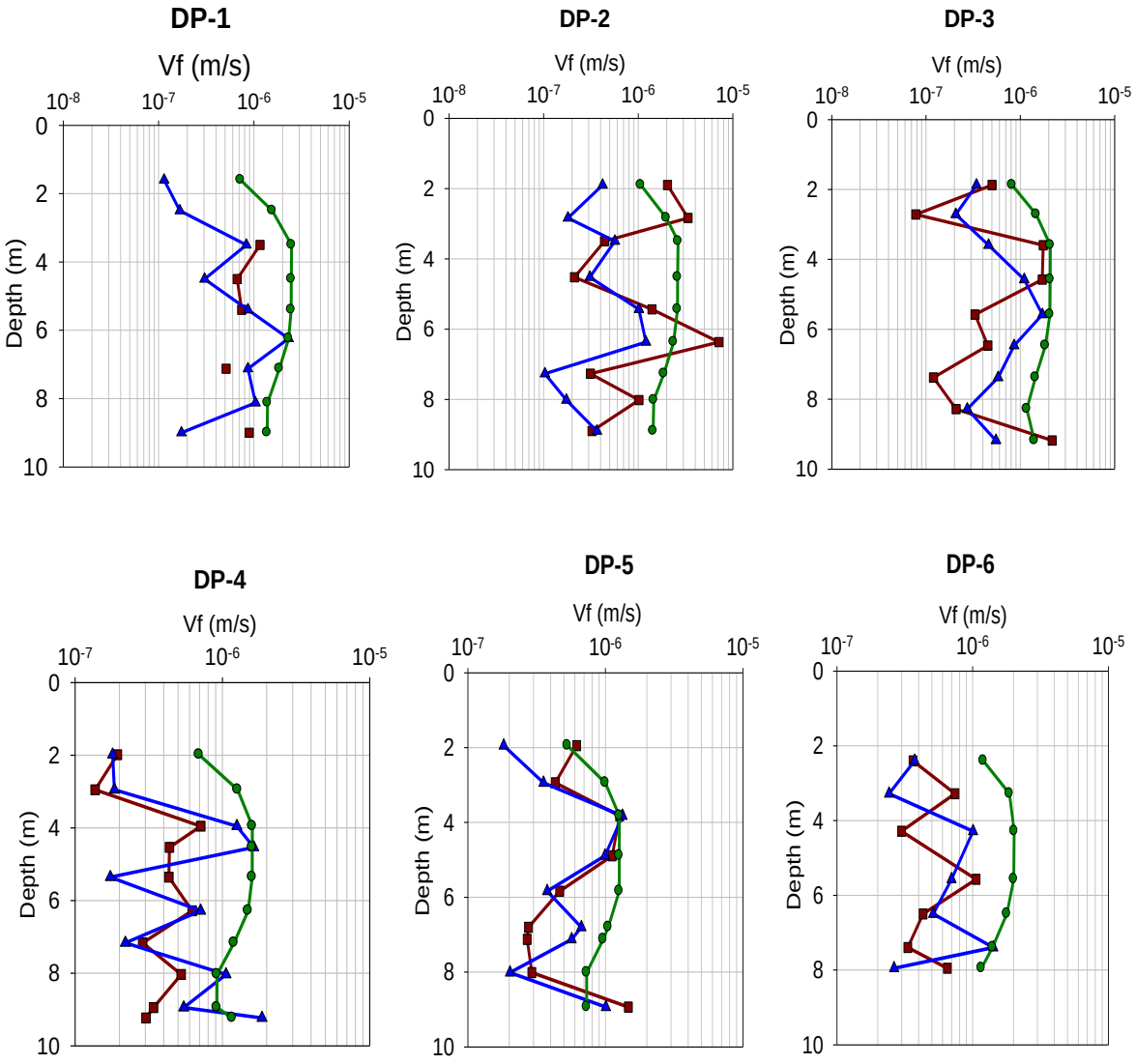

Figure 2.5: Comparison of groundwater velocities determined through borehole-dilution tests (red), calculated with the Darcy equation and slug tests (blue), and simulated by the numerical model (green) for the different drive-point locations.

2.5 Summary and Conclusion

The current study showed the possibilities and challenges of incorporating field data into a numerical model. A detailed field characterization of the Wall and Curtain site was performed in 2011-2012. Field data were used to set up a numerical flow model of the study site. The flow model was calibrated by comparing observed and simulated heads across the domain. The overall fit was good, with an R^2 value of 0.85and the data following a linear trend. The agreement between observed heads and simulated heads close to the Wall and Curtain had a lower R^2 of 0.67, which was acceptable as the data followed a linear trend and scattered equally above and below the 1:1 line. Possibly, the 10 extraction wells that represented the flow rate of the Wall and Curtain in the simulation affected the simulated heads in the proximity of the system. The simulation results indicate that the upgradient drain of the system intercepted shallow groundwater, whereas the Wall and Curtain intercepted deeper, contaminated groundwater, as intended by design. A comparison between simulated velocities and velocities determined through field tests showed that the model generally overestimated velocities. However, a significant number of good matches was observed and the simulated velocities followed the same trend as velocities determined from field data. Overall, the results from the simulation with incorporated field data indicate that the numerical model was describing the system accurately and realistically, especially considering the simplifications of the input data. The flow model will be used as a basis for future reactive transport simulations in order to estimate the longevity of the system.

Chapter 3
Geochemical characterization of the Wall and Curtain Site

3.1 Introduction

^{90}Sr is a mobile, radioactive isotope, which decays with a half-life of 28.8 years through β decay to ^{90}Y, another pure β emitter. ^{90}Y decays with a half-life of 64 hours into ^{90}Zr. ^{90}Sr can substitute for calcium in the bones, leading to increased risk of leukemia and other diseases (Pors Nielsen, 2004; O'Hara et al., 2009). After ^{90}Sr is released, it has the potential to be mobile and remains a major contaminant for around 10 half-lives (Wallace et al., 2012). Permeable reactive barriers (PRBs) are passive remediation systems that are installed along a contaminant plume flow path. A reactive material either promotes chemical reactions that lead to products that do not cause health concerns or adsorbs the contaminant. PRBs have been successfully implemented for the remediation of inorganic and organic contaminants, as well as radionuclides (e.g. Blowes et al., 2000). At the Atomic Energy of Canada Limited (AECL) Chalk River Laboratories, Chalk River, Ontario, a permeable reactive barrier system with adjustable outflow drains was installed in 1998 to remediate a ^{90}Sr plume. It is the first PRB system known to use clinoptilolite as a reactive material. Clinoptilolite is the most abundant member of the 48 minerals in the zeolite group, occurring frequently in the Earth's crust as part of zeolite-rich tuffs in sedimentary rocks (Dyer et al., 2006; Osmanlioglu, 2006). It consists of a SiO_4 tetrahedral honeycomb framework with consistent-diameter connecting channels that vary in size from 2.5 to 5 Å (Osmanlioglu, 2006) and exhibits a net negative surface charge. Clinoptilolite can be described by the formula $(Na, K)_6(Al_6Si_{30}O_{72}) \cdot 20H_2O$ (Palmer and Gunter, 2001); however, the exact composition and purity can vary widely even within the same deposit (Smiciklas et al., 2006). The high sorption capacity of clinoptilolite has caused interest in its use in the treatment of wastewaters containing radioactive nuclides and heavy metals (Pabalan and Bertetti, 1998). Several studies on sorption and ion exchange

onto clinoptilolite have been performed. Smiciklas et al. (2006) found that sorption of Sr^{2+} on clinoptilolite follows a Langmuir isotherm. Sorption is consistent between pH 2 and 10 and increases strongly at pH > 10. Due to the variability of the material, distribution coefficients (K_d) for Sr on clinoptilolite vary in studies from 90 mL/g (Smiciklas et al., 2006) to 1,200 mL/g to 5,500 mL/g (Elizondo et al., 1999). Calcium is expected to be the chief competitor for sorption sites with Sr due to its abundance and preference (Rabideau et al., 2005; Cantrell et al., 1994; Fuhrmann et al., 1995). Fuhrmann et al. (1995) predicted that clinoptilolite would work efficiently to adsorb Sr (K_d = 650 mL/g) with a calcium concentration of 120 mg/L as a competing cation in the groundwater. In these studies, Sr^{2+} is used as a substitute for ^{90}Sr as it does not cause health concerns. Rabideau et al. (2005), however, pointed out that the assumption of equal behaviour of ^{90}Sr and Sr^{2+} has not been tested, and only few studies exist that use ^{90}Sr in experiments. Wallace et al. (2012) observed that the sorption of ^{90}Sr onto sandy loam sediments increases strongly at pH between 4 and 6, and is highest between pH 6 and 8. ^{90}Sr sorption decreases with increasing ionic strength of the solution, in both Na- or Ca-bearing solutions (Wallace et al., 2012). The most important mechanism in the sorption of ^{90}Sr is ion exchange. Jackson and Inch (1989) studied a ^{90}Sr plume at the Chalk River Laboratories, Ontario, in a similar geological setting to this study. They found that ^{90}Sr transport is retarded, travelling at 3% of the groundwater velocity. A mean K_d of 10 mL/g for ^{90}Sr onto the sediment was determined, in which biotite is the phase with the strongest adsorption capacity. Leach tests of Jackson and Inch (1989) show that one third of ^{90}Sr is readily exchangeable with 0.1 M $MgCl_2$, and two thirds of the ^{90}Sr is specifically adsorbed onto Fe (III) and Mn (IV) oxyhydroxides. Jackson and Inch (1989) found that competition with stable Sr or Ca does not control the distribution coefficient, and that the specific surface area is the most important factor influencing ^{90}Sr sorption onto aquifer sediments.

The objective of this study was to characterize the pore-water chemistry across the permeable reactive barrier site at the Chalk River Laboratories and to determine the geochemical parameters and mechanisms of ^{90}Sr sorption onto the clinoptilolite. The results

will provide insight in the efficiency and longevity of the system, and will be used to construct a reactive transport model of ^{90}Sr migration at the site (Chapter 4).

3.2 Site description

The study site is located on the property of the AECL Chalk River Laboratories in Chalk River, Ontario, Canada, approximately 193 km northwest of Ottawa. In the early 1950s, concentrated ammonium nitrate solutions containing mixed fission products were stored in pits lined with crushed limestone. Portions of these solutions, which contained ^{90}Sr and tritium, leaked into the lower half of a predominantly sandy aquifer. The aquifer has a saturated thickness of 5 to 13m. The bedrock is overlain in many locations by glacial stony till. At some locations post-depositional fluvial action has washed the fine fraction from the stony till, resulting in the formation of a thin layer of gravel at the bottom of the aquifer. Fine to medium fluvial sands overlie the till or are in direct contact with the bedrock. These sands are overlain by fine sands and, in many locations, a silty very fine sand unit, which is considered to form the transition from fluvial to aeolian sediments (Killey and Munch, 1987). The aeolian deposits contain fine sands and interstratified sand and silt units. Hydraulic conductivity values on the site, determined through permeameter tests and grain size data, range from 3.5×10^{-6} m/s to 1.2×10^{-4} m/s (Killey and Munch, 1987). Groundwater velocities are estimated to range between 100 m/a to 150 m/a (Klukas and Moltyaner, 1995). Strontium transport is retarded due to geochemical interactions with the sand, resulting in a travel time of more than 40 years for ^{90}Sr to reach Duke Swamp, 440 m downgradient of the source area (Lee and Hartwig, 2005).

In 1998, a permeable reactive barrier system known as the Wall and Curtain (Fig. 1.1) was installed to prevent the ^{90}Sr plume to discharge into Duke Swamp. The system consists of a 30 m long sheet-piling wall (Waterloo Barrier®) which contacts the bedrock or till. An 11 m wide, 2 m thick and 6 m deep curtain of reactive material, granular clinoptilolite, is placed in front of the sheet-piling wall. Two wings of sheet-piling wall are installed on either side of the clinoptilolite, as well as a low-permeability plastic liner and bentonite-impregnated felt at

the bottom of the reactive cell. Ten vertical wells at the back of the cell, connected by a horizontal drain, collect the discharge of the reactive barrier system, which drains into a manhole. The height of the pipe and thus the hydraulic head of the system can be adjusted in the manhole. A second horizontal drain 60 m upgradient of the system intercepts shallow uncontaminated groundwater. By intercepting shallow groundwater, the upgradient drain prevents loading the reactive material with dissolved constituents other than ^{90}Sr, in turn prolonging the time to replacement of the groundwater system. The upgradient drain also discharges into the manhole and features an adjustable outflow height. This means that the system has the unique advantage to control the hydraulic gradient and the capture zone of the system. Another advantage is that the discharge of the system can be sampled and the discharge of the upgradient drain can be monitored for electrical conductivity, as the plume resides in the lower half of the aquifer, which is labelled with road salt.

3.3 Methods

3.3.1 Groundwater Characterization

Six 1.9 cm (¾ inch, nominal pipe diameter) drive-point piezometers were installed on site in a transect parallel to the sheet-piling of the Wall and Curtain system (see Figure 3.1). The screened, 15.24 cm (6 inches) long drive-points were connected to 1.52 m (5 feet) stainless steel pipe sections, which were connected by long shoulder couplings. The drive-points were driven into the ground with a handheld electric hammer. After reaching their maximum depth of 9 m, drive-point piezometers were pulled out of the ground using a truck jack with a crank and a chain.

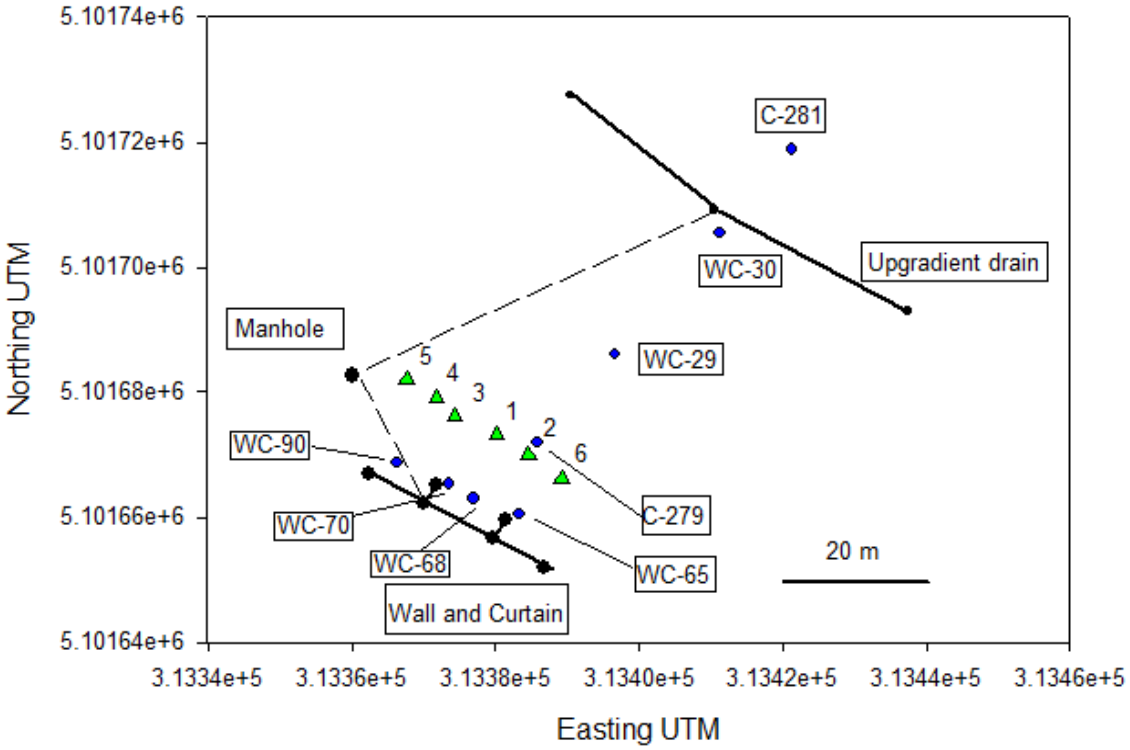

Figure 3.1: Site schematics with locations of Wall and Curtain sheet-piling wall, preinstalled wells sampled and the upgradient drain. Drive-point piezometers DP-1 to DP-6 are depicted by green triangles and numbered accordingly.

Pore-water samples were taken from each piezometer of selected pre-installed multi-level wells, as well as from drive-point piezometers (see Figure 3.1). Installed wells were purged of three well volumes prior to sampling. Measurements of Eh, pH and electrical conductivity (EC) were taken while purging the well until stable readings were observed. Samples for anion, cation and gross beta determinations were taken from each location, as well as separate samples for alkalinity titrations. Samples were filtered with 0.45 µm Waterra inline filters and cation and gross beta samples were acidified with concentrated nitric acid to a pH < 2. Alkalinity was determined in the laboratory as soon as possible, usually within 24 hours, with a Hach digital titrator using 0.16 N sulfuric acid. A similar sampling procedure was used for the drive-point piezometers; with the only difference that little purging was necessary before stable readings of *in situ* measurements were observed. In the drive-point

piezometers, samples were first collected at 1 m intervals, starting at 1 m below the water table, to a depth of 4.5 m. At depths > 4.5 m, the sampling interval was decreased to 30.48 cm (1 foot) in order to delineate the ^{90}Sr plume in an accurate and detailed way. The samples were collected through an inflated packer to ensure that the sample was taken from the 15.24 cm (6 inch) long interval of the drive-point isolated from the shallower aquifer.

Cations and anions were analysed by inductively coupled plasma atomic emission spectroscopy (ICP-AES) and ion chromatography (IC), respectively. Samples taken for gross beta measurements were dripped and evaporated on previously-weighed planchettes. The residual mass on the planchettes as well as the dripped mass from the bottle were recorded. The solids were fixed on the planchettes using a few drops of a 10% Collodion – 90% acetone mixture. Collodion (Fisher Scientific) is a solution of nitrocellulose in ether and alcohol. The air-dried planchettes were counted for 30 min each in an OXFORD Tennelec Series 5 XLB beta counter.

3.3.2 Characterization of reactive material

3.3.2.1 Column test

A column containing 5 volume % 14 x 50 mesh clinoptilolite and 95 volume % silica sand was set up at the University of Waterloo in 2010 (Yung, 2010). The column experiment has still been running, and because of the relevancy of the experiment the interpretation of the data was incorporated into this study. The solution pumped through the column was similar in composition to the groundwater composition at the Wall and Curtain site, substituting for ^{90}Sr with stable Sr (Table 3.1). In the experiment, a control column containing 100% 20 x 30 mesh silica sand was also run, which showed complete breakthrough of Sr within 10 days. Flow through both columns was maintained at 331.2 mL/day, which was approximately one pore volume per day.

Table 3.1: Simulated groundwater composition in column experiment.

Component	Concentration (mg/L)
Ca^{2+}	7.24
Mg^{2+}	1.82
Sr^{2+}	0.111
Na^{+}	23.6
Cl^{-}	47.1
CO_3^{2-}	1.92
SO_4^{2-}	7.19

The 5% clinoptilolite column was sampled for cations and anions, as well as for measurements of pH, Eh and alkalinity.

3.3.2.2 Solid samples from the PRB

Solid samples of the reactive material were collected from locations in the Wall and Curtain shown in Figure 3.2. A hole was dug through approximately 35 cm of overburden to the top of the reactive material. A 6 m long, 0.95 cm (3/8 inch) inside diameter (ID) stainless steel pipe, kept upright by attaching it to a wooden pole that was tied down, was used for sample collection. The bottom end of the pipe was plugged with a plastic tip with flap sides so it would stay on the pipe and prevent entry of solids when pushed down, and be left in the ground when the pipe was pulled up. The pipe was then filled with water to prevent the entry of solids while manually pushing it to a depth of 5.5 m. A 6 m long 0.79 cm (5/16 inch) outer diameter (OD) and 0.48 cm (3/16 inch) ID polyethylene tube perforated with 0.24 cm (3/32 inch) diameter holes, was inserted through the pipe. The perforated tip of the tube was 10 cm long, of which 4 cm of the lower end were wrapped with a Nitex (Sefar America Inc.) mesh (236 micron) screen attached with hot glue, which was also used to plug the end of the tube. The pipe was then lifted out of the clinoptilolite while holding the sampling tube in place.

Pore-water samples (500 mL), containing small amounts of sediment, were pumped out of the sampling tube at vertical intervals of 5 cm to 10cm, at the leading edge of the Sr plume. The samples were checked for radiation with a pancake style Geiger-Mueller detector in the field. Between sampling points, the grains in the tube were flushed out before the tube was lifted to the next depth.

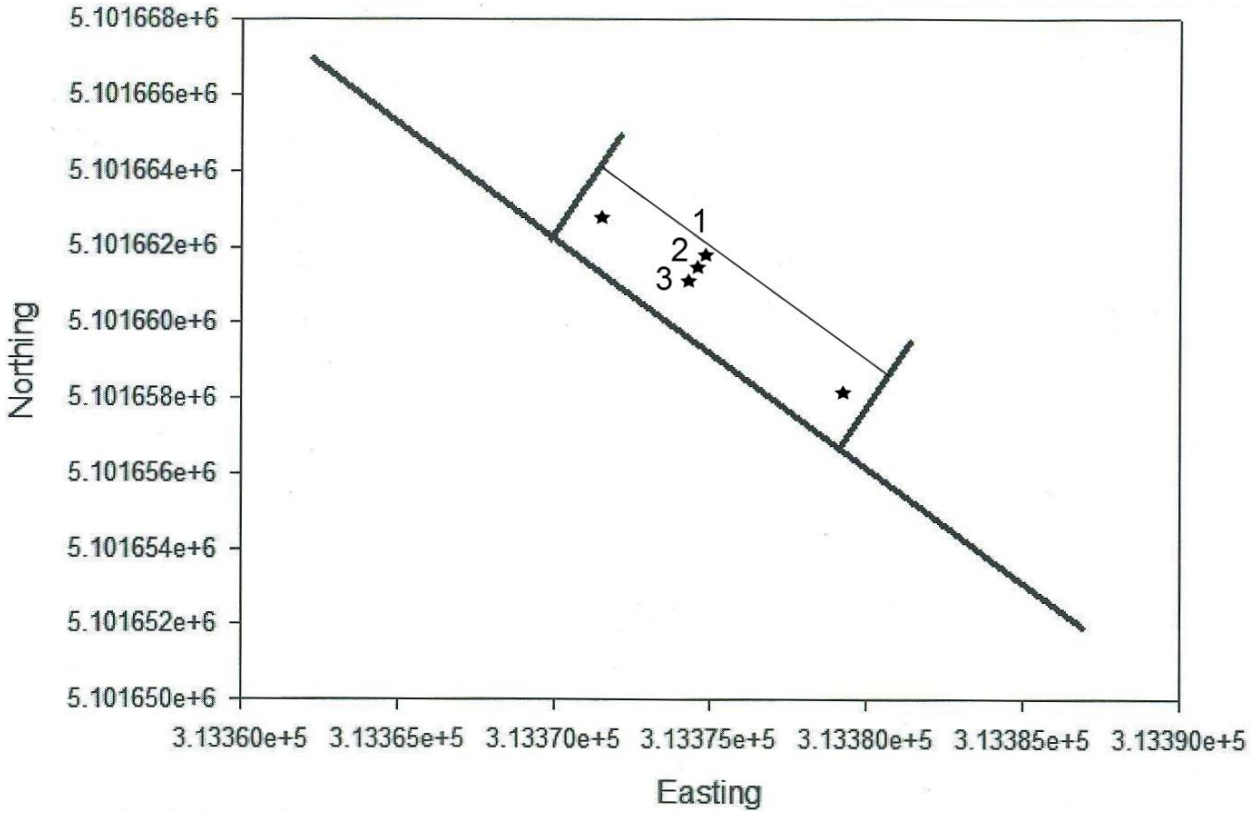

Figure 3.2: Solid sampling locations in the clinoptilolite.

After collection, the samples were stored until the suspended solids had settled, then filtered by vacuum filtration. The filtrate was acidified and analyzed to determine gross beta activity levels and cation concentrations. The solids were oven-dried at 40°C and counted for gross beta activity. Two batches of experiments were set up at the Chalk River Laboratories, 24 hr sequential extractions on samples collected from a profile taken from the leading edge of the plume (location 2) and a time to equilibrium study on combined

radioactive samples from a profile over 1.8 m in location 1. The time to equilibrium study was conducted to determine if kinetics play an important role in the sorption/desorption of beta activity and cations onto clinoptilolite. The dry sample weight was approximately 1 g; the solution volume to solid mass ratio was 20:1 (20 mL water to 1 g solids). Extractions were performed sequentially with four solutions, namely deionized (DI) water, 1 M KCl, a 0.1M acetic acid/sodium acetate solution and 0.5 M nitric acid. Samples were agitated on a rotary mixer at 20 rpm, which was considered low enough for the fine particles to prevent crushing and grinding of the solid material.

To analyze the stable Sr on the clinoptilolite, piston cores of 0.5 m depth were taken in the shallow, uncontaminated clinoptilolite and the Winter Sand, which is placed in front of the clinoptilolite, at the eastern end of the Curtain. These samples were also counted for gross beta and showed no contamination. Extractions with a contact time of 24 hours and a setting of 5.5 rpm on the rotary mixer were conducted on these samples at the University of Waterloo.

3.4 Results and Discussion

3.4.1 Results of pore-water samples

Detailed geochemistry profiles for each well and drive-point are provided in Appendix A. Samples were taken over the course of two years, and are representative only of the specific date they were collected; however, some general trends could be well identified across the site. The pH was relatively uniform across site and with depth, ranging between 5 and 6. A slight decrease within the ^{90}Sr plume was observed in some locations. The redox potential, measured through the Eh, decreased with depth, probably due to increased isolation from atmospheric oxygen, oxygen consumption along the flow path and the reduced conditions in the lakebed of Lake 233, the recharge area of the lower aquifer. The alkalinity was low across site, generally being less than 40 mg/L as $CaCO_3$. It often increased with depth, but remained below 100 mg/L as $CaCO_3$. The electrical conductivity (EC) increased with depth, reaching values of $\geq$ 100 μS/cm at depths $\geq$ 6 m. At many locations, a strong increase in EC

was observed at depths of 7 m to 8 m, which coincided with the location of the plume. The higher EC at depth was in agreement with the findings of Killey and Munch (1987) that the recharge area of the deeper portion of the aquifer was more distant than the one of the shallow aquifer and transverse vertical dispersion was low along the groundwater flow path.

Chloride was the most prominent anion in the aquifer; Cl concentrations increased strongly with depth. High Cl concentrations in the lower half of the aquifer were in agreement with the reported presence of a road-salt label. The maximum Cl concentration on site was found in drive-point piezometer DP-5 with 155 mg/L at a depth of 8.3 m. Sulfate concentrations fluctuated across site and with depth between 2 mg/L and 9 mg/L. The highest sulfate concentration was 15 mg/L, measured in WC-65 at a depth of 5 m. Nitrate concentrations were low across site, with maximum values of 3 mg/L, often showing a peak concentration in shallow depths ($\leq$ 6 m). Only small amounts of fluoride were present across site, which consequently was not considered to have an influence in the geochemistry of the aquifer.

Sodium was the most prominent cation across site, with concentrations of up to 53 mg/L. A strong increase with depth was associated with the road-salt label in the lower half of the aquifer. In wells WC-65 to WC-90, i.e. close to the Wall and Curtain, a peak concentration at depths of 8 m was observed, directly coinciding with the ^{90}Sr plume. The outflow of the Wall and Curtain showed a Na concentration of 17 mg/L. This concentration was within the range of concentrations found on site, so no conclusion of the fate of Na in the Curtain can be drawn from this sample. Sodium concentrations from the upgradient drain and the sample from the weir were typical of shallow and deep groundwater on site, respectively. Calcium concentrations were around 10 mg/L across site. Some increase with depth was observed. Calcium concentrations were substantially higher in wells WC-68 and WC-70 directly in front of the Wall and Curtain, reaching values of 43 mg/L. The Ca concentration in the outflow of the upgradient drain was 4.1 mg/L, reflecting shallow groundwater. Calcium concentrations from the weir downgradient of the Wall and Curtain and the outflow of the Wall and Curtain were 10 mg/L and 5.9 mg/L, respectively. The Ca concentration in the weir reflected deeper groundwater. The Ca concentration from the outflow of the Wall and Curtain was lower than typical Ca concentrations in deeper groundwater, which could

indicate that Ca was taken up by the clinoptilolite. Potassium concentrations were low across site and variable with depth, in some locations showing a small peak between depths of 7 m and 9 m. The K concentration in the outflow of the Wall and Curtain was the highest one found on site. This observation indicates that Potassium was released from the clinoptilolite during ion exchange. Magnesium concentrations were low across site (≤ 3 mg/L), and increased with depth. The outflow of the upgradient drain and the sample from the weir showed Mg concentrations typical for shallow and deep groundwater, respectively. Barium concentrations increased with depth, showing a peak concentration of 0.11 mg/L at depths of 8 m to 9 m on either side of the Curtain (WC-65 and WC-90), and a peak at depths of 6 m to 7 m directly upgradient of the Curtain (WC-68 and WC-70). Barium concentrations in the outflow of the upgradient drain and the weir were consistent with groundwater concentrations. The mean Ba concentration in the outflow of the Wall and Curtain (0.0037 mg/L) was substantially lower than anywhere else on site, indicating that Ba adsorbed onto the clinoptilolite. Iron and Mn concentrations were not detectable or very low in the shallow part of the aquifer. Manganese concentrations began to increase at depths ≥ 6 m, reaching maximum concentrations 1.2 mg/L at depths of 10 m. Manganese concentrations from the outflows of the upgradient drain and the Wall and Curtain were 0.11 mg/L and 0.16 mg/L, respectively, reflecting shallow groundwater and some possible sorption of Mn onto the clinoptilolite. The Mn concentration in the sample from the weir (0.36 mg/L) reflected deeper groundwater. Iron concentrations started increasing at depths ≥ 7 m. The maximum Fe concentration was found in drive-point piezometer DP-1 with 22.2 mg/L at a depth of 9.6 m. The outflow of the upgradient drain showed a high Fe concentration of 3.6 mg/L, and Fe oxides clogged the drain. The Fe concentration in the outflow of the Wall and Curtain was low compared to deeper groundwater, which could indicate that some ferrous iron adsorbs onto the clinoptilolite. Strontium concentrations were low across site (0.02 mg/L to 0.05 mg/L) and variable with depth. Some increase of Sr concentrations with depth was observed, especially in wells close to the Wall and Curtain (WC-65 to WC-90), as well as a peak at a depth of 8 m (0.08 mg/L to 0.22 mg/L). The outflow of the upgradient drain and the sample from the weir showed Sr concentrations of 0.043 mg/L and 0.11 mg/L, respectively,

indicating again that the upgradient drain intercepted shallow groundwater, whereas some deeper groundwater was discharged into the swamp downgradient of the system. The outflow of the Wall and Curtain showed the lowest Sr concentration on site (0.0048 mg/L), which indicates that Sr was retained on the clinoptilolite. Silica concentrations varied across site and with depth between 5 mg/L and 10 mg/L, which was expected to be the result of equilibration between the silica sand and groundwater. In some locations, trace amounts of Zn were detected. Charge balance errors were calculated for each sample, and were for the majority of samples ≤ 5%or ranged between 5% and 10%. Larger errors were only found in a small number of samples.

The plume location was determined through gross beta measurements. The samples taken in small vertical intervals in the drive-point piezometers helped to determine the plume location precisely with depth. Gross beta measurements showed a clear peak at depths of 6.24 m to 8.40 m, with the highest beta activity of 3,506 Bq/L in DP-1 at a depth of 7.44 m. Along the groundwater flow path, gross beta activities peaked in C-281, WC-30 and WC-29 at the same depth below the water table as DP-1, but showed a shallower peak in WC-68 close to the Wall and Curtain. This indicates that deeper groundwater was drawn upward close to the Wall and Curtain, which ensured the effective treatment of the contaminant plume.

In wells upgradient of the system, beta activities were highest in WC-29, ca. 30 m upgradient of the Wall and Curtain, but decreased with further distance in WC-30 (1,550 Bq/L) and C-281 (676 Bq/L). It is important to note that beta activities were higher west of the system than east of it. In DP-6 and WC-65, only low beta activities (≤ 1.9 Bq/L) were detected. In WC-90 and DP-4, beta activities were substantially higher with a maximum of 541 Bq/L. This could indicate the bypass of the system by a second, smaller plume. However, beta activity at the weir was low (1.50Bq/L). The outflow of the Wall and Curtain and the upgradient drain showed low beta activities of 2.58 Bq/L and 12.6 Bq/L, respectively. The result of the sample from the Wall and Curtain indicates that the system effectively removes radioactive ^{90}Sr from the groundwater. The sample from the upgradient drain showed a beta activity that exceeded the drinking water guideline of 5 Bq/L; however,

other samples collected from the upgradient drain during continuous monitoring of the upgradient drain showed beta activities that meet the drinking water guideline. Thus, the high beta activity in this sample might be due to faulty sample analysis or accumulation of beta activity on the precipitated ferrioxyhydroxides in the drain, which were then flushed out. The results from the upgradient drain indicate that it generally intercepted shallow groundwater, but will have to be continued to be monitored to ensure that the beta activity of the effluent does not increase.

From average beta activities from wells WC-65, WC-68 and WC-70, which are located directly in front of the clinoptilolite, an average advective mass flux was calculated by:

$$\overline{J_A} = \overline{q_A}\bar{C},$$

Where q_A is the average advective flow. Using an average flow rate of 0.35 L/s of the system and an average beta activity of 38.76 Bq/L, the mass flux of the system was 0.21 Bq/m^2s or 17,749 Bq/m^2dayacross the cross section of the Wall and Curtain perpendicular to the groundwater flow direction. As the outflow showed no contamination, the system was highly efficient in remediating a large amount of beta activity.

3.4.2 Results of column experiment

Cation profiles through the column after nearly 2 years (670 days indicate that Sr had accumulated in the first few centimeters of the column, but only reached a concentration of 0.5 C/C_0 at a distance of 7 cm, indicating that it was still far from breakthrough (Figure 3.3). Dissolved Ca and Na had reached equilibrium with the solid phase and showed complete breakthrough. Dissolved K concentrations showed a strong increase with distance, indicating that it was released from the clinoptilolite in the ion exchange process. Silica concentrations showed a slight increase with distance, which was not surprising as the silica sand was expected to equilibrate with the input solution. Manganese showed a stronger increase with distance, indicating that it was released from silica sand surfaces during ion exchange. An increase in dissolved Li over the profile indicates that it was also released in the ion exchange

process, probably from the smectite portion of the clinoptilolite material. The distribution coefficient K_d was calculated to be 1215 mL/g for the reactive column overall by comparing Sr transport to Cl breakthrough in the column; the overall retardation factor R being 4594. The distribution coefficient was calculated though the retardation equation

$$R = 1 + \frac{\theta}{\rho_b} K_d,$$

where θ is the effective porosity and ρ_b is the bulk density of the material. The Retardation factor R was determined by dividing the water velocity by the velocity of the retarded constituent:

$$R = \frac{v_w}{v_R}$$

By comparing the transport velocity of Sr in the reactive column containing 5% clinoptilolite and the transport velocity of Sr in the control column, a retardation factor of 2709 was calculated. Assuming that this retardation was only due to sorption of Sr on the clinoptilolite, a distribution coefficient for Sr on clinoptilolite was determined by only incorporating the bulk density and porosity of clinoptilolite into the retardation equation. Using 0.8 g/cm^3 as a bulk density and 0.4 as a porosity for clinoptilolite (see Rabideau et al., 2005), the K_d was calculated to be 1354 mL/g. The equations above assume a linear isotherm and that no ion exchange along the flow path occurs, which would be inapplicable in this case, as results indicated that ion exchange was occurring. However, Jackson et al (1980) found that the distribution coefficient value for ^{90}Sr on aquifer sands determined through the retardation equation was in agreement with values determined through analyses of contaminated sediments and pore-waters (Jackson et al., 1980), making the retardation equation applicable.

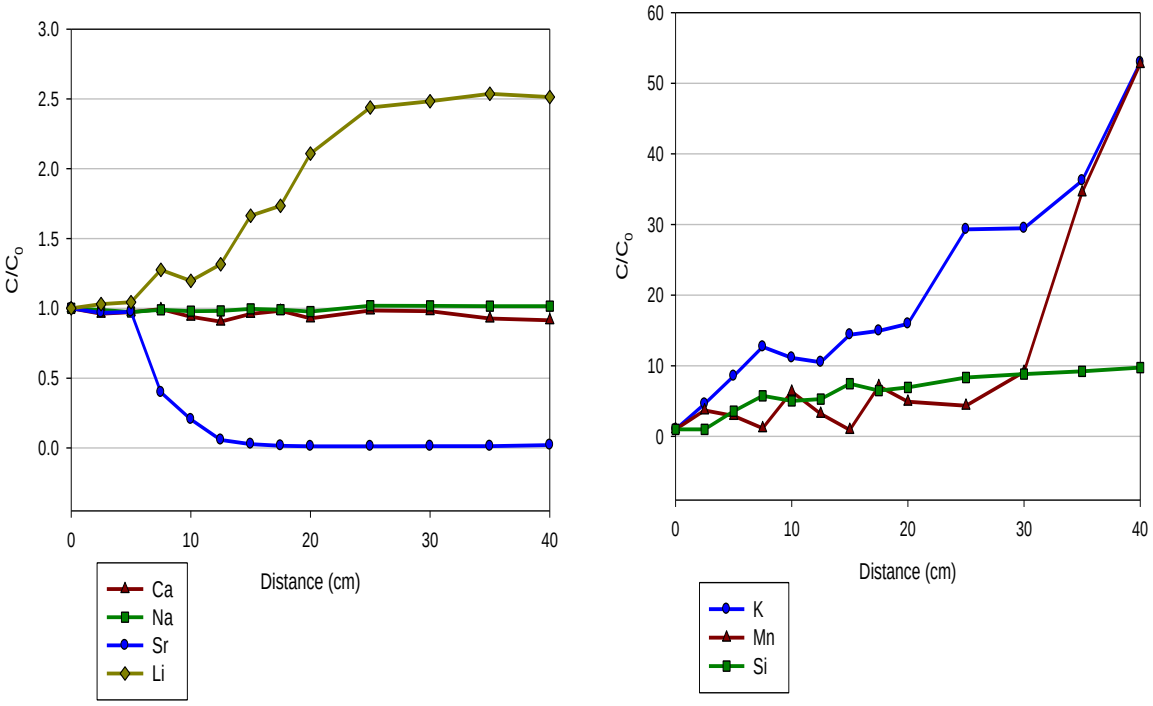

Figure 3.3: Cation profiles of the column tests after 670 days.

3.4.3 Solid samples and *in situ* distribution coefficient

Profiles of the gross beta activity of solid sampling locations 1 and 2 at the Curtain can be seen in Figure 3.4. A clear peak is visible at a depth of 4.4 m in both locations, with a higher activity in the location further upgradient. It is important to note that no elevated counts per minute were observed in other samples taken from the clinoptilolite, e.g. from location 3, which is 42 cm downgradient of location 2. A gross beta determination on a sample from location 3 at 4.5 m only showed background beta activity. Pore-water samples collected together with the solids were analyzed for gross beta to determine an *in situ* distribution coefficient for ^{90}Sr on clinoptilolite, which is shown in Figure 3.5. The sorption isotherm was linear, showing a very good fit to the linear regression line. One sample point (red in Figure 3.5) was excluded from this plot to improve the regression fit. The K_d from *in situ* sampling was determined to be 76,159 mL/g, which is more than an order of magnitude greater than

the one calculated from the results of the column experiment. One reason for this discrepancy is a bias for small grain sizes in the sampling method. Only small masses of grains were desired from sampling due to health and safety reasons when handling radioactive material. The dominant grain size of the collected solid samples was silt, which has a higher sorption capacity than larger grains due to the increased surface area.

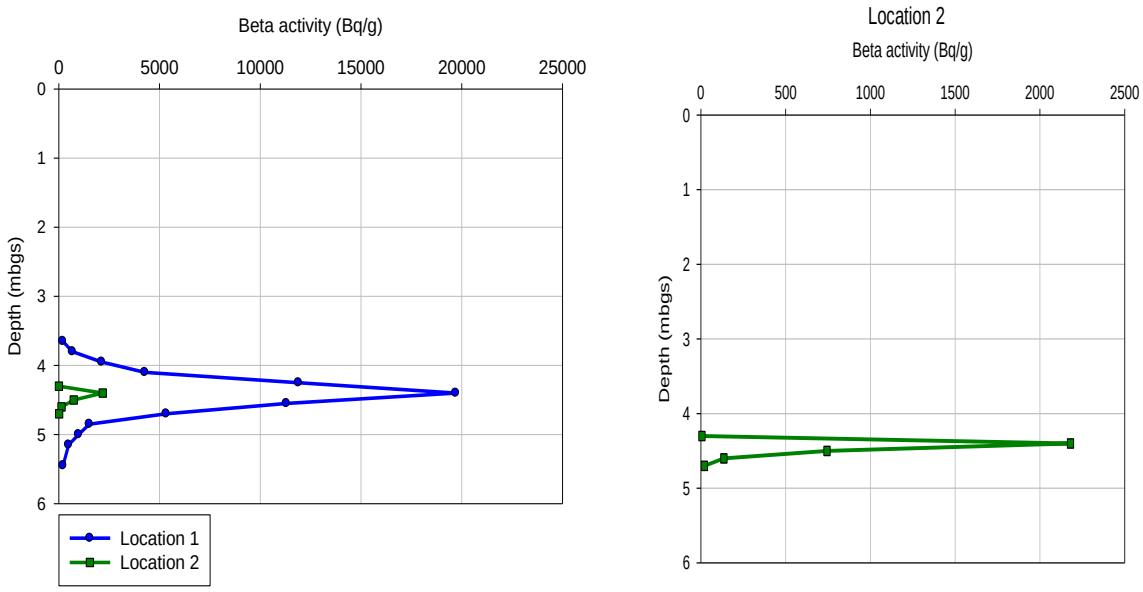

Figure 3.4: Beta activity profiles of solid sampling location 1 and 2 (magnification on the right) in the clinoptilolite.

As adsorbed cation concentrations were not determined prior to the leach test due to small sampling sizes, no K_d can be determined from the cation results of the liquid samples. However, differences between dissolved concentrations close to the reactive material and in the aquifer were compared. Calcium concentrations in the clinoptilolite ranged between 5 and 13 mg/L, reflecting deeper groundwater concentrations, although not reaching maximum concentrations that were present in the aquifer. This could indicate that Ca was taken up by the clinoptilolite. Barium concentrations from pore-water samples in the clinoptilolite were one order of magnitude lower than in the aquifer. As Ba has a small hydrated radius, it is

expected to be preferentially adsorbed onto the clinoptilolite compared to other divalent ions (Stumm and Morgan, 1996). The substantially lower dissolved concentrations in the clinoptilolite were consistent with this observation. Dissolved Sr concentrations in the clinoptilolite ranged from 0.0035 mg/L to 0.0850 mg/L, which was lower than in the aquifer. Strontium concentrations at location 1 were higher than at location 2; higher Sr concentrations in the pore-water coincided with higher beta activity of the solid sample. These findings suggest that Sr was still being adsorbed on the clinoptilolite at location 2, reflected by lower dissolved Sr concentrations than in the aquifer. At location 1, higher dissolved Sr concentrations were similar to aquifer concentrations, indicating that the clinoptilolite had already reached the maximum sorption capacity with respect to Sr and that adsorbed and dissolved Sr are in equilibrium. Strontium was the only ion for which a good fit to a sorption isotherm was observed when using the total amount leached as an estimate for the sorbed concentration. The isotherm (see Figure 3.5, right) was linear, with a K_d of 426.66 L/g.

Some Fe might have been adsorbed to the clinoptilolite, as dissolved Fe concentrations from pore-water samples in the reactive material were as low as in the shallow aquifer. Other cations were at concentrations that were similar to the concentrations from deeper groundwater in the aquifer.

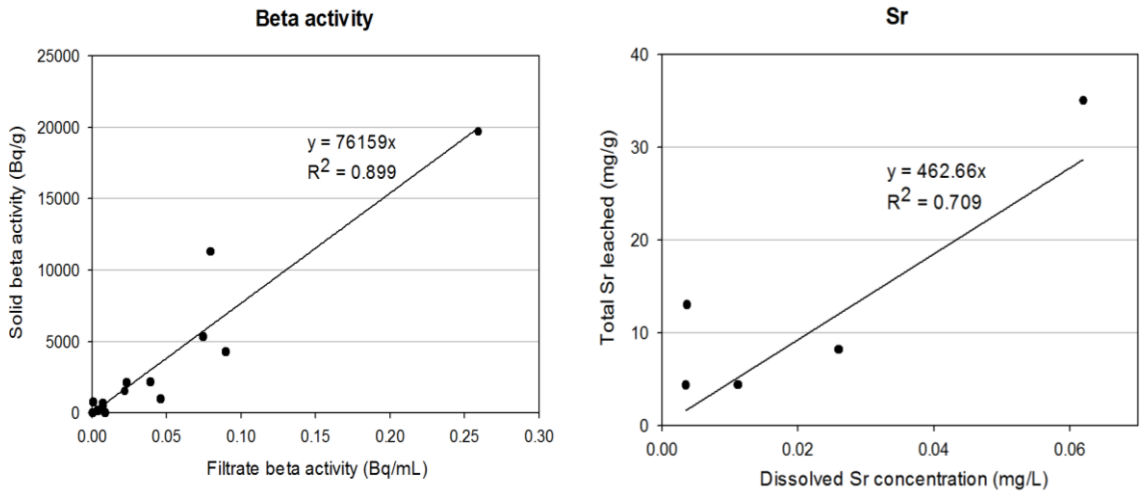

Figure 3.5: Sorption isotherms for beta activity (left) and Sr (right), including a best fit for the data.

3.4.4 Leach tests

During the leach tests, solid and liquid samples were measured with a pancake style Geiger-Mueller (GM) detector, which gives a gross measure of beta and gamma radiation in counts per minute, during the leach tests, and were counted for beta activity after the leach test. A calibration between counts per minute and beta activity could be established from these measurements (see Figure 3.6). As water shields beta activity much more efficiently than air, the calibration was different for liquid and solid samples, but behaved linearly in both cases. For solid samples, the linear regression line was y = 0.26x -54.84. The fit was very good with the data plotting linearly and an R^2 value of 0. 972. Only one sample did not fall on the line and was left out in the calibration (see Figure 3.6). For liquid samples, the linear regression line was y = 136.2x – 10526, the fit also being good with the data following a linear trend and an R^2 value of 0.919. This calibration assists in estimating the beta activity from *in situ* GM radiation readings to be made in the future. For application in the field, the calculation can be simplified by setting the intercept of the regression line to 0. For the solid samples, the equation then becomes y = 0.26x, and still showed a good fit to the data with the data still plotting linearly and an R^2 value of 0.968. For liquid samples, the slope of the linear

regression line with an intercept at 0 was 136.2, the R^2 value being slightly lower, but still good, with 0.852 and the data still following a linear trend.

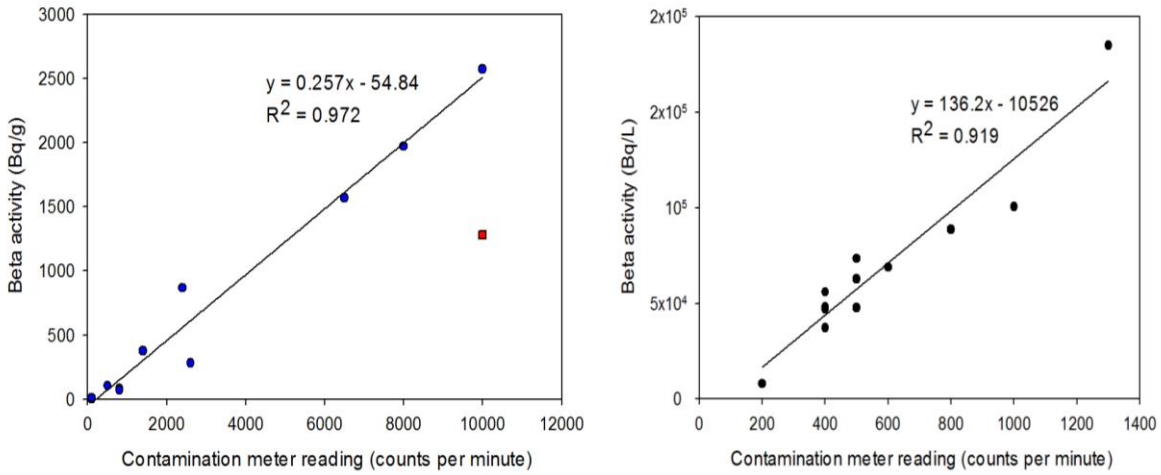

Figure 3.6: Calibration of contamination meter readings and beta activity measurements for solid samples (left) and liquid samples (right). On the left in red the only sample that did not show a good fit to the regression line.

The results of the extraction experiments are shown in Figure 3.7, using gross beta activity as a proxy for the ^{90}Sr concentration on the clinoptilolite. Gross beta activity was strongly retained on the material, with 17% of the initial amount still remaining after the extraction experiments. DI extracted very little gross beta activity from the clinoptilolite, leaching less than 1 % of the beta activity and less than 0.5% of the total leached cation concentration for all cations considered. The 1 M KCl solution was the most efficient solution used in leaching beta activity and cations from the clinoptilolite, indicating that ion exchange was the major mechanism for sorption and desorption of ^{90}Sr on clinoptilolite. The process was clearly kinetically controlled, as the percent leached increased over time. From the cation results, a preference of exchangeable ions was observed. The proportions of Ba and Sr desorbed were highest (92 % and 93% after 10 days, respectively), followed by Mn (82 % after 10 days) and Ca (80 % after 10 days). These findings indicate that equilibrium had not yet been reached after a contact time of 10 days, although a decrease in the slope of the graphs can be

observed (see Figure 3.8). It is important to note that the percentage of leached beta activity in Figure 3.8 did not correspond to the percentage of leached Sr, as only total Sr concentrations were determined

Interestingly, Mg desorption due to ion exchange did not seem to be kinetically controlled, the percentage leached ranging from 66 % to 75% overall.

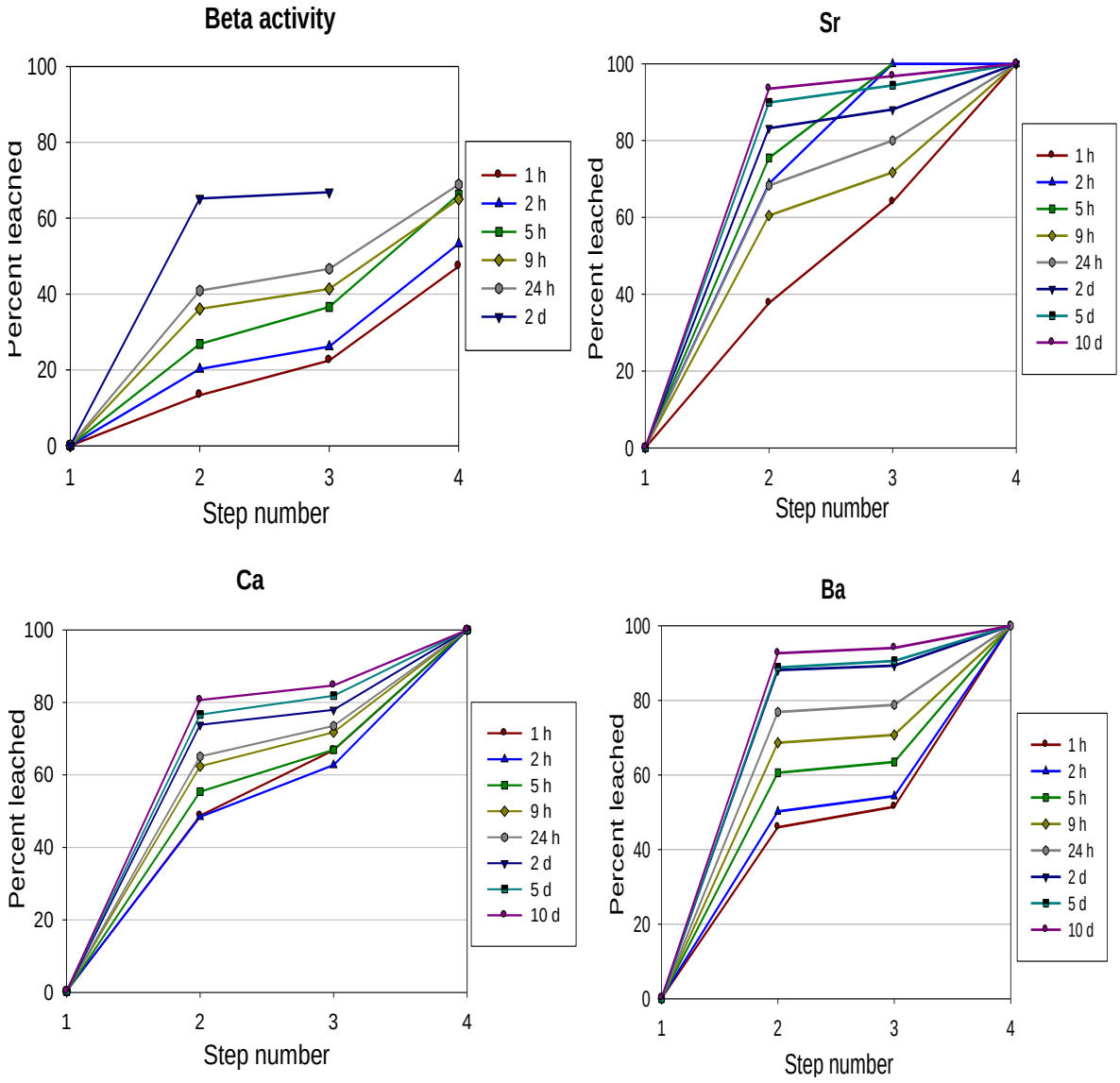

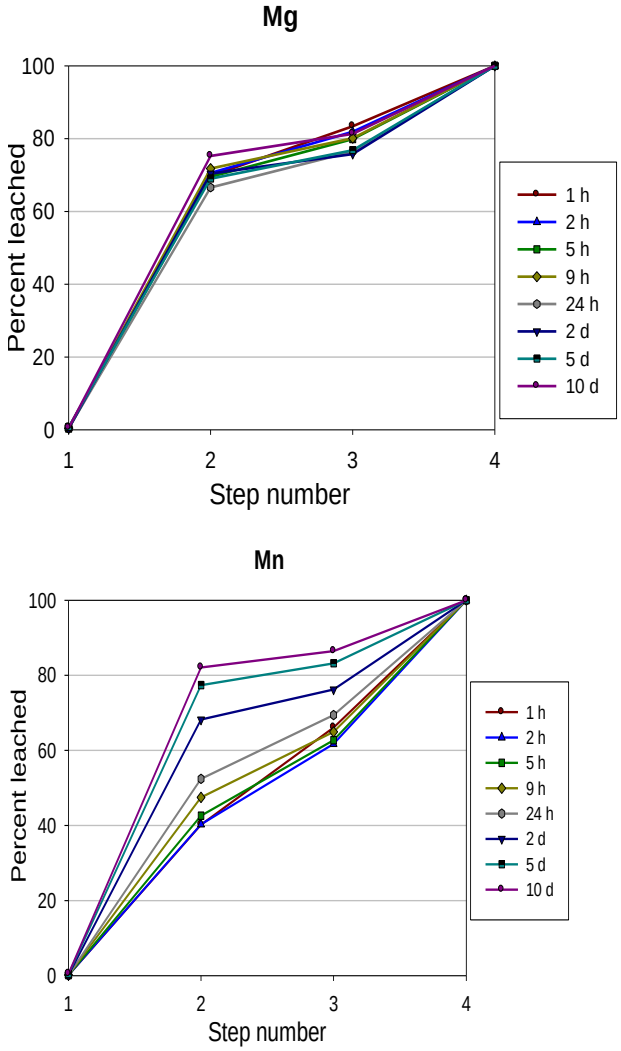

Figure 3.7: Accumulative percentage of gross beta and cations leached off the clinoptilolite in the different extraction steps for the time to equilibrium study.

The 0.1 M acetic acid/Na acetate solution was not quite as effective as KCl, but still leached off an additional 4% to 10% of the initial gross beta and 1% to 20% of the total leached cation concentration from the clinoptilolite. Both, the percentage leached and the pH, seemed to be independent from the contact time, which indicates that equilibrium was reached rapidly. The same was observed with 0.5M HNO_3 solution, which was the second most efficient solution in desorbing ^{90}Sr from the clinoptilolite, usually leaching an

additional 20 % to 30 % of the initial beta activity and 3 % to 40 % of the total leached cation concentration. Cation results also showed high concentrations of Fe, Al, Si and P, indicating that 0.5 M nitric acid did not only leach off ions from the surface of the clinoptilolite, but disintegrated the internal structure of it.

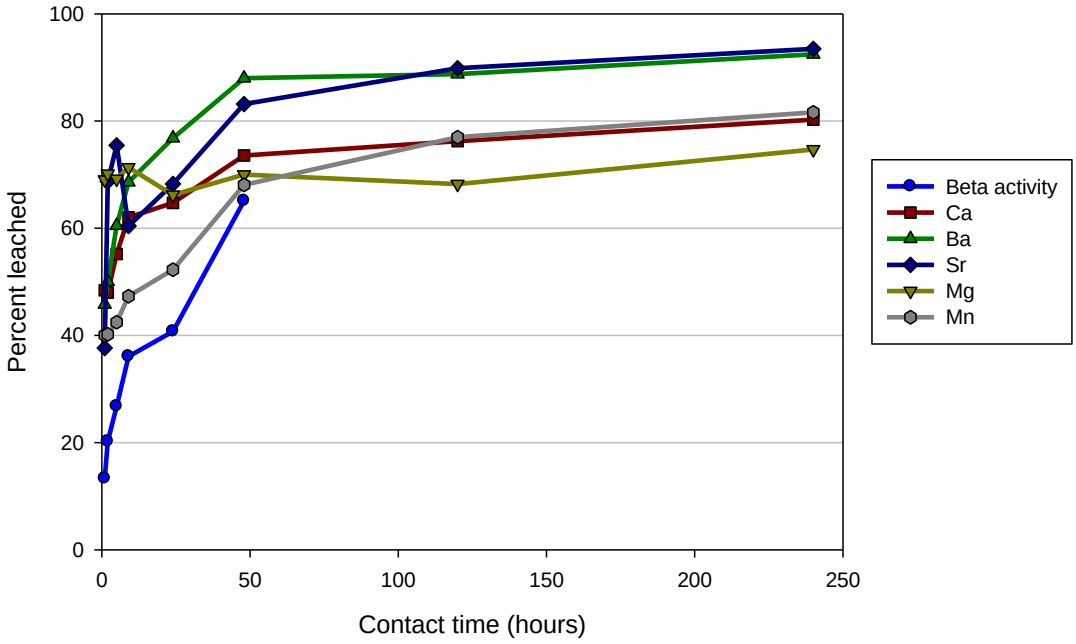

Figure 3.8: Time dependence of ion exchange for beta activity and selected cations using the 1 M KCl solution (step 2).

Overall, ^{90}Sr desorption was most sensitive to kinetically controlled ion exchange as well as to the pH of the solution. At a pH of 4.6, 4 % to 10 % of the initial ^{90}Sr is leached from the clinoptilolite. This amount increased to 20 % to 30 % when the pH is decreased to 0.7. After the remediation of the ^{90}Sr plume, the clinoptilolite will equilibrate with the "new" groundwater that moves through it. However, the results showed that Sr was well sorbed on the clinoptilolite except in situations with low pH and high cation concentrations. At the Wall and Curtain site, a pH between 5 and 6 is expected; cation concentrations were low, so not much leaching of radioactive Sr is expected to occur.

3.5 Conclusions

The aquifer and reactive material of the Wall and Curtain site were characterized in this study. Pore-water samples from the aquifer and the outflow of the permeable barrier system indicate that the system efficiently intercepted deep groundwater containing ^{90}Sr. Gross beta results from samples taken in 30 cm (1 foot) intervals in drive-point piezometers were used to determine the precise position of the ^{90}Sr plume, between depths of 6.3 m bgs and 8.4 m bgs. The system treated a mass flux of 17,749 Bq/m^2day, which was determined with average beta activities and average flow rates of the Wall and Curtain. Cation results indicate that Ba and Sr were adsorbed onto the reactive material, whereas K was released showing that retention is predominantly due to an ion exchange process.

The leading edge of the ^{90}Sr plume was identified through a sampling method that allowed the collection of small sample sizes. Nearly 14 years after the installation of the system, elevated gross beta activity was only detected 40 cm into the reactive material. The *in situ* distribution coefficient was determined to be 76,159 mL/g for beta activity on the clinoptilolite. This leads to the conclusion that ^{90}Sr is adsorbed on the clinoptilolite surface and is highly immobile in the reactive material. Cation results from samples in the reactive material supported the assumption that Sr and Ba were taken up by the clinoptilolite. Sequential extractions were performed on the reactive material using four different extraction solutions. Ion exchange was the most important mechanism in desorption of ^{90}Sr, as 1M KCl was the most efficient solution in leaching off Sr from the clinoptilolite. Ion exchange was kinetically controlled and equilibrium was not attained after a contact time of 10 days. Low pH (< 4) and high ionic strength are expected to be the two most important factors influencing Sr sorption. As the site conditions showed neither of these characteristics, and clinoptilolite samples still contained 17% of the initial beta activity fixed after the leach tests, no significant desorption of ^{90}Sr is expected to occur on site.

The results from this study can be used to construct a reactive transport model of the site, which will give more refined estimates of the longevity of the system.

An ongoing column experiment at the University of Waterloo was sampled after nearly two years, resulting in a calculated distribution coefficient of Sr on clinoptilolite of 1354 mL/g. The overall retardation factor of 4594 leads to the conclusion that it will still take 2315 days or 2349 pore volumes until breakthrough of Sr through the column will occur.

Chapter 4
Longevity estimates of the Wall and Curtain System

4.1 Introduction

Strontium-90 (^{90}Sr) is a mobile radionuclide which decays through beta decay with a half-life of 28.8 years to yttrium-90 (^{90}Y). ^{90}Y, another pure beta emitter, decays with a half-life of 64.4 hours to stable zirconium-90 (^{90}Zr). ^{90}Sr is a by-product of fission reactions and causes health concerns as it has the affinity to replace calcium in bones (O'Hara et al., 2009). In groundwater, ^{90}Sr is a mobile contaminant that will remain in the aquifer for around 10 half-lives, i.e. 300 years (Wallace et al., 2012). Permeable reactive barriers (PRBs) are passive remediation systems that are installed along the groundwater flow path of a contaminant plume. The reactive material in the barrier promotes chemical reactions that retain the contaminant within the PRB or transform the contaminant into products that do not cause health concerns. The reactive material can adsorb the contaminant, thus making it immobile. PRBs have been successfully applied to a wide range of contaminants, including inorganic and organic compounds and radionuclides (e.g. Blowes et al., 2000).

Numerical models have been increasingly used in assessments of field sites over the last decades and are considered an important tool in understanding the hydrological cycle (Brunner and Simmons, 2012). Although numerical models need to be calibrated, they cannot be validated and verified as their calibration to field sites results in a non-unique solution (Konikow and Bredehoeft, 1992). In this study, two different numerical codes were used to describe a field site, HydroGeoSphere and MIN3P. HydroGeoSphere is a three dimensional, physically based, finite element, fully integrated numerical code developed at the University of Waterloo (Therrien et al., 2010). HydroGeoSphere is designed to simulate flow and solute transport in variably saturated and fractured porous media as well as in surface water (Brunner and Simmons, 2012). A unique feature of HydroGeoSphere is the

fully-integrated fashion of simulating flow, which means that precipitation partitions into different components such as evaporation, overland flow and groundwater recharge (Therrien et al., 2010). Other features in HydroGeoSphere include variable-density flow and transport, first-order decay reactions (including branching decay reactions), the transport of reactive chemical species and heat transport (Brunner and Simmons, 2012). The ability to model flow and transport in the unsaturated zone and discrete fractures, as well as the possibility to include wells, tile drains and surface water bodies, make HydroGeoSphere applicable to a wide range of hydrological settings, such as regional-scale watershed studies (e.g. Li et al., 2008), the impact of glaciation on groundwater flow systems (e.g. Lemieux et al., 2008), surface water/groundwater interactions (e.g. Brunner et al., 2009) and the reclamation of oil sands (e.g. Price et al., 2010).

MIN3P is a mechanistic multicomponent reactive transport model, which can model variably saturated flow and reactive transport in one, two and three dimensions (Mayer et al., 2002). It considers secondary aqueous species of the components specified, as well as mineral precipitation-dissolution reactions. Ion exchange species and redox reactions can be included in the simulations. Another feature of MIN3P is the possibility to include intra-aqueous kinetically controlled reactions, including irreversible reactions and reactions following Monod kinetics, in the simulation. Additional kinetically controlled reactions can be added by the user to the database, including threshold and inhibition terms. All these features make MIN3P a useful tool in modeling a large variety of variably saturated geochemical situations, which is shown by the use of MIN3P in simulating geochemical transport of acid-mine drainage (e.g. Amos et al., 2004; Jurjovec et al., 2004), TCE treatment (Jeen et al., 2007) and attenuation of organic compounds in the vadose zone (Molins et al., 2010)

Previous chapters focused on the hydrological and geochemical characterization of a permeable reactive barrier system treating a ^{90}Sr plume. The reactive transport modeling study used the parameters determined through field and laboratory experiments and included them into numerical simulations of the study site. Both codes, HydroGeoSphere and MIN3P,

were used in this study to provide refined estimates of the longevity of the permeable reactive barrier system known as the Wall and Curtain.

4.2 Site description

The study site is located 193 km northwest of Ottawa, on the property of the Atomic Energy of Canada (AECL) Chalk River Laboratories, in Chalk River, Ontario. In the early 1950's, concentrated ammonium nitrate solutions containing a variety of fission products including ^{90}Sr and tritium were disposed of in pits lined with crushed limestone. Mobile constituents in these solutions entered the lower half of an unconfined, sandy aquifer. The aquifer has a saturated thickness of 5 to 13 m and is underlain by Precambrian gneiss (Killey and Munch, 1987). In most areas, a glacial stony till overlies the bedrock, followed by a thin gravel layer in some areas. Above the till, fine to medium fluvial sands are dominant. Next in sequence is a silty very fine sand layer, which is assumed to mark the transition from fluvial deposits to aeolian deposits (Killey and Munch, 1987). The aeolian sediments that reach to the surface are mainly composed of fine sands, which are intercepted by interstratified silt and sand units (Killey and Munch, 1987). Hydraulic conductivities determined through permeameter tests range from 3.5×10^{-6} m/s to 1.2×10^{-4} m/s (Killey and Munch, 1987). The average linear groundwater velocities estimated by numerical modelling range from 100 m/a to 150 m/a (Klukas and Moltyaner, 1995). However, transport of ^{90}Sr is retarded due to geochemical interactions with the aquifer, resulting in a travel time of over 40 years from the source area to Duke Swamp, 440 m downgradient (Lee and Hartwig, 2005).

In order to intercept the ^{90}Sr plume and prevent discharge into Duke Swamp, a permeable reactive barrier system was installed in December 1998. The system is known as the Wall and Curtain (see Figure 1.1), and consists of a 30 m long sheet-piling cut off wall (Waterloo Barrier®), which is in contact with the bedrock or till. In front of the wall, an 11 m wide, 2 m thick and 6 m deep curtain of reactive material, clinoptilolite, is placed. The Wall and Curtain is the first PRB known to employ clinoptilolite, a zeolite, as a reactive material. Clinoptilolite has a high sorption capacity and a strong affinity to both Sr and Ca (Fuhrmann at al., 1995;

Cantrell et al., 1994; Rabideau et al., 2005). Two wings of sheet-piling on either side of the reactive curtain help to keep the clinoptilolite in place. Ten vertical wells at the back of the curtain collect water from the barrier, which is discharged into a manhole by a horizontal drain. A second horizontal drain installed 60 m upgradient of the system intercepts shallow, uncontaminated groundwater to prevent loading of the sorption sites on the reactive material by ions competing with ^{90}Sr. The outflow height of both drains can be adjusted in the manhole, giving the Wall and Curtain the unique advantage to adjust the hydraulic gradient across site as well as the capture zone of the system.

4.3 Conceptual Model

From field and laboratory experiments, a conceptual model of the site was constructed. A detailed physical characterization of the aquifer in the proximity of the Wall and Curtain included single-well response tests and borehole-dilution tests. A water-table map of the site was constructed from water-table measurements. In the proximity of the system, water-table measurements from all piezometers of pre-installed wells were taken, indicating that there was a strong vertical upward component to the hydraulic gradient. Hydraulic conductivities determined through single-well response tests were used to refine hydraulic conductivity values of the aquifer in numerical simulations. Simulated velocities were compared with average groundwater velocities determined through borehole-dilution tests (see Chapter 2). The aquifer was horizontally rather homogeneous; as a result, hydraulic conductivities and average groundwater velocities could be interpolated laterally. Some variation of hydraulic conductivity estimates were seen with depth. Hydraulic conductivities were lower in depths $\leq$ 3.5m (in the order of 10^{-6} m/s) and increased to values in the order of 10^{-5} m/s in depths between 3.5 m and 8 m. In depths > 8 m, hydraulic conductivities decreased to values on the order of 10^{-6} m/s. A detailed description of the physical characterization of the site is provided in Chapter 1.

A detailed description of the geochemical characterization of the aquifer and the reactive material at the Wall and Curtain site can be found in Chapter 3. A large number of pore-

water samples from the aquifer across site were taken to characterize the composition of the plume and the uncontaminated groundwater in detail. Solid and pore-water samples from the clinoptilolite were analyzed to determine an *in situ* distribution coefficient (K_d) of ^{90}Sr on clinoptilolite; the K_d was found to be 76,159 mL/g. During the solid sampling, the leading edge of the plume in the clinoptilolite was found. Beta activity above background levels could only be found in the first 40 cm of the reactive material after 14 years of operation. Sequential extractions performed on the radioactive clinoptilolite samples showed that kinetically controlled ion exchange was the dominant mechanism for sorption/desorption of cations and beta activity onto/from the clinoptilolite. The results of the field and laboratory experiments described above indicate that the Wall and Curtain system worked efficiently in intercepting a ^{90}Sr plume.

The results from previous work indicate that groundwater flow is horizontal, until it is upward in the vicinity of the Wall and Curtain. Ionic concentrations were generally higher in the lower aquifer (> 6 m bgs) due to the more distant source area, Lake 233, which is labelled with road salt. The ^{90}Sr plume was very discrete at depth of 6 m to 8 m in the aquifer. In the proximity of the PRB, the vertical component of the gradient increased, resulting in a localized maximum of beta activity in the reactive material at depths of 4.3 m to 4.7 m. Sr and Ba were retained on the clinoptilolite, whereas K was released. As the sorption capacity of the clinoptilolite is high and the leading edge of the ^{90}Sr plume was only 40 cm in the clinoptilolite after 14 years of operation, indicating that the system might function for up to another 50 years. To provide refined longevity estimates, numerical simulations were set up in HydroGeoSphere and MIN3P.

4.4 Numerical Implementation

4.4.1 HydroGeoSphere

The construction details of the Wall and Curtain and the conceptual model were used as a guide to construct numerical reactive transport models using two different codes, HydroGeosphere and MIN3P. Prior to including reactive transport in HydroGeoSphere, a

well calibrated physical flow model was constructed (for calibration details, see Chapter 2). However, the representation of flow through the barrier in the model by 10 pumping wells had to be changed to a passive horizontal drain. This was necessary to include reactive transport in the simulation, as pumping well outflows showed a stabilization of solute concentrations.

The model domain was rectangular, being 200 m long in the direction of flow (x-dimension), 150 m wide (y-dimension) and 12 m thick (z-dimension). Grid spacing in the x-dimension was 1 to 3 m upgradient and downgradient of the Wall and Curtain, and was refined to 0.5 m in the curtain (see Figure 2.1). Spacing in the y dimension was 1 m on each side of the Wall and Curtain, and was refined to 0.5 m within the Curtain. Spacing in the z-dimension was 1 m. The inflow and outflow boundaries were constant head boundaries, lateral boundaries and the bottom of the domain were no-flow boundaries. A uniform recharge of 9.51×10^{-9} m/s was applied to the top boundary, which corresponds to the reported recharge estimate of 0.3 m/a (Klukas and Moltyaner, 1995). Based on field measurements, the aquifer was divided into three zones with different hydraulic conductivities, which were assumed to be isotropic . For modelling purposes, the gravel layer was represented by a 0.5 m thick layer with a hydraulic conductivity of 3.8×10^{-5} m/s. This value was a weighted average of 0.49 m sand (3.6×10^{-5} m/s) and 0.01 m gravel (1.3×10^{-4} m/s). The stony till at the base of the aquifer was represented in the bottom meter of the domain, with an assigned isotropic hydraulic conductivity of 1.4×10^{-6} m/s. Table 4.1 shows the input parameters of the simulation.

The 30 m long, 12 m deep sheet-piling cut-off wall and wings on either side of the clinoptilolite were included as impermeable zones at 115 m in the direction of flow in the center of the y-dimension. In front of the cut-off wall, a curtain of clinoptilolite was placed, which had the same dimensions as on site and an assigned isotropic hydraulic conductivity of 2.0×10^{-4} m/s, which was decreased slightly from reported values from the Chalk River Laboratories from 2010 (2.6×10^{-4} m/s) to achieve a better fit of simulated to observed heads. The upgradient drain was represented by a 58 m long passive tile drain at x = 51 m. The swamp downgradient of the Wall and Curtain was represented by a 300 m^2 large seepage

area with an applied uniform flux based on weir measurements. A passive horizontal tile drain (flow rate set to 0) represented the Wall and Curtain drain. However, to draw water into the curtain with an assigned flow rate of 0, it was necessary to specify the hydraulic head within the drain. Ten observation wells at the back of the curtain were included to indicate breakthrough of ^{90}Sr in the reactive material and to give easier access to longevity estimates.

Only five solutes could be incorporated into the simulation. For this simulation under transient, fully-saturated conditions, radioactive ^{90}Sr and the daughter products of ^{90}Sr, ^{90}Y and ^{90}Zr were included as solutes, as well as the major cations on site, Na and Ca. The 20 m wide plume started permeating at time 0 in the lower half of the aquifer (z = 0 m to 6 m) and continuously infiltrated until 100 years, the end of the simulation. Free solution diffusion coefficients of 1×10^{-20} m^2/s were assigned for all solutes. The decay constants of ^{90}Sr and ^{90}Y were specified as 7.6×10^{-10} s^{-1} and 3.0×10^{-6} s^{-1}, which correspond to half-lives of 28.8 years and 64 hours, respectively. Distribution coefficients were 0 for all porous media zones for ^{90}Y, ^{90}Zr and Na. Calcium sorption on the aquifer sands was assumed to be low, so no distribution coefficient was assigned for Ca onto the aquifer. A distribution coefficient of 79.1 mL/g was assigned for sorption of Ca onto the clinoptilolite. This value was determined through analysis of *in situ* samples from the Curtain. The distribution coefficient for ^{90}Sr was specified as 8.5 mL/g for the aquifer material (from Killey and Munch, 1987), and 76,159 mL/g for the clinoptilolite (determined through analysis of samples field and laboratory experiments; Chapter 3). Typical concentrations were specified for the solutes, being 0 for the decay products Y and Zr, and 30 mg/L and 10 mg/L for Na and Ca, respectively. The assigned Sr concentration in the plume was 39 Bq/L.

A two-dimensional simulation in HydroGeoSphere was run to receive more insight in the magnitude of the transverse vertical dispersivity of the aquifer. For this purpose, the model domain was enlarged in the x-dimension and Chloride was included as a conservative tracer, which originated from the surface 490 m upgradient of the Wall and Curtain system. These conditions were chosen to represent the source of the road salt label in Lake 233. If the flow model is representative of flow conditions in the aquifer, then the Chloride plume should be present only in depths of 6 to 12 m.

Table 4.1: Model input parameters.

Parameter (Unit)	Input value in model
Influent boundary head (m)	10.9
Effluent boundary head (m)	8.3
K1 (m/s), upper third of aquifer (z = 8 – 12)	5.5×10^{-6}
K2 (m/s), central aquifer (z = 4.5 – 8)	2.2×10^{-5}
K3 (m/s), lower aquifer (z = 1.5 – 4.5)	1.2×10^{-5}
K4 (m/s) gravel above till (z = 1 – 1.5)	3.8×10^{-5}
K5 (m/s) till above bedrock (z = 0 – 1)	1.4×10^{-6}
K6 (m/s) curtain	2.0×10^{-4}
K7 (m/s) wall and base of curtain	1.0×10^{-10}
Seepage area discharge (m^3/s)	7.0×10^{-5}
Area of downgradient seepage (m^2)	300
Seepage area specific discharge (m/s)	2.3×10^{-7}

4.4.2 MIN3P

In the code MIN3P, only reactive transport under transient, fully-saturated conditions through the clinoptilolite curtain was simulated, as parameters such as the cation exchange capacity (CEC) can be specified for only one material instead of multiple ones. However, MIN3P provided more opportunities for the incorporation of geochemical interactions, such as ion exchange and sorption, than HydroGeoSphere. The one-dimensional model domain was 2 m long, with a grid spacing of 0.1 m. The entire model domain consisted of clinoptilolite, which had an assigned porosity of 44%. An isotropic hydraulic conductivity of

2 x 10^{-4} m/s was specified for the clinoptilolite; the specific storage coefficient of clinoptilolite was set to 1.0 x 10^{-5} m^{-1} and the longitudinal dispersivity to 9.8 x 10^{-3} m. For simulating ion exchange, the cation exchange capacity and bulk density of the material have to be specified. For clinoptilolite at the Wall and Curtain site, the bulk density is 0.78 kg/m^3. The CEC of clinoptilolite was assigned to be 165 meq/100 g (as reported from Teague Mineral Products in Rabideau et al., 2005). The inflow and outflow boundaries of the domain were assigned constant head boundaries, with inflow and outflow heads of 6.00 m and 5.95 m, respectively. All other boundaries were no flow boundaries. As an initial condition for the reactive transport simulation, the background chemistry of the aquifer was specified. The chemistry of the plume, which continuously infiltrated the clinoptilolite, was specified from averages in a simplified fashion in the inflow boundary condition of the reactive transport simulation. Sr was specified as an average value in Bq/L; however, it was treated in the simulation as mg/L. The composition of the aquifer and the plume can be found in Table 4.2. Simplifications included the inclusion of high Na and Cl concentrations in the Sr plume, although the Sr plume is known to be much more discrete that the road salt label. Seven species were considered to take part in ion exchange in the simulation, namely Na, Ca, K, Sr, Ba, Mg and Mn.

If a cation is exchanged with a cation of the same charge, then the exchange equation can be written as, e.g.:

$$Ba^{2+} + Sr - X \leftrightarrow Ba - X + Sr^{2+}$$

If a monovalent cation on the surface is exchanged with a divalent cation, then the exchange equation becomes, e.g.:

$$Ca^{2+} + K - X \leftrightarrow Ca - X + K^{+}$$

Radioactive decay of Sr to Y was added as an intra-aqueous, irreversible kinetic reaction in the MIN3P database.

Table 4.2: Geochemical composition of uncontaminated groundwater and plume used in the simulation with MIN3P.

Component (unit)	Concentration in background groundwater	Concentration in plume
pH	6.00	5.50
Sr (Bq/L)	0.10	39.0
Fe^{2+} (mg/L)	0.04	2.50
Ba^{2+} (mg/L)	0.013	0.08
Cl^- (mg/L)	19.7	52.2
Ca^{2+}(mg/L)	5.68	8.97
K^+ (mg/L)	1.21	1.83
Mg^{2+} (mg/L)	1.23	2.37
Mn^{2+} (mg/L)	0.009	0.36
Na^+ (mg/L)	9.97	26.3
CO_3^{2-} (mg/L)	7.64	15.8

An updated version of MIN3P was used that, in addition to the geochemical reactions described above, considers kinetic sorption of components, in this case of Sr onto the clinoptilolite. A distribution coefficient of 76,159 mL/g was specified for sorption of ^{90}Sr onto clinoptilolite. The kinetics of the reaction are considered in MIN3P by the equation:

$$\frac{\partial \hat{C}_{sorb}}{\partial t} = \alpha \left(\frac{K_d(1-\theta)}{\theta} \rho_s C_{aq} - \hat{C}_{sorb} \right), \quad \textbf{(4.1)}$$

(from Yin, in prep.) where $\hat{C}_{sorb}$ is the sorbed concentration normalized to the pore-water (mol/L), C_{aq} is the aqueous concentration, θ is the porosity, ρ_b is the solid density of the material, K_d is the distribution coefficient and α is the first-order kinetic rate. The rate has been determined to be 9.97×10^{-2} day^{-1} through fitting to results from column experiments performed by Yin et al. (in preparation). Simulations were run with both versions of MIN3P, the one that only includes equilibrium ion exchange and the updated version that additionally considers kinetic sorption of Sr onto clinoptilolite, to determine the influence of kinetic sorption on the resulting longevity estimates of the system.

A sensitivity analysis on the simulation including kinetic sorption was performed to determine if the distribution coefficient and/or the first-order kinetic rate have a major

influence on the resulting longevity estimates. For this purpose, two simulations were run in which the distribution coefficient was changed to 2045 mL/g, as determined by Rabideau et al (2005), and to 10,000, respectively. Two additional simulations, in which the kinetic rate was varied, included a simulation with a kinetic rate double the initially used rate (0.199 day^{-1}) and a simulation with a kinetic rate that was increased by an order of magnitude (0.997 day^{-1}).

4.5 Results and Discussion

4.5.1 HydroGeoSphere

The concentration of the considered solutes after 100 years in the aquifer can be seen in longitudinal cross-sections in Figure 4.1. As Ca and Na behaved very similarly, only Na is shown. Sodium and Zr showed a clear plume with maximum concentrations of 0.038 kg/m^3 and 0.049 kg/m^3, respectively. Yttrium concentrations were high in the front of the model domain (x = 0), as Yttrium was produced through radioactive decay of ^{90}Sr. The Y concentration then decreased throughout the aquifer, as it decayed quickly to ^{90}Zr.

Strontium showed low concentrations in the aquifer due to the inclusion of radioactive decay, which was only simulated in the sorbed phase, but clearly accumulated in the clinoptilolite.

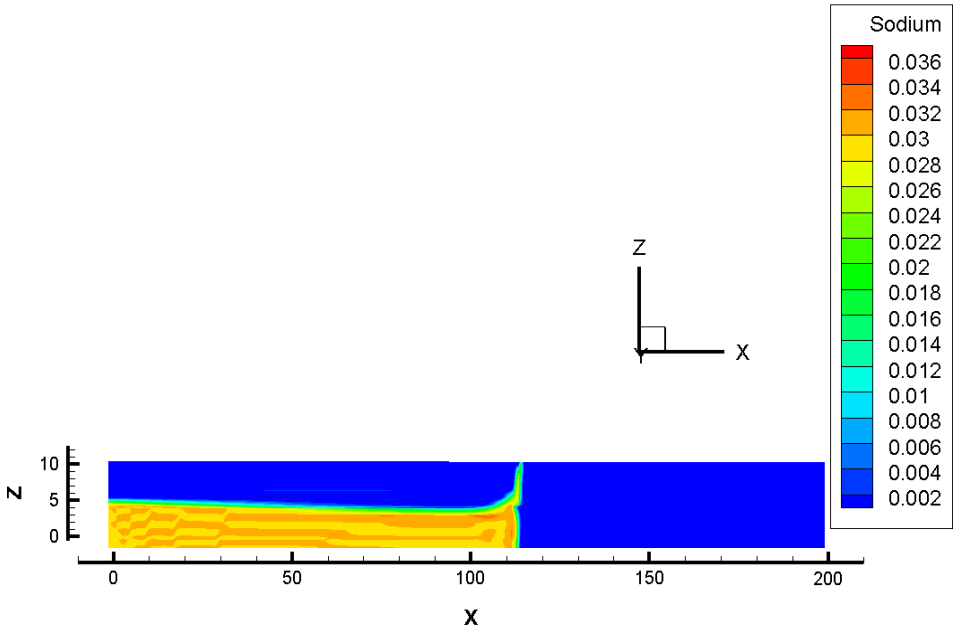
Sodium
0.036
0.034
0.032
0.03
0.028
0.026
0.024
0.022
0.02
0.018
0.016
0.014
0.012
0.01
0.008
0.006
0.004
0.002
Z
X
10
5
0
Z
0
50
100
150
200
X

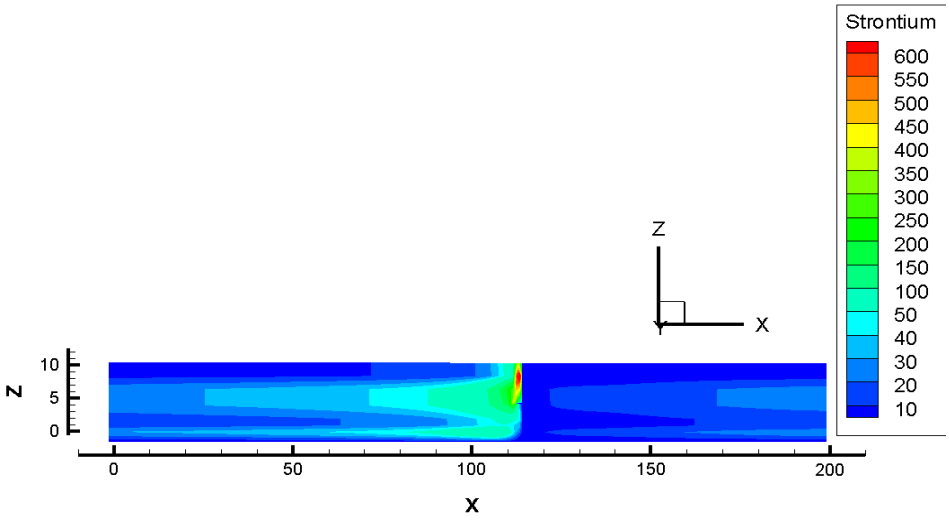
Strontium
600
550
500
450
400
350
300
250
200
150
100
50
40
30
20
10
Z
X
10
5
0
Z
0
50
100
150
200
X

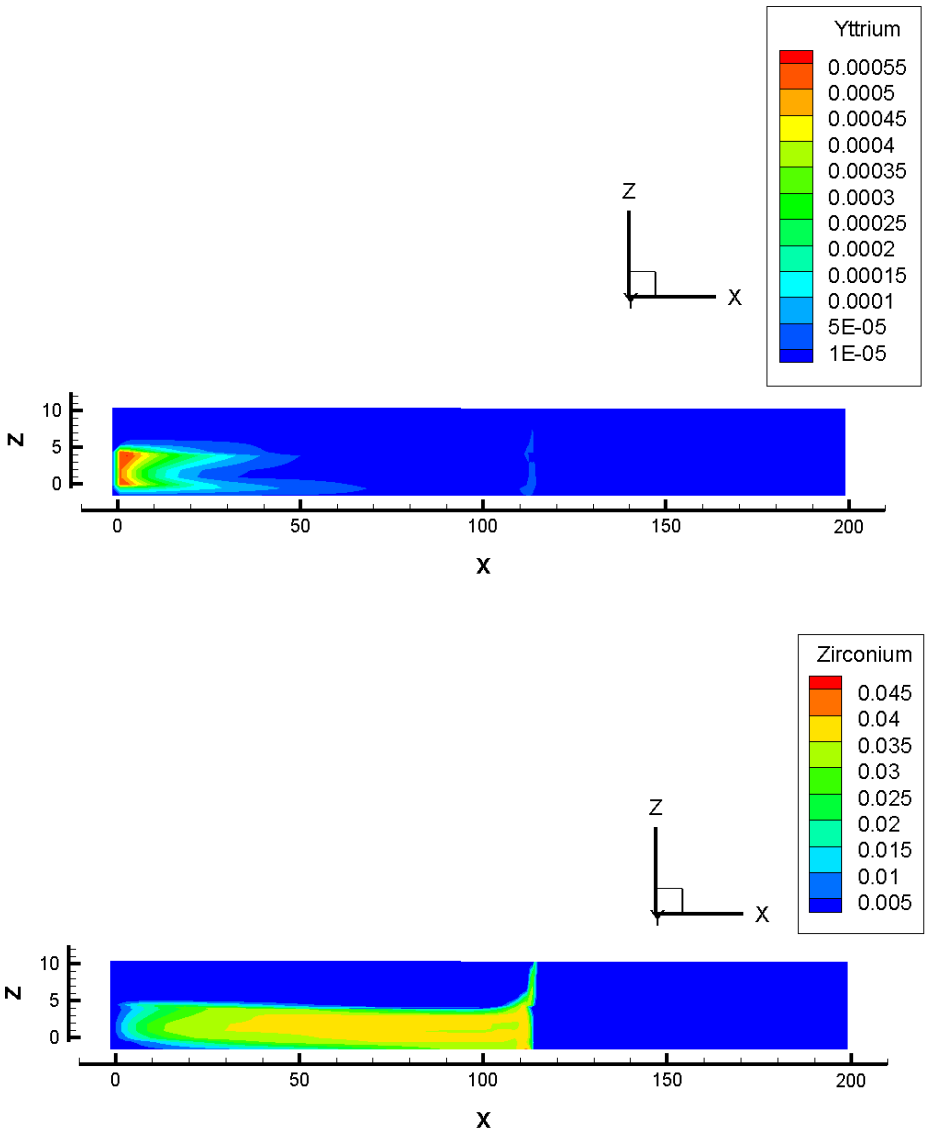

Figure 4.1: Longitudinal cross sections of solute concentrations along the center line of the domain.

The outflow of the observation wells (see Figure 4.2) showed that Na stabilized quickly at a concentration of 3.8 x 10^{-6} kg/m^3 or 3.8 x 10^{-3} mg/L, which was lower than expected, considering that an input concentration of 30 mg/L was specified and that Na was not included in sorption processes. However, the longitudinal cross section showed that the mass

of the plume was in the lower aquifer, and only the dispersed leading edge of the Na plume reached the clinoptilolite. Strontium concentrations in the observation well started increasing markedly after a transport time of 2.2 x 10^9 seconds or approximately 70 years, indicating that the sorption capacity of the clinoptilolite was exhausted and breakthrough started to occur. As Y was not specified to take part in sorption processes, the concentration of Y started increasing earlier, at 1.8 x 10^9 seconds or 57 years. Although the concentrations of Sr and Y did not reach the threshold level of 2 Bq/L after 100 years, the sharp increase in their concentration suggested that breakthrough was occurring. Thus, the longevity estimate of the Wall and Curtain system based on the simulation with HydroGeoSphere was around 100 years, after treating a total mass of 1200 MBq of ^{90}Sr (see Figure 4.2).

The two-dimensional simulation with Chloride as a conservative tracer showed that the Chloride plume was only present in the lower half of the aquifer. However, it extended at depths between 4 m and 12 m in the simulation, meaning that the plume extended to shallower depths than in the field. Only by decreasing the hydraulic conductivity of the central aquifer, a good fit to field observations of the extent of the high EC plume was achieved. These results indicate that some adjustments of the specified hydraulic conductivity in the central aquifer will be helpful in the future, including more comparisons of simulated groundwater velocities and velocities determined through field tests.

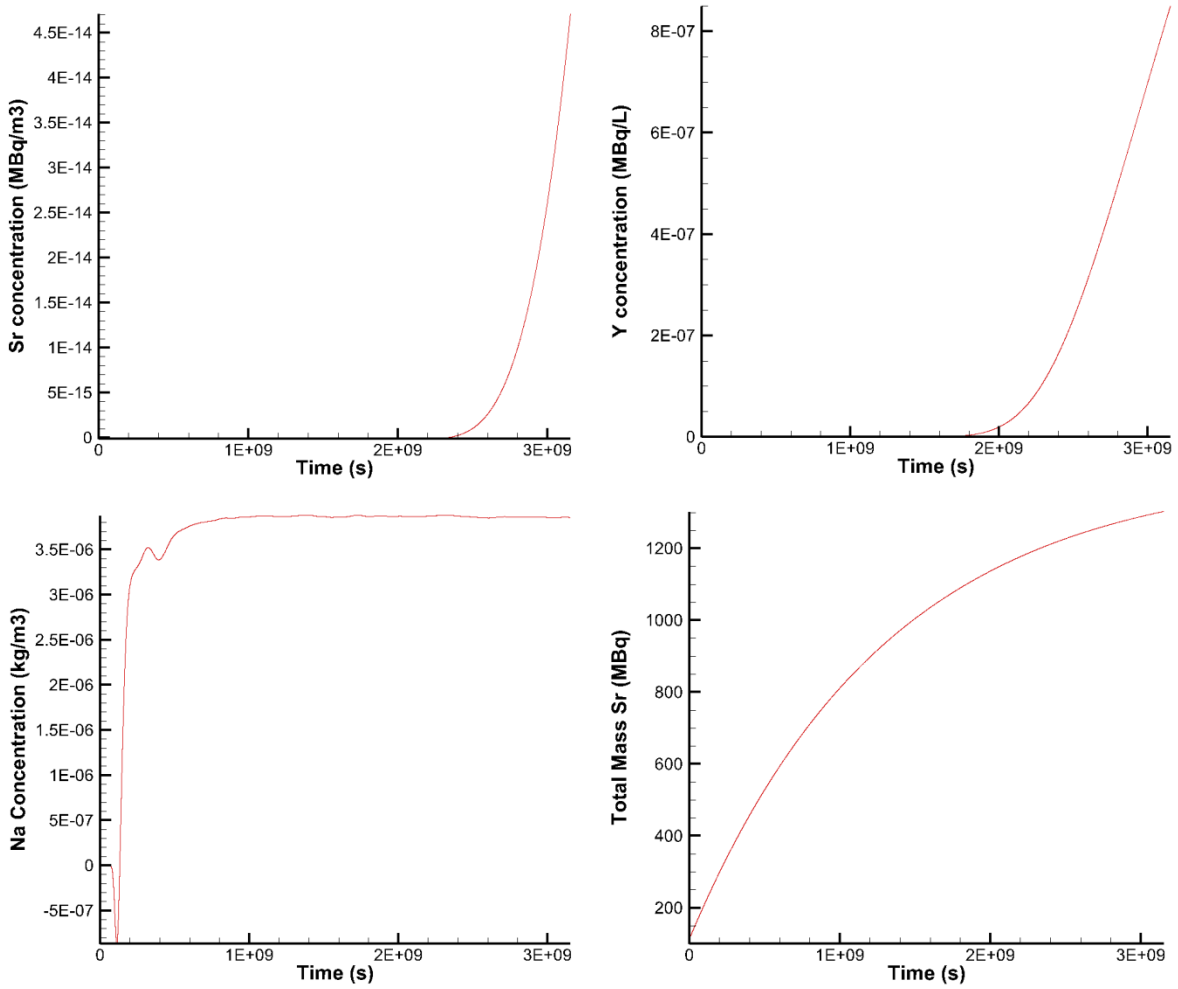

Figure 4.2: Outflow concentrations of Sr and Y in observation well 3 (top) and Na in observation well 1 (bottom left). Observation well 3 is located in the center, observation well 1 at the western end of the reactive material. On the bottom right, the mass balance of Sr over time is shown.

4.5.2 MIN3P

The breakthrough time of different solutes varies in the updated version of MIN3P that considers kinetic sorption of ^{90}Sr onto the clinoptilolite (see Figure 4.3). The pH was stable at the first output time, 20 years. The pH was with 3.3 lower than expected, which was most likely due to the fact that because of modeling memory limitations, not all possible secondary

aqueous species were included in the simulation. Cl^-, CO_3^{2-} and Fe^{2+} all showed complete breakthrough after 20 years, their concentration across the entire domain equalling their respective input concentration. This was not surprising as none of these components were specified to take part in exchange reactions. Potassium concentrations were higher in the back of the curtain (the last 30 cm), indicating that it was released in ion exchange processes. Sodium showed a slightly higher concentration in the back of the curtain than in the front after 20 years. Magnesium reached up to 1.75 m into the curtain; Ca and Ba were more retarded and reached up to 1.7 and 1.5 m into the curtain, respectively, indicating that Ca and Ba were preferred over Mg on the clinoptilolite surface. Mn showed a maximum at x= 1.68 m. Sr only reached 0.1 m into the simulated curtain of clinoptilolite. The distribution of sorbed species due to ion exchange in the domain showed that sorbed Na and K concentrations were highest in the last 30 cm of the domain. Sorbed Mg concentrations showed a thin, discrete maximum at 1.68 m; sorbed Mn concentrations showed a maximum at 1.8 m. The maximum of sorbed Ca was between 0.40 m to 1.13 m, the maximum of sorbed Ba was located between 0.35 m to 0.87 m after 20 years. The concentration of Sr on the surface due to kinetic sorption was only high in the first 10 cm after 20 years. These results indicate that Sr was the most retarded component in the system due to kinetic sorption; Ca, Ba and Mg were sorbed onto the clinoptilolite, whereas Na and K were released from it, which was in agreement with results from field and laboratory experiments.

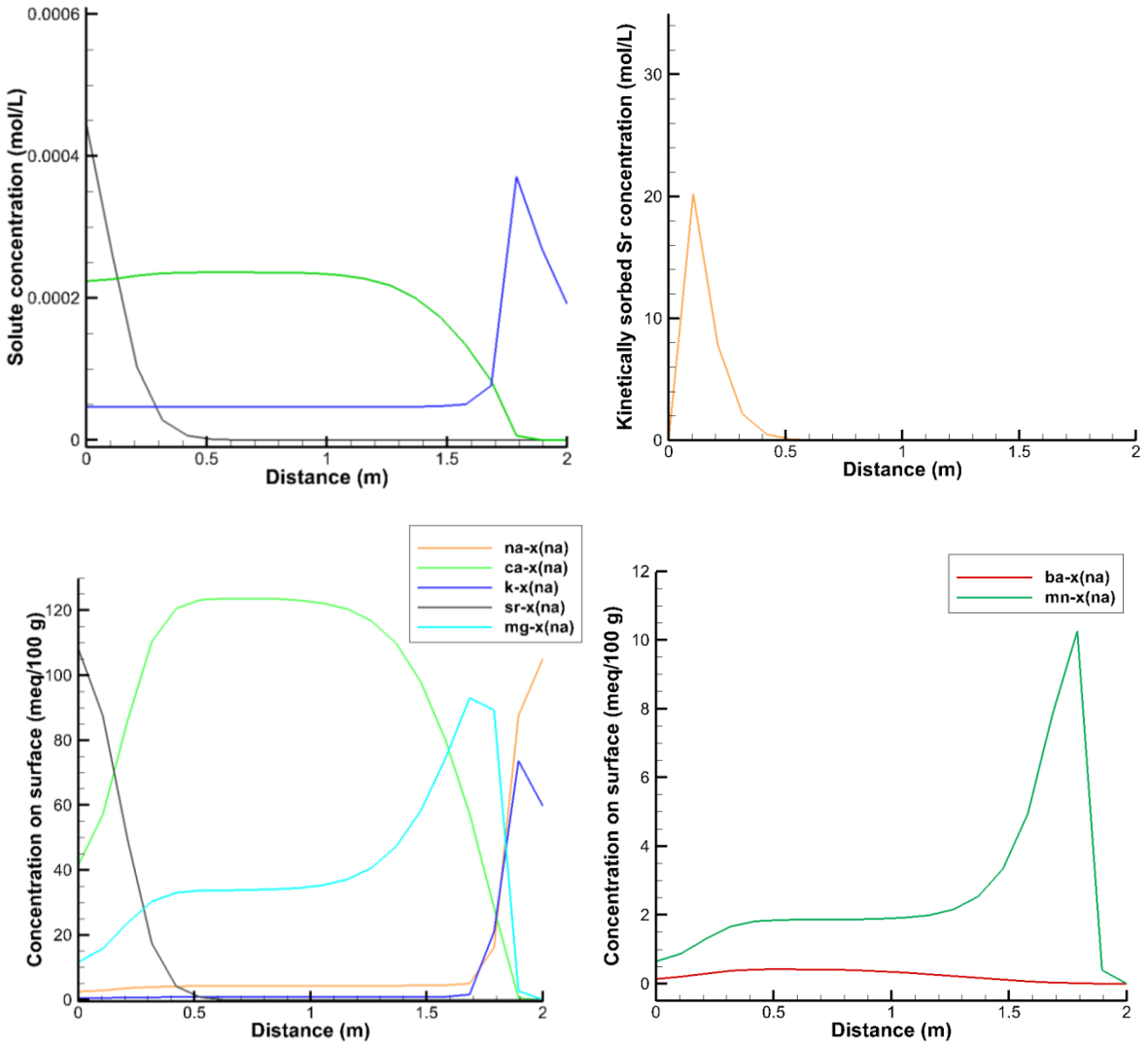

Figure 4.3: Concentration profiles in the clinoptilolite after 20 years. Top left: Total aqueous Sr (grey), Ca (green) and K(blue) concentrations. Top right: Kinetically sorbed Sr concentration. On the bottom concentrations of ion exchange species on the surface.

At an output time of 50 years (see Figure 4.4), Sr had arrived at 40 cm into the clinoptilolite. Ca, Mg, Mn, Na and K all showed low concentrations in the front of the curtain and maximum concentrations at the back of the curtain. Ba showed a maximum concentration between 0.60 m and 1.60 m; however, concentrations remained high

throughout the last meter of clinoptilolite. The concentration of sorbed Sr due to kinetic sorption continued to increase in the first 10 cm of the domain.

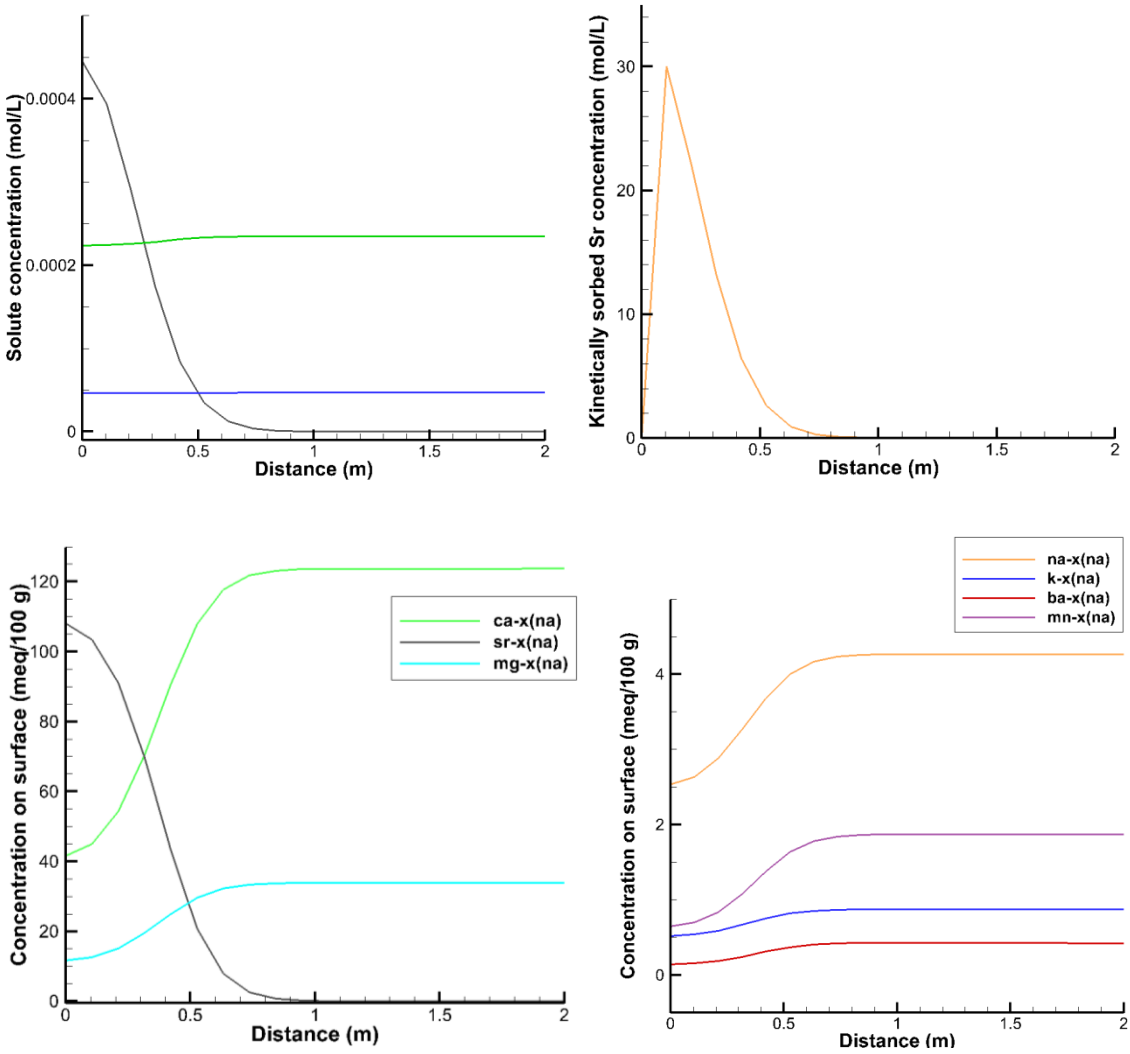

Figure 4.4: Concentration profiles in the clinoptilolite after 50 years. Top left: Total aqueous Sr (grey), Ca (green) and K(blue) concentrations. Top right: Kinetically sorbed Sr concentration. On the bottom concentrations of ion exchange species on the surface.

At output times of 100 years and 200 years (see Figure 4.5), the trend seen after 50 years continued. Na, Ba, Ca, Mn, K, and Mg had low concentrations in the front of the domain; their maximum concentrations reached the back of the curtain. Between 100 and 200 years,

the front of low concentrations in the first 20-50 cm of the curtain moved further inward. The sorbed species of the components above followed the same trend. Sr concentrations only reached 70 cm into the clinoptilolite after 200 years. These results indicate that Ba, Ca, Mg, Mn, K and Na were all released from the clinoptilolite surface; Sr adsorbed on the surface of the clinoptilolite.

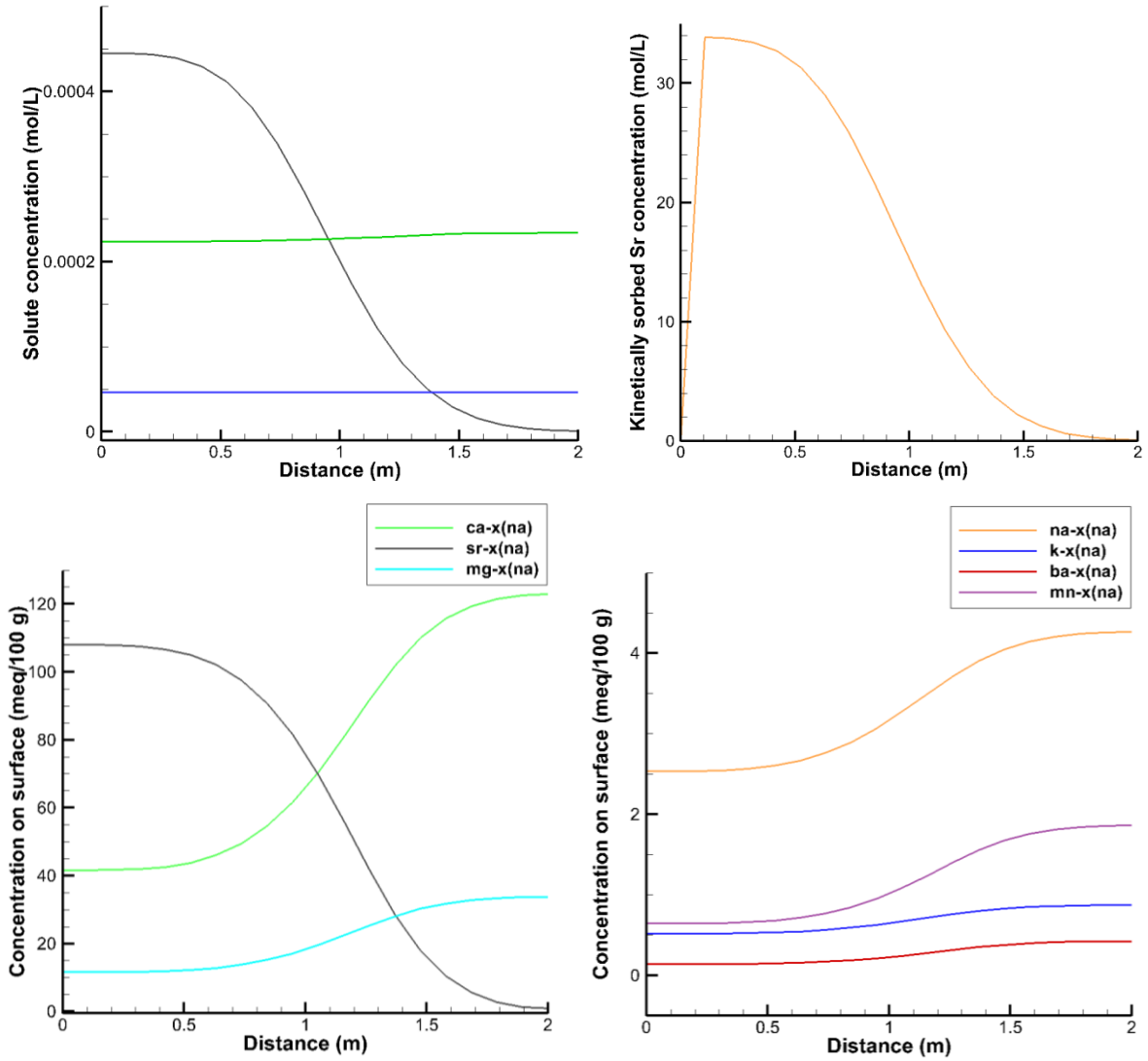

Figure 4.5: Concentration profiles in the clinoptilolite after 200 years. Top left: Total aqueous Sr (grey), Ca (green) and K(blue) concentrations. Top right: Kinetically sorbed Sr concentration. On the bottom concentrations of ion exchange species on the surface.

According to the simulation results, the longevity of the system is more than 200 years (see Figure 4.7).

In the simulation run with the version of MIN3P that does not consider kinetic sorption of ^{90}Sr, Sr^{2+} breakthrough was achieved after a time of less than 30 years (see Figure 4.6), showing that the kinetic sorption of Sr onto clinoptilolite had a major influence on the results.

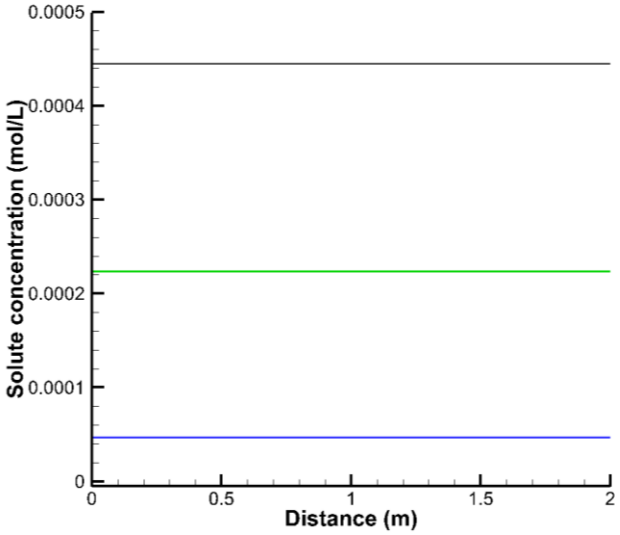

Figure 4.6: Total aqueous Sr (grey), Ca (green) and K (blue) concentrations in the clinoptilolite after 30 years in the simulation only including equilibrium ion exchange.

4.5.3 Sensitivity analysis

Varying the distribution coefficient had a major influence on the simulation results. When the Kd was changed to 2045 mL/g, Sr concentrations were equal to the input concentrations up to 1 m in the clinoptilolite after 20 years (see Figure 4.7). It can be seen in Figure 4.9 that the sorption capacity of the clinoptilolite was exhausted to a distance of 1.5 m, however, Sr concentrations at x = 2 m were already above drinking water guidelines (5 Bq/L).

When the distribution coefficient was changed to 10,000 mL/g, Sr reached up to 0.8 m after 20 years and kinetically sorbed Sr showed a broader peak than in the original simulation (see Figure 4.8), indicating that the sorption capacity of the clinoptilolite was exhausted

faster. After 100 years, the sorption capacity of the clinoptilolite was exhausted and complete Sr breakthrough occurred (see Figure 4.9).

Increasing the kinetic rate by an order of magnitude only resulted in a difference of 2 x 10-4 mol/L in the concentration of kinetically sorbed Sr after 200 years and a difference of 2 x 10-9 mol/L in the total aqueous Sr concentration, indicating that the simulation is not sensitive to a varied rate.

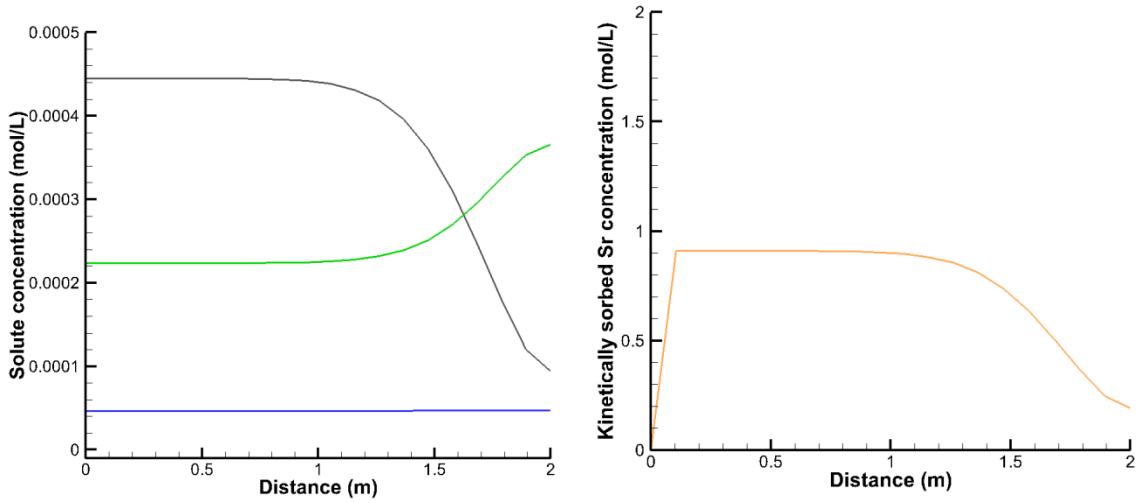

Figure 4.7: Concentration profiles in the clinoptilolite after 20 years in the simulation with Kd = 2045. Left: Total aqueous Sr (grey), Ca (green) and K(blue) concentrations. Right: Kinetically sorbed Sr concentration.

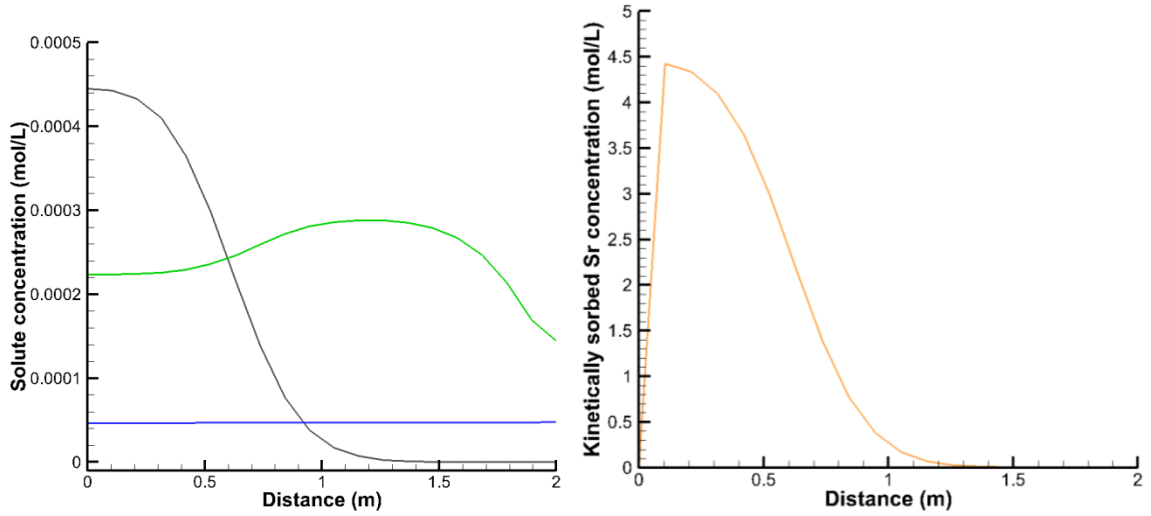

Figure 4.8: Concentration profiles in the clinoptilolite after 20 years in the simulation with Kd = 10,000. Left: Total aqueous Sr (grey), Ca (green) and K(blue) concentrations. Right: Kinetically sorbed Sr concentration.

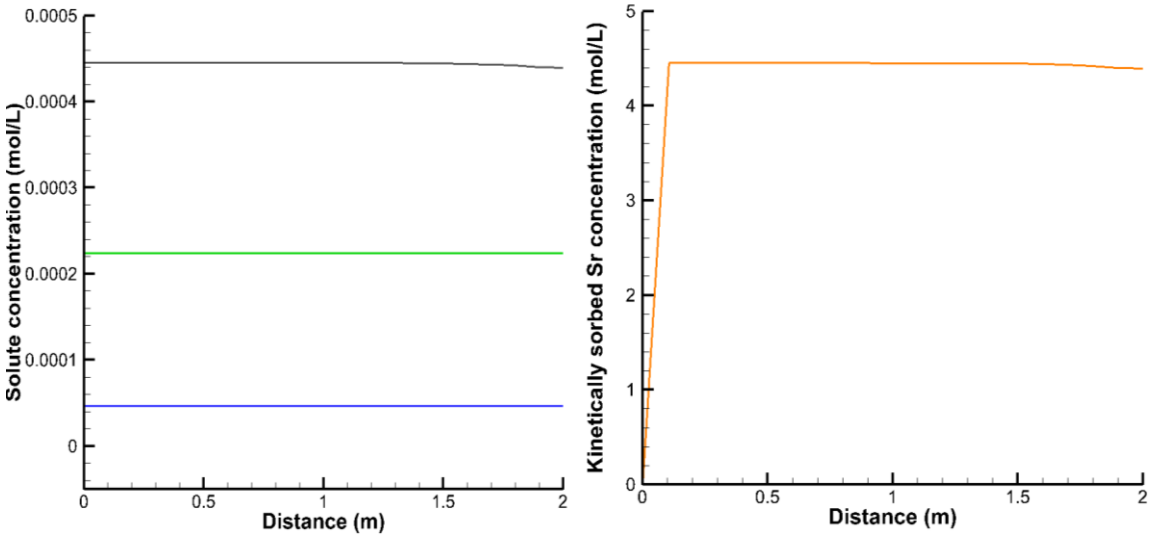

Figure 4.9: Concentration profiles in the clinoptilolite after 100 years in the simulation with Kd = 10,000. Left: Total aqueous Sr (grey), Ca (green) and K(blue) concentrations. Right: Kinetically sorbed Sr concentration.

Considering that the leading edge of the plume was found through field sampling 40 cm within a vertically limited area in the clinoptilolite after 14 years of operation, a longevity of 30 years overall seemed an underestimate; however, the longevity estimate of over 200 years seemed large. The simulation did not consider small-scale dispersion and plume fingering or the limited thickness of the ^{90}Sr plume; however, this process was found in the field. Furthermore, it is unlikely that all the Ca, Mg, Ba and K on the sorption sites will progressively be replaced by Sr, making 200 years an overestimate. From field and laboratory experiments, longevity estimates of 80 to 100 years seemed much more realistic than estimates of over 200 years. An updated version of MIN3P that considers kinetically controlled ion exchange, rather than kinetic sorption of ^{90}Sr, would be useful to test if simulated longevity estimates are then closer to estimates derived from the field.

4.6 Summary and Conclusions

Based on empirical data, collected in the field, the Wall and Curtain system installed 14 years ago to remediate a ^{90}Sr plume is working efficiently. From field and laboratory experiments, a conceptual model of the site, including sorption mechanisms on the reactive material, was constructed. Using field data and construction details of the system, two different numerical codes were used to construct reactive transport models. The model in HydroGeoSphere employed a large model domain and physical parameters of the aquifer and the Wall and Curtain. However, reactive transport abilities were limited to include only five solutes. Radioactive decay of ^{90}Sr and ^{90}Y was included, as well as distribution coefficients that were specified for different material zones. At an output time of 100 years, the ^{90}Sr plume had clearly reached the clinoptilolite, and breakthrough of ^{90}Sr and ^{90}Y started to occur. Flow and transport of the plume through the curtain of clinoptilolite was simulated with MIN3P. In this code, concentrations of all major components of the uncontaminated groundwater and the ^{90}Sr plume could be specified in a simplified form. Radioactive decay of ^{90}Sr was included. Six components that were expected to take part in ion exchange were included. An updated version of MIN3P was used, which also considered kinetic sorption of Sr onto clinoptilolite.

The results of the simulation indicated that the longevity of the curtain was over 350 years; however, this was largely due to the fact that all ion exchange species other than Sr were released over time as the ^{90}Sr plume moved further into the system. In consequence, Sr was sorbed onto the clinoptilolite. It is highly unlikely that all other ion exchange species would be replaced by Sr in reality. From field and laboratory experiments, longevity estimates of 80 years to 100 years for the system would be much more realistic. As input parameters of the simulations are simplified, empirical field and laboratory data are considered more dependable than the results of the simulations. The incorporation of kinetically controlled ion exchange, which was determined to be the major sorption mechanism of Sr onto clinoptilolite, into the MIN3P code might be helpful to provide refined longevity estimates of the system. Further field and laboratory work, mainly the sampling and analysis of the reactive material, including SEM and XRF and additional leach tests with previously loaded clinoptilolite, will give a more detailed view of the mechanisms and the kinetics of the system. The results from these tests and continuous monitoring of the outflow of the Curtain will be helpful to further refine longevity estimates, as well as give recommendations of how to replace the barrier after the ^{90}Sr plume is remediated.

Appendix A

Groundwater chemistry profiles for sampled wells and drive-point piezometers

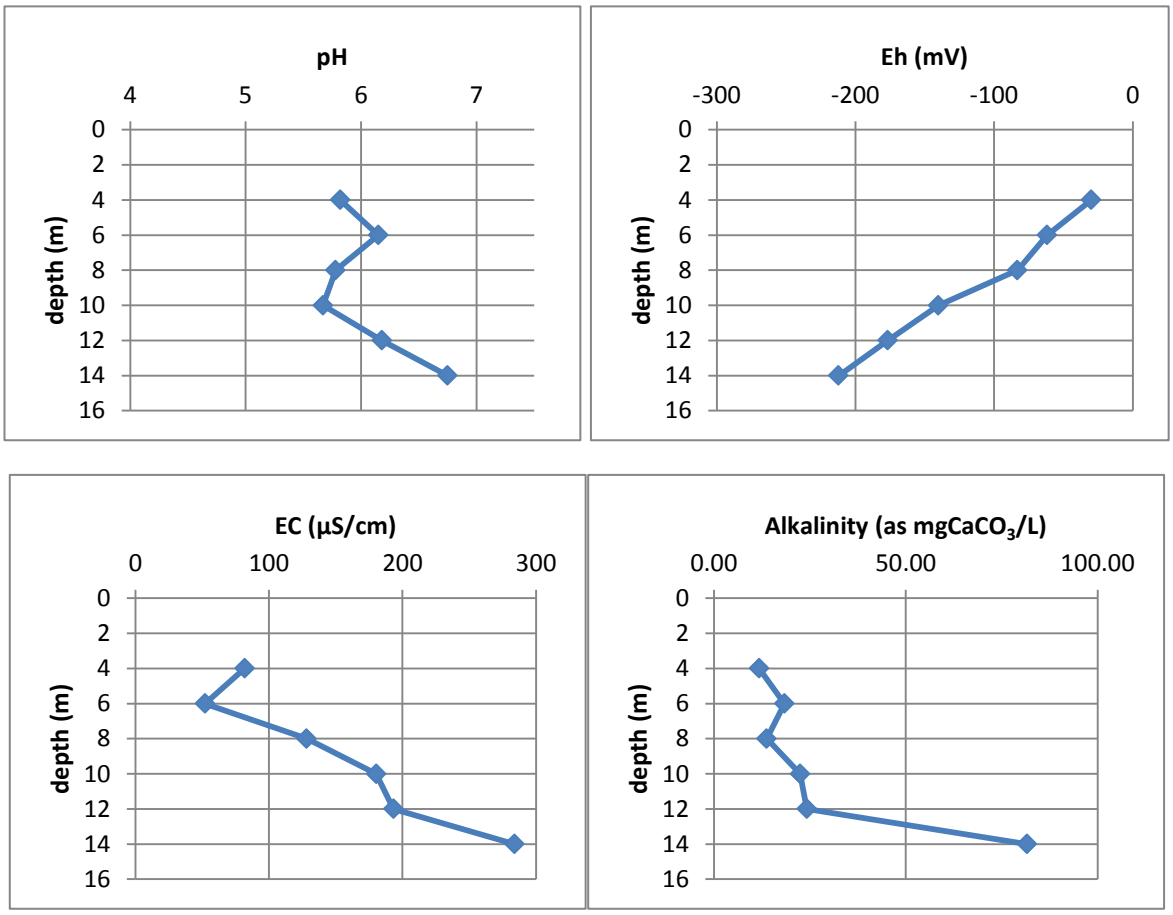

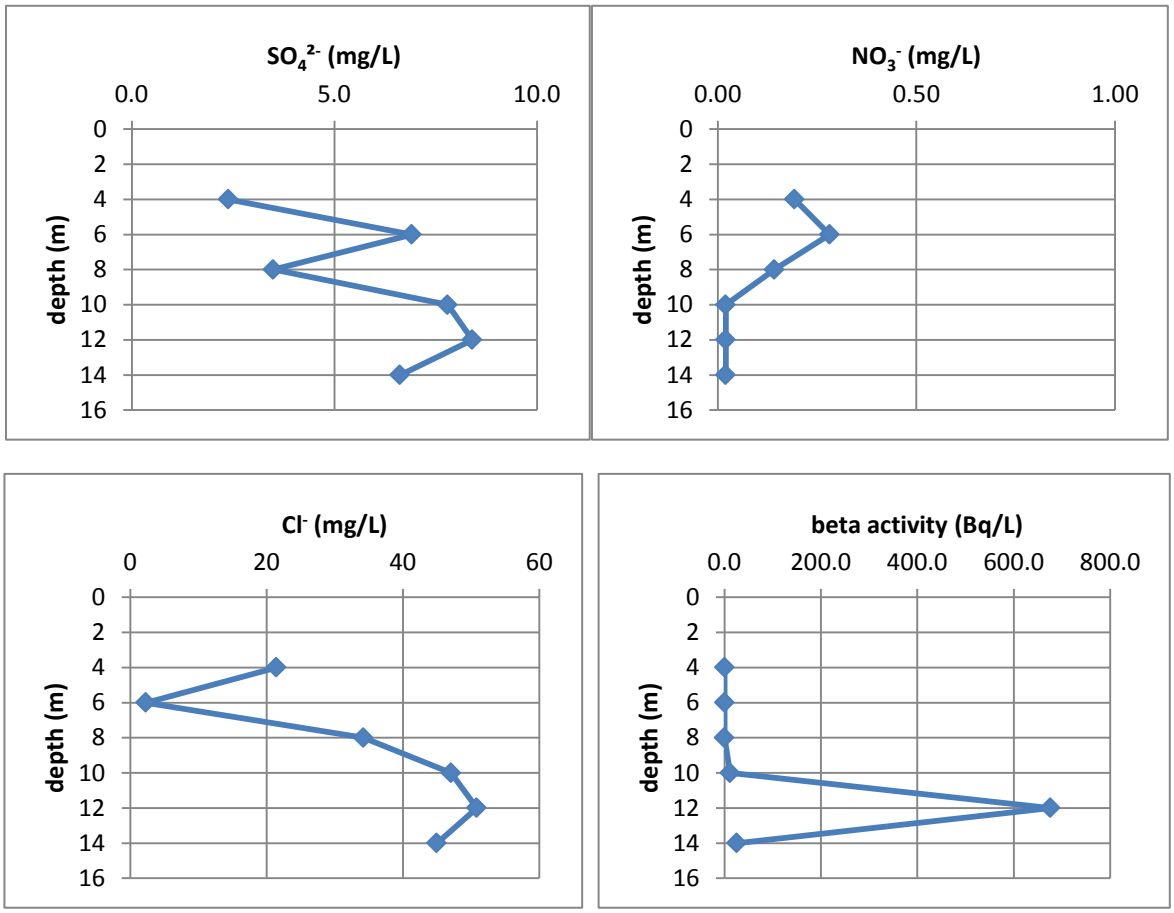

Figure A.1: Groundwater chemistry profiles for well C-281.

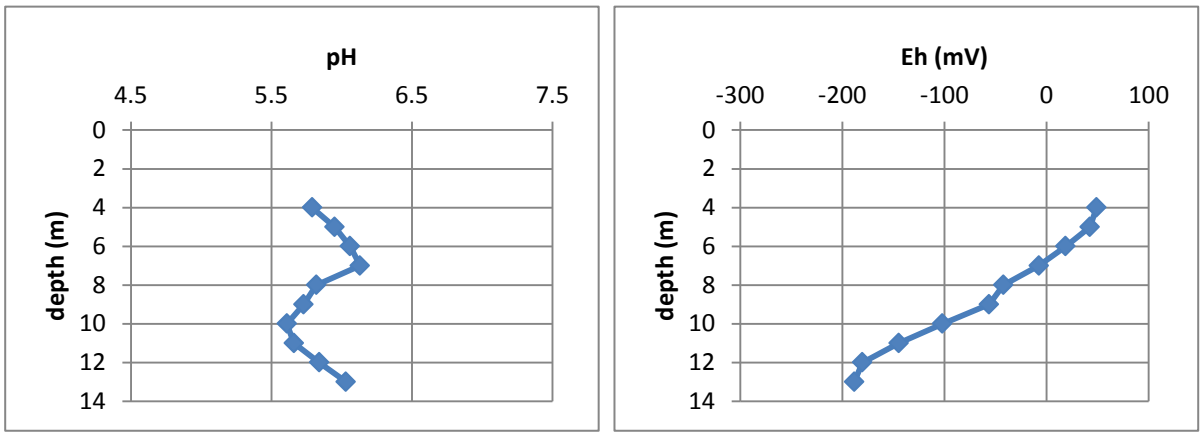

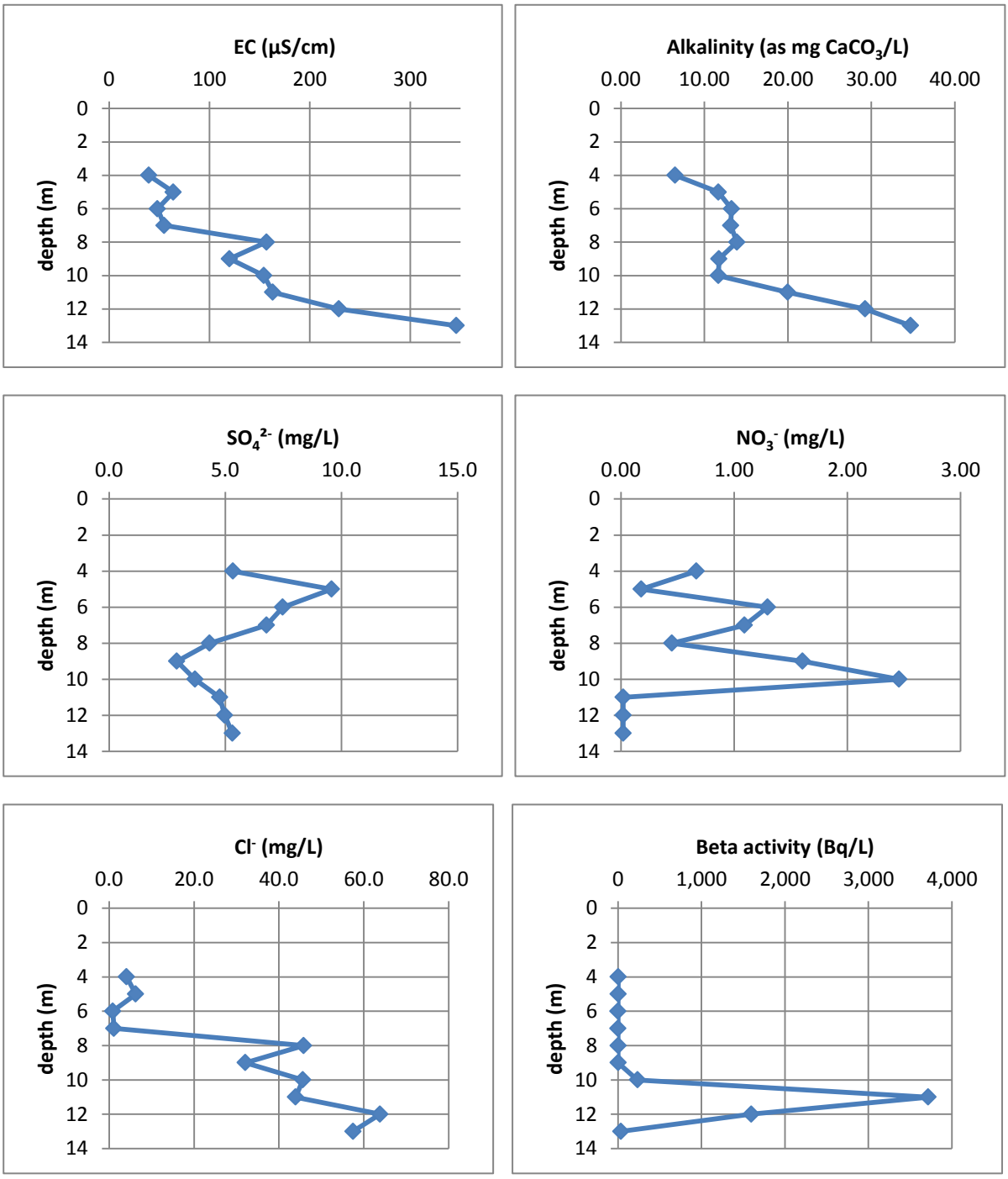

Figure A.2: Groundwater chemistry profiles of *in situ* measurements and anions for well WC-29.

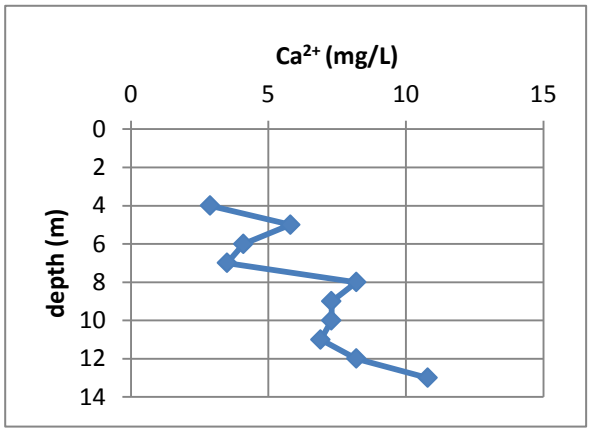
Ca2+ (mg/L)
0
5
10
15
depth (m)
0
2
4
6
8
10
12
14

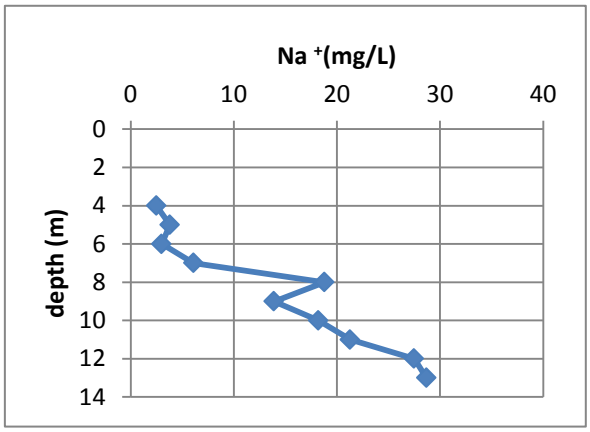
Na +(mg/L)
0
10
20
30
40
depth (m)
0
2
4
6
8
10
12
14

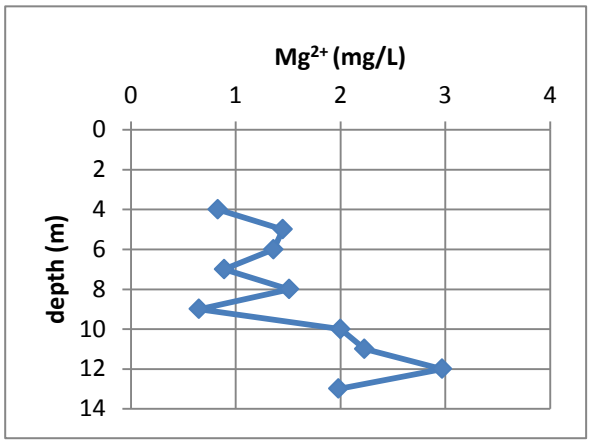
Mg2+ (mg/L)
0
1
2
3
4
depth (m)
0
2
4
6
8
10
12
14

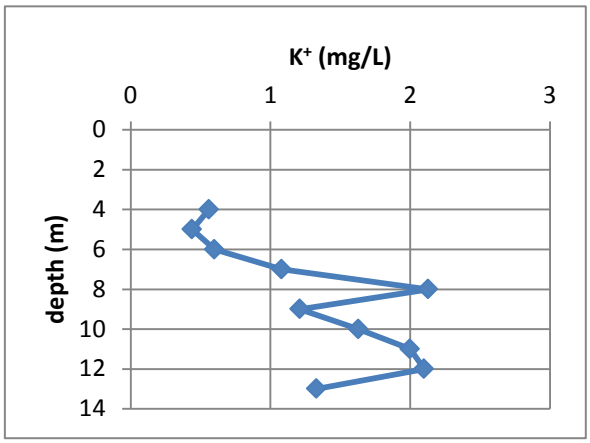
K+ (mg/L)
0
1
2
3
depth (m)
0
2
4
6
8
10
12
14

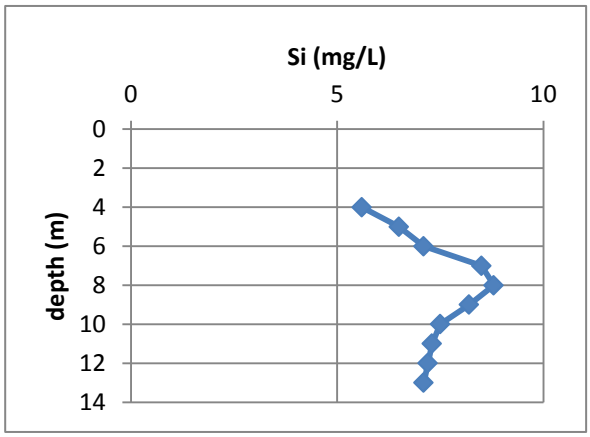
Si (mg/L)
0
5
10
depth (m)
0
2
4
6
8
10
12
14

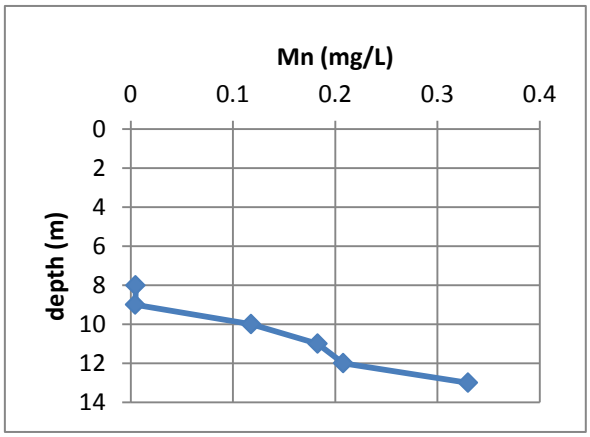
Mn (mg/L)
0
0.1
0.2
0.3
0.4
depth (m)
0
2
4
6
8
10
12
14

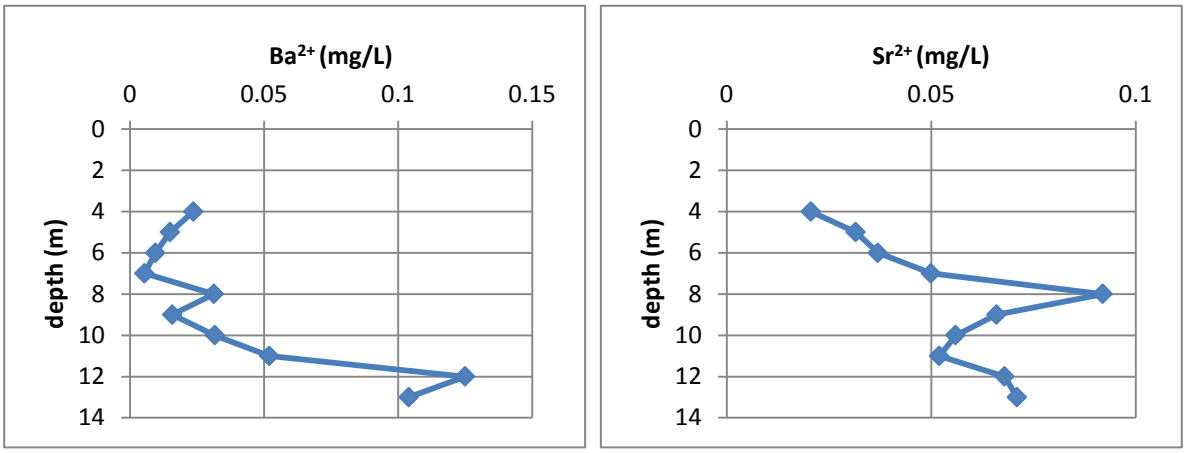

Figure A.3: Cation chemistry profiles for Well WC-29. Fe is not shown as it is only above detection limit at 12 and 13 m (7.4 mg/L).

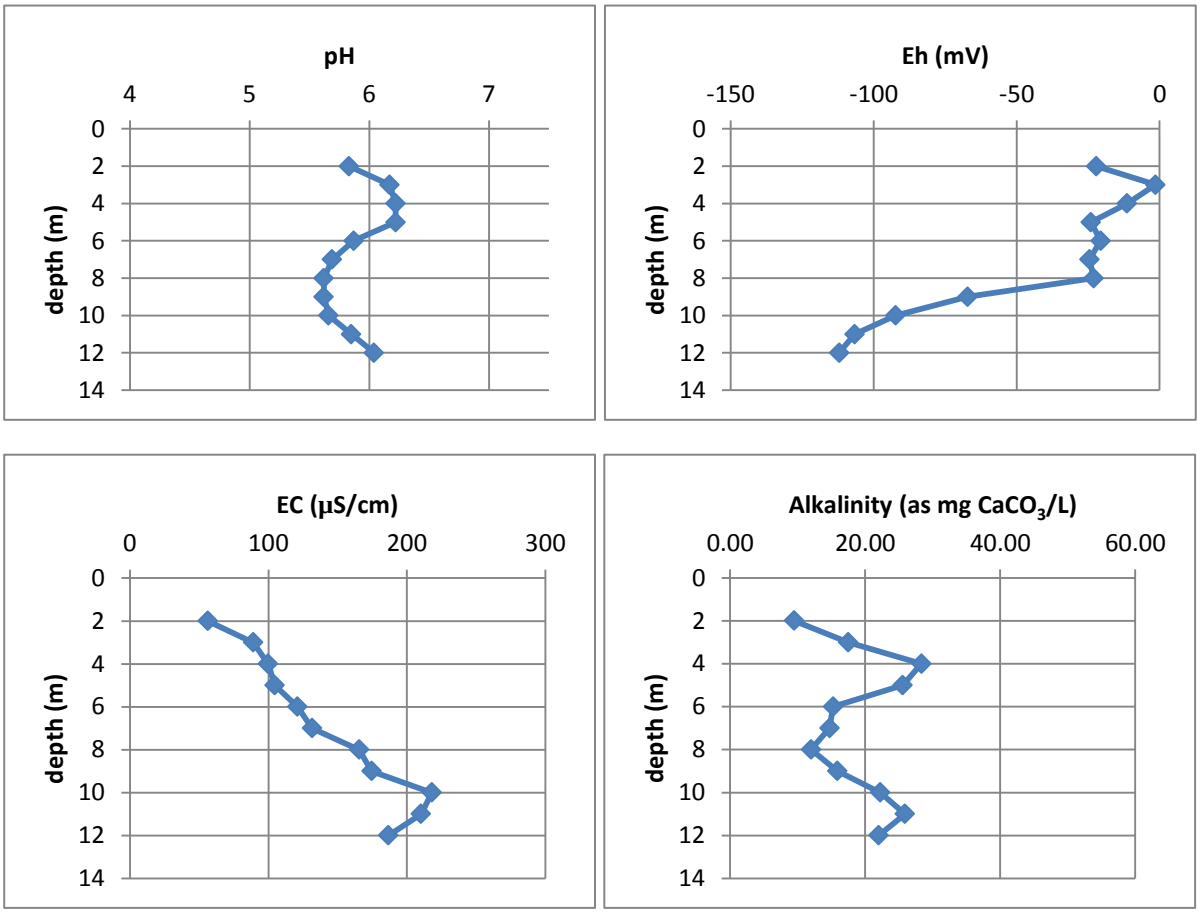

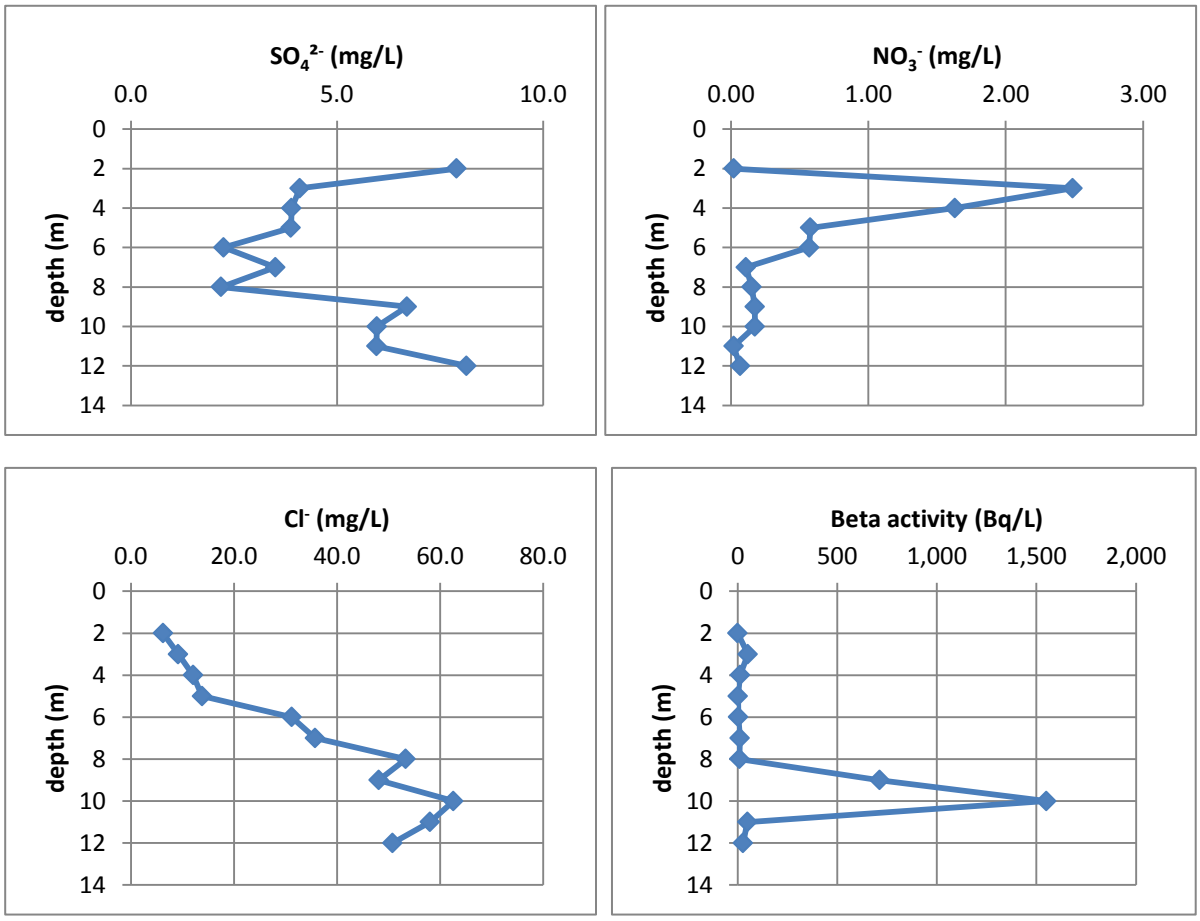

Figure A.4: Groundwater chemistry profiles of anions, *in situ* measurements and beta activity for well WC-30.

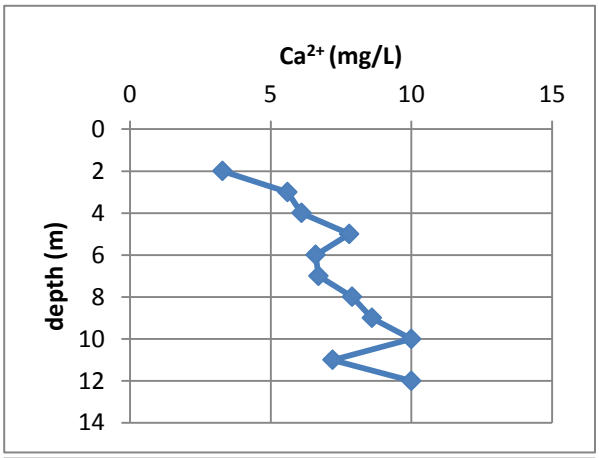
Ca2+ (mg/L)
0
5
10
15
depth (m)
0
2
4
6
8
10
12
14

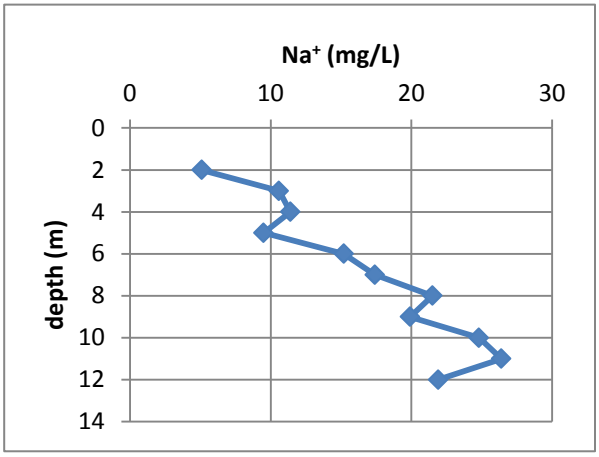
Na+ (mg/L)
0
10
20
30
depth (m)
0
2
4
6
8
10
12
14

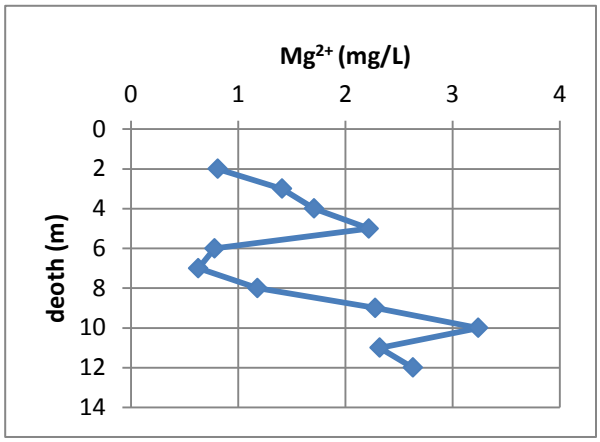
Mg2+ (mg/L)
0
1
2
3
4
deoth (m)
0
2
4
6
8
10
12
14

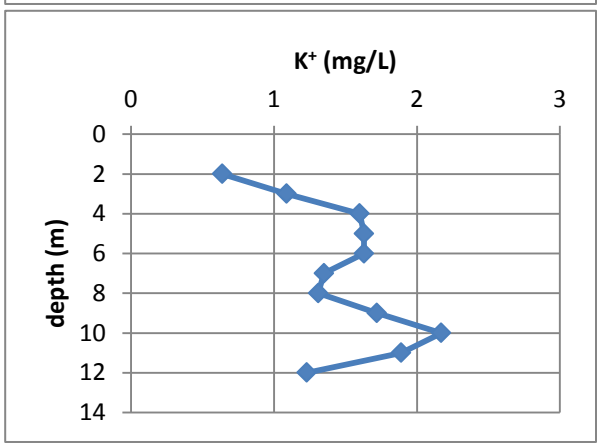
K+ (mg/L)
0
1
2
3
depth (m)
0
2
4
6
8
10
12
14

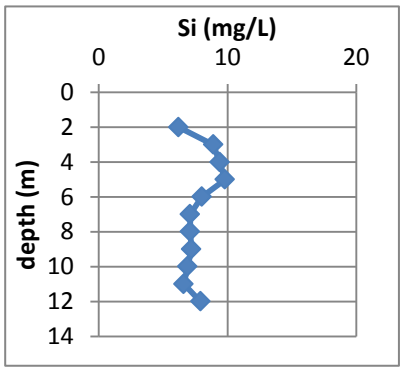
Si (mg/L)
0
10
20
depth (m)
0
2
4
6
8
10
12
14

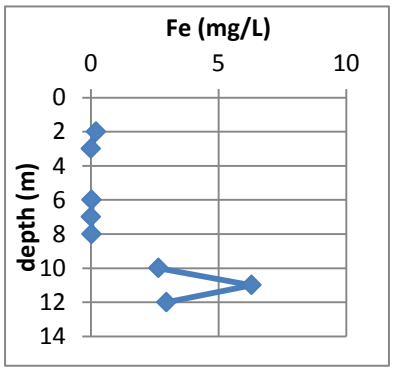
Fe (mg/L)
0
5
10
depth (m)
0
2
4
6
8
10
12
14

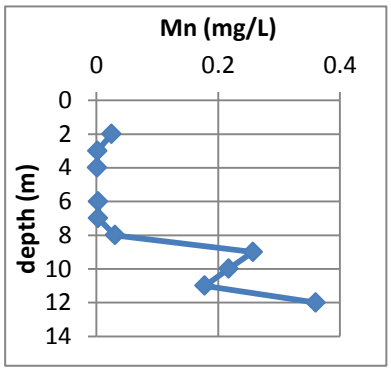
Mn (mg/L)
0
0.2
0.4
depth (m)
0
2
4
6
8
10
12
14

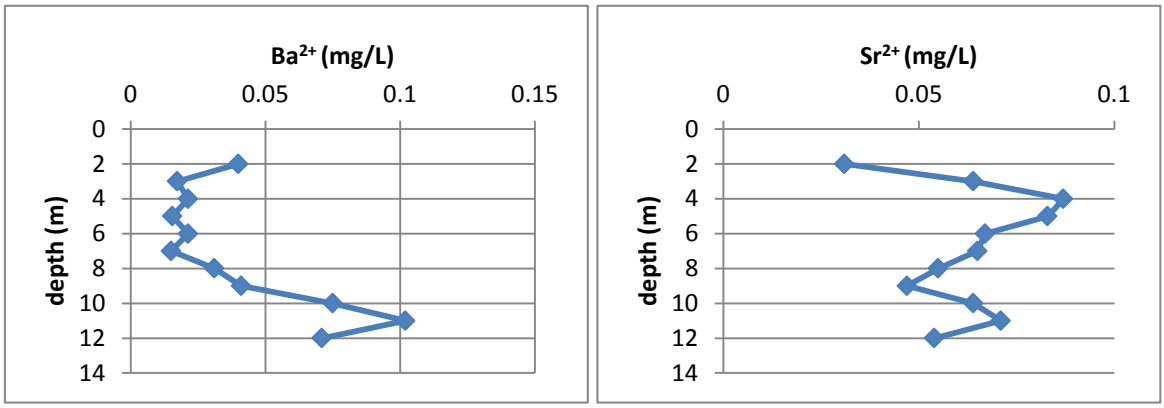

Figure A.5: Cation profiles for WC-30.

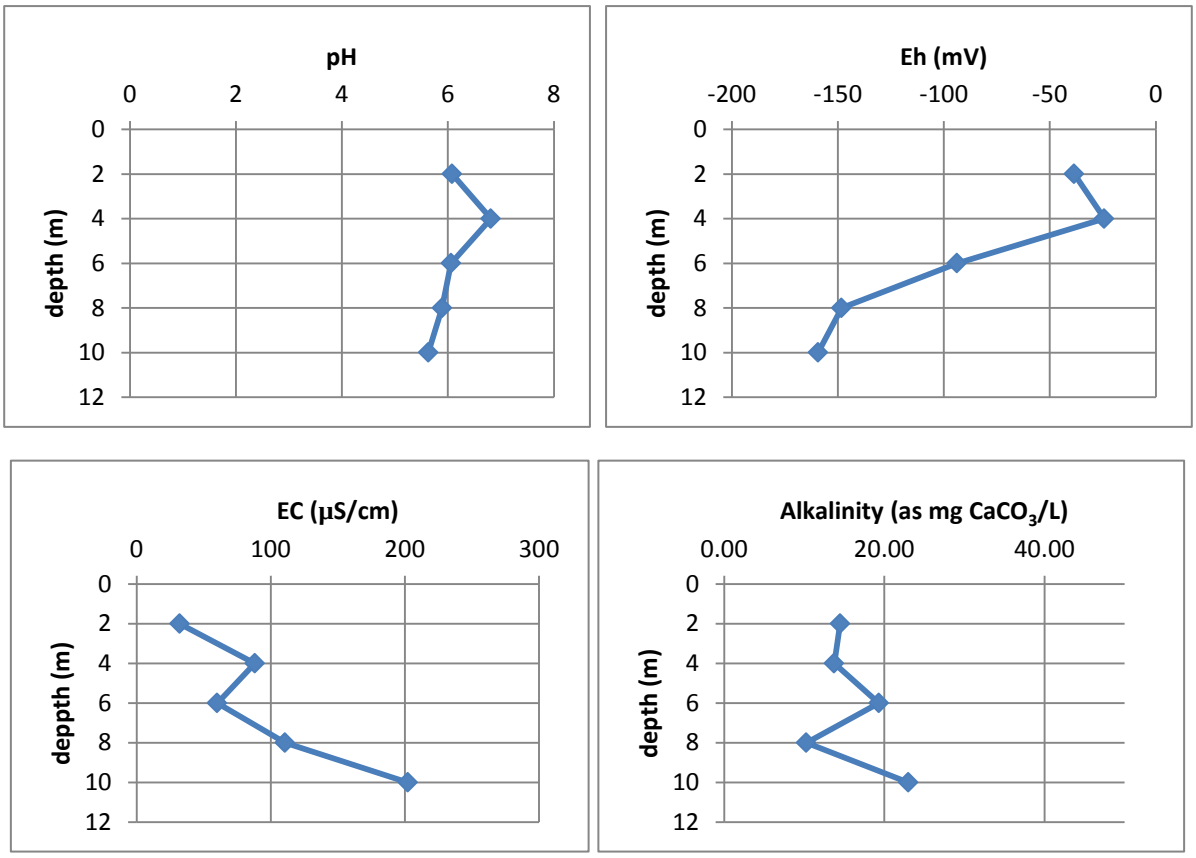

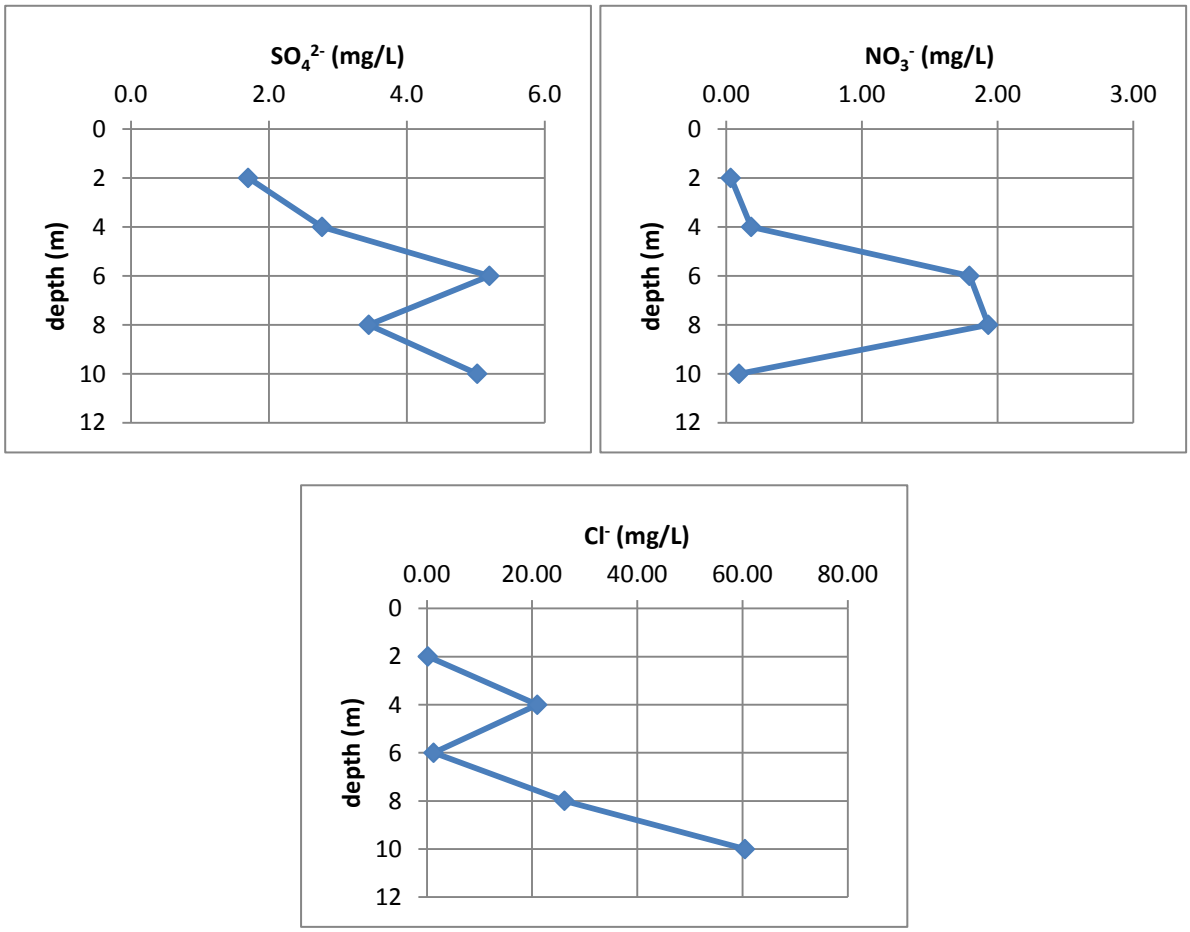

Figure A.6: Groundwater chemistry profiles for well C-279.

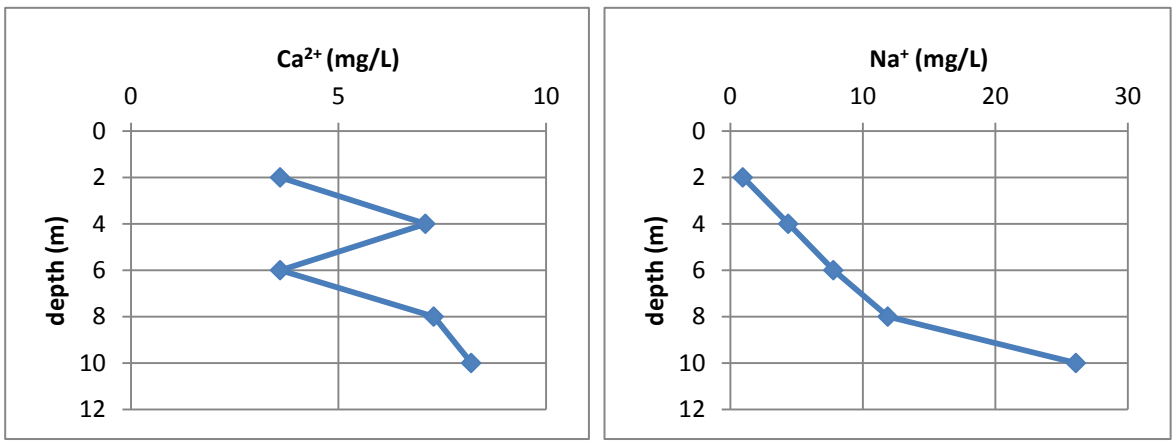

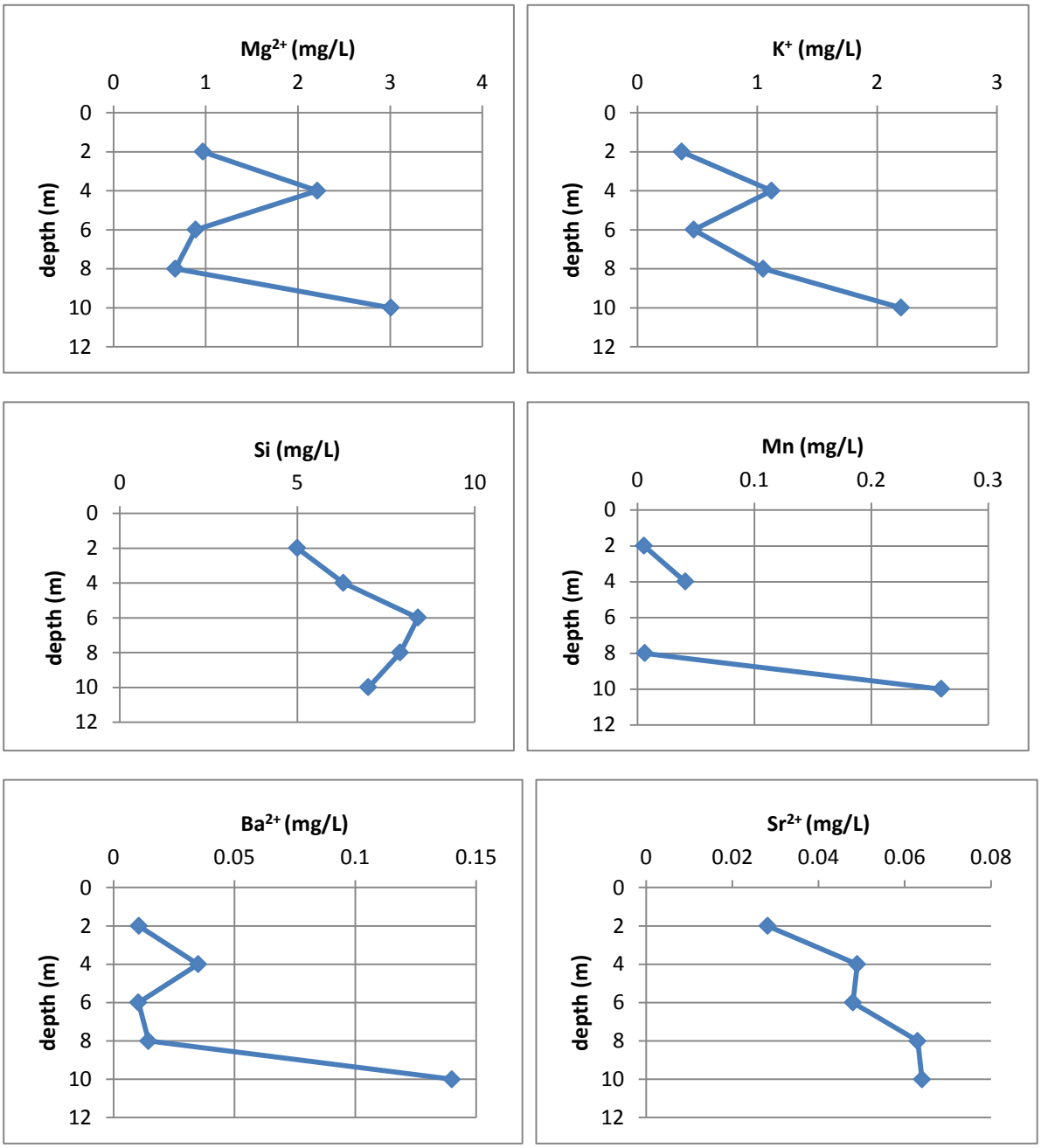

Figure A.7: cation profiles for C-279. Fe profile is not shown as the only data point is 1 mg/L at a depth of 10 m.

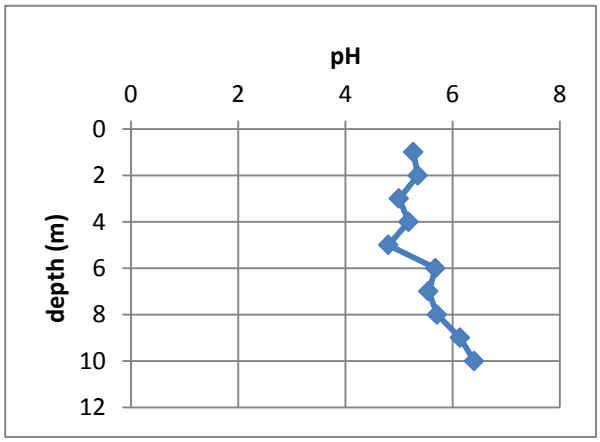
pH
0
2
4
6
8
depth (m)
0
2
4
6
8
10
12

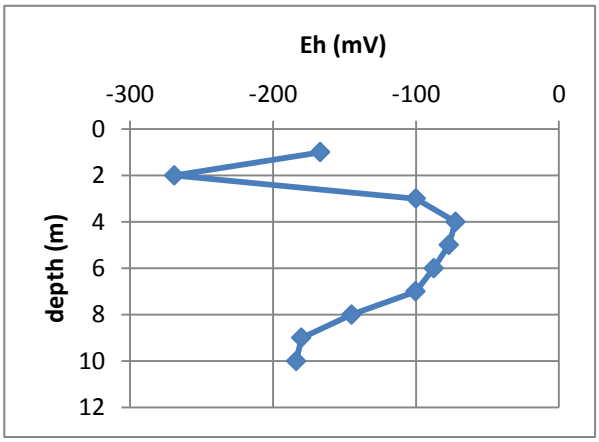
Eh (mV)
-300
-200
-100
0
depth (m)
0
2
4
6
8
10
12

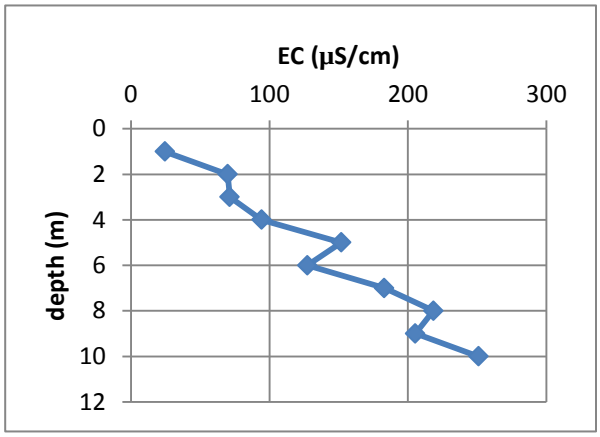
EC (µS/cm)
0
100
200
300
depth (m)
0
2
4
6
8
10
12

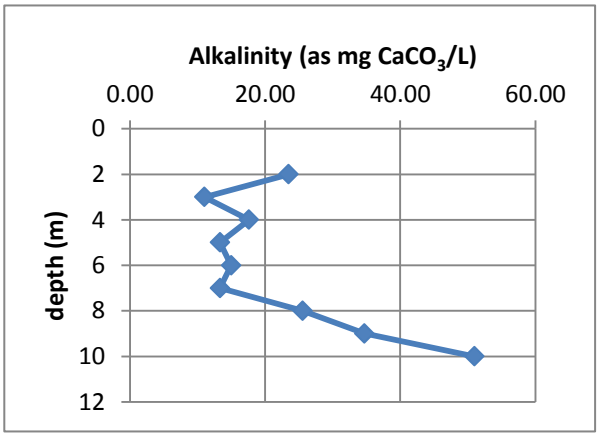
Alkalinity (as mg CaCO3/L)
0.00
20.00
40.00
60.00
depth (m)
0
2
4
6
8
10
12

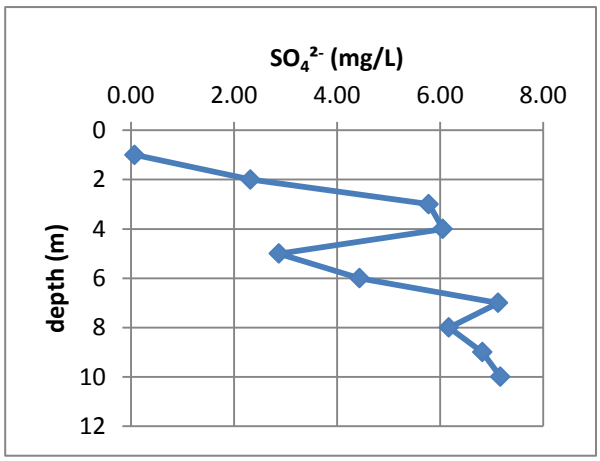
SO4 2- (mg/L)
0.00
2.00
4.00
6.00
8.00
depth (m)
0
2
4
6
8
10
12

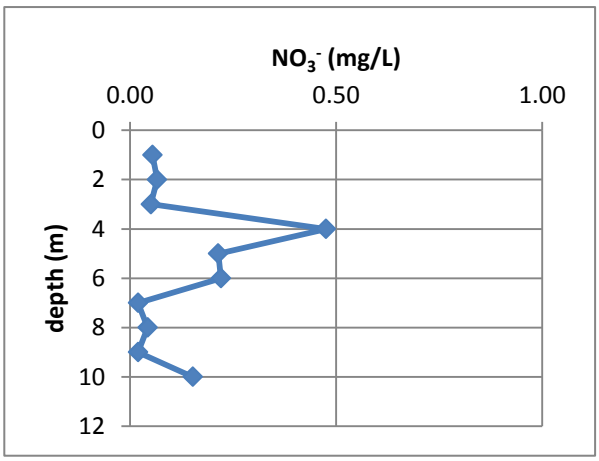
NO3 - (mg/L)
0.00
0.50
1.00
depth (m)
0
2
4
6
8
10
12

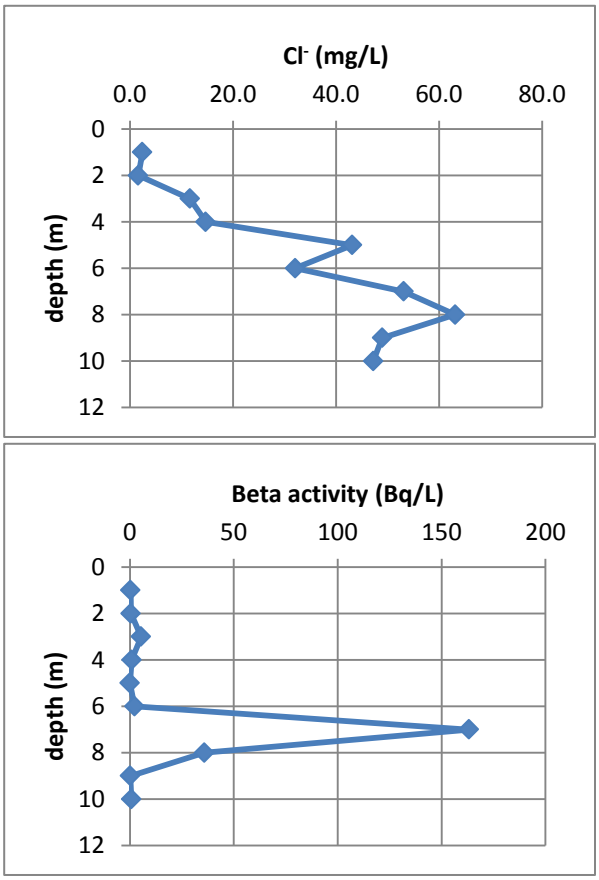

Figure A.8: Groundwater chemistry profiles of anions, *in situ* measurements and beta activity for well WC-90.

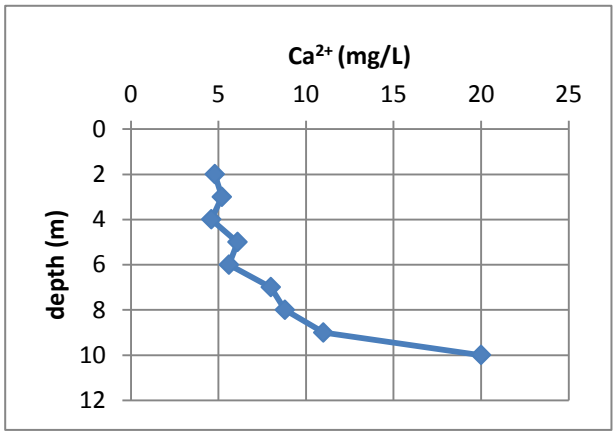
Ca2+ (mg/L)
0
5
10
15
20
25
depth (m)
0
2
4
6
8
10
12

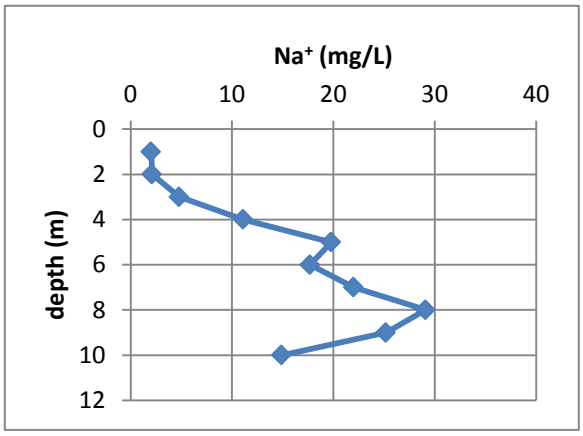
Na+ (mg/L)
0
10
20
30
40
depth (m)
0
2
4
6
8
10
12

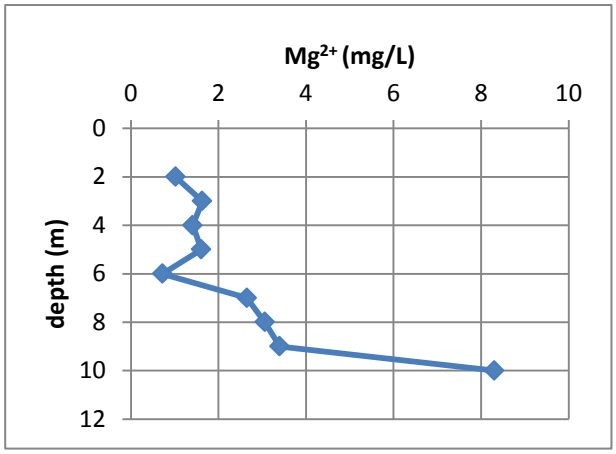
Mg2+ (mg/L)
0
2
4
6
8
10
depth (m)
0
2
4
6
8
10
12

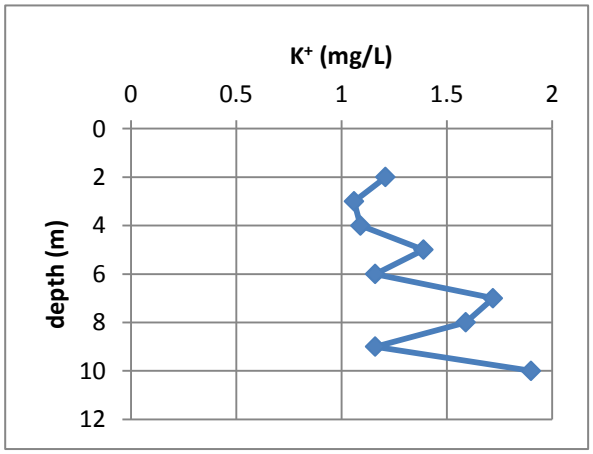
K+ (mg/L)
0
0.5
1
1.5
2
depth (m)
0
2
4
6
8
10
12

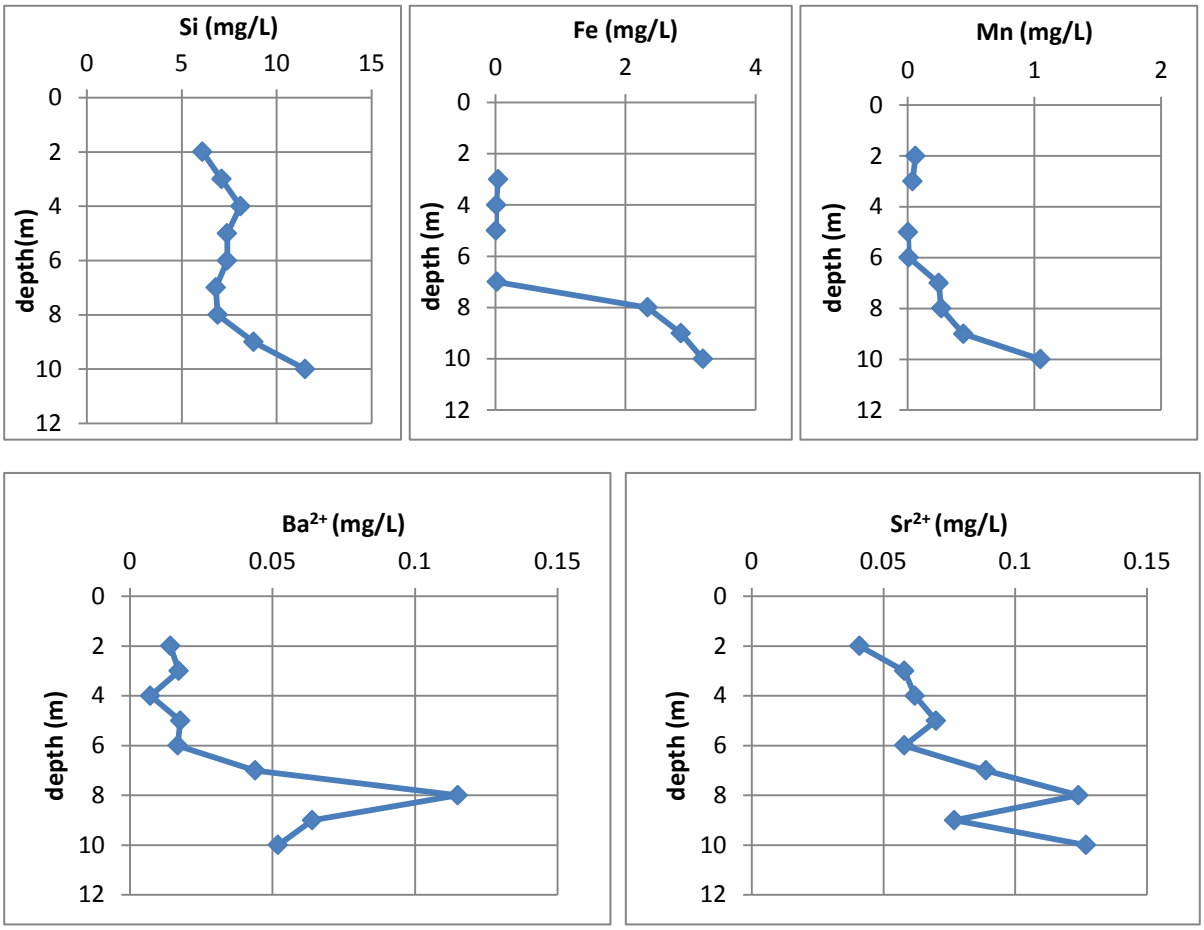

Figure A.9: Cation profiles for WC-90.

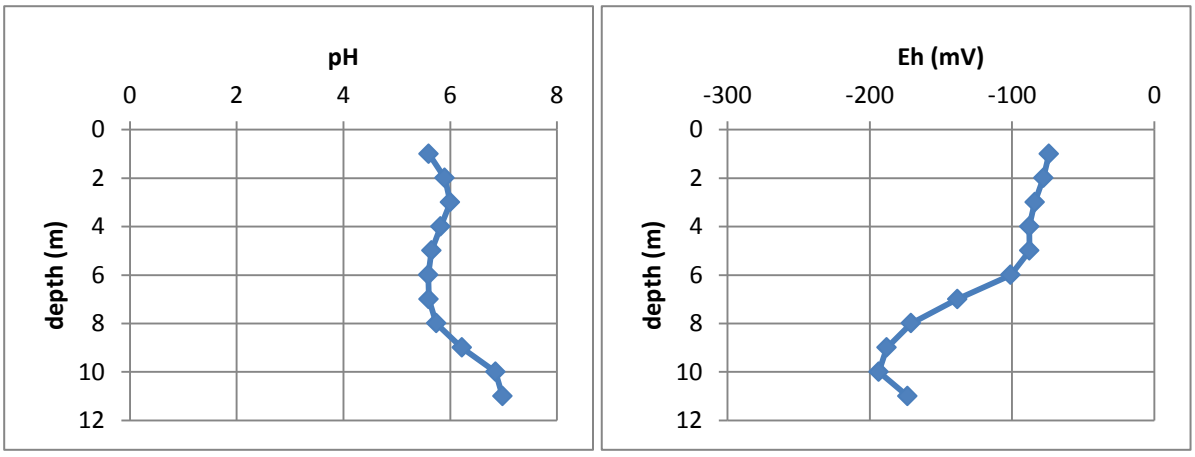

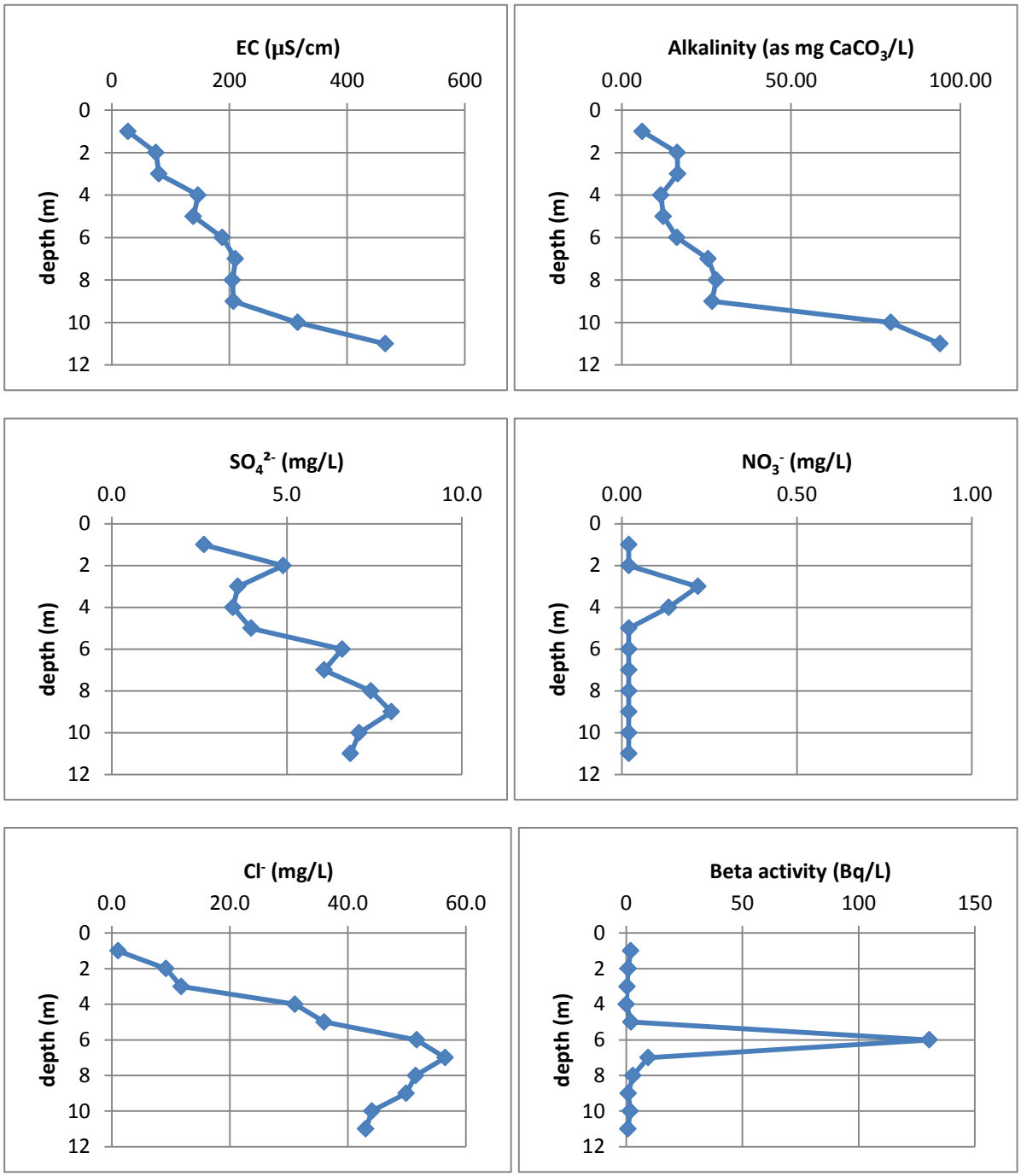

Figure A.10: Groundwater chemistry profiles of anions, *in situ* measurements and beta activity for well WC-70.

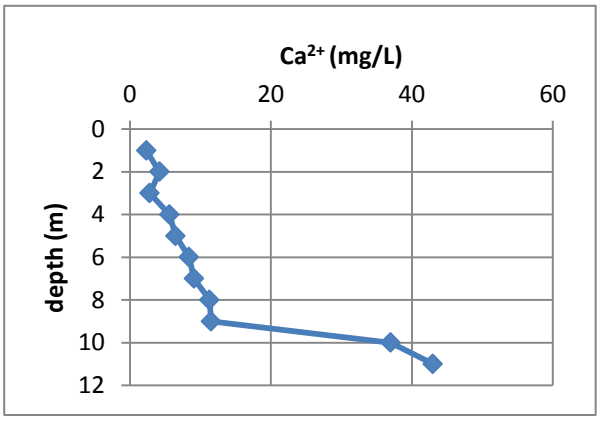
Ca2+ (mg/L)
0
20
40
60
depth (m)
0
2
4
6
8
10
12

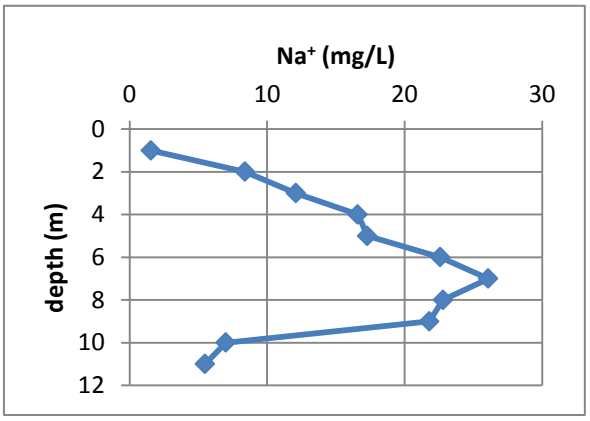
Na+ (mg/L)
0
10
20
30
depth (m)
0
2
4
6
8
10
12

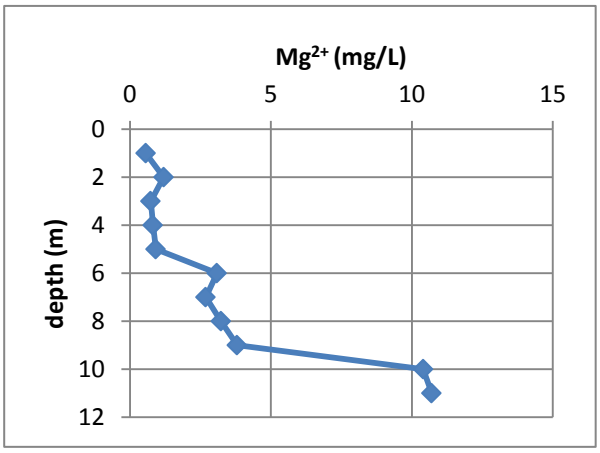
Mg2+ (mg/L)
0
5
10
15
depth (m)
0
2
4
6
8
10
12

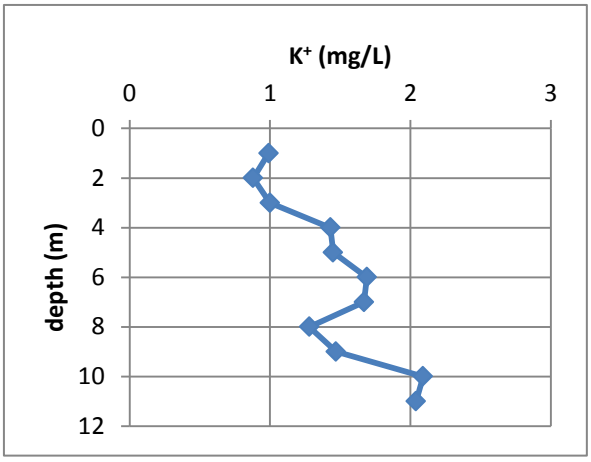
K+ (mg/L)
0
1
2
3
depth (m)
0
2
4
6
8
10
12

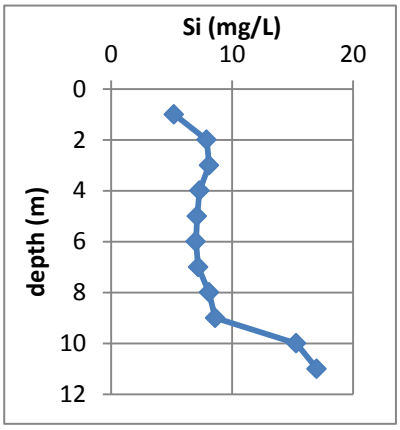
Si (mg/L)
0
10
20
depth (m)
0
2
4
6
8
10
12

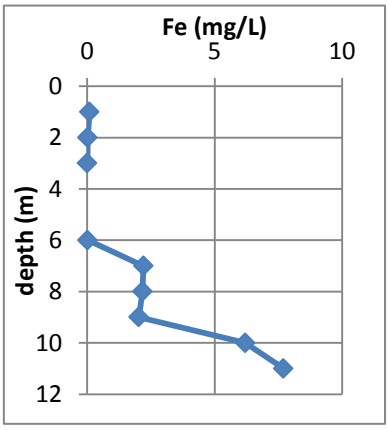
Fe (mg/L)
0
5
10
depth (m)
0
2
4
6
8
10
12

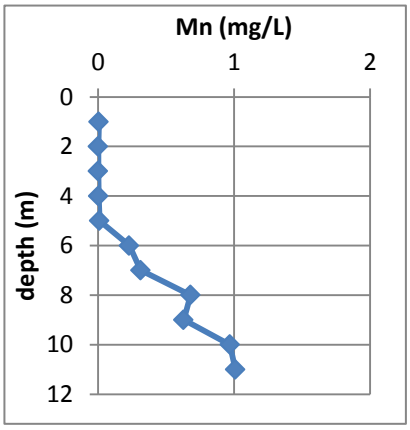
Mn (mg/L)
0
1
2
depth (m)
0
2
4
6
8
10
12

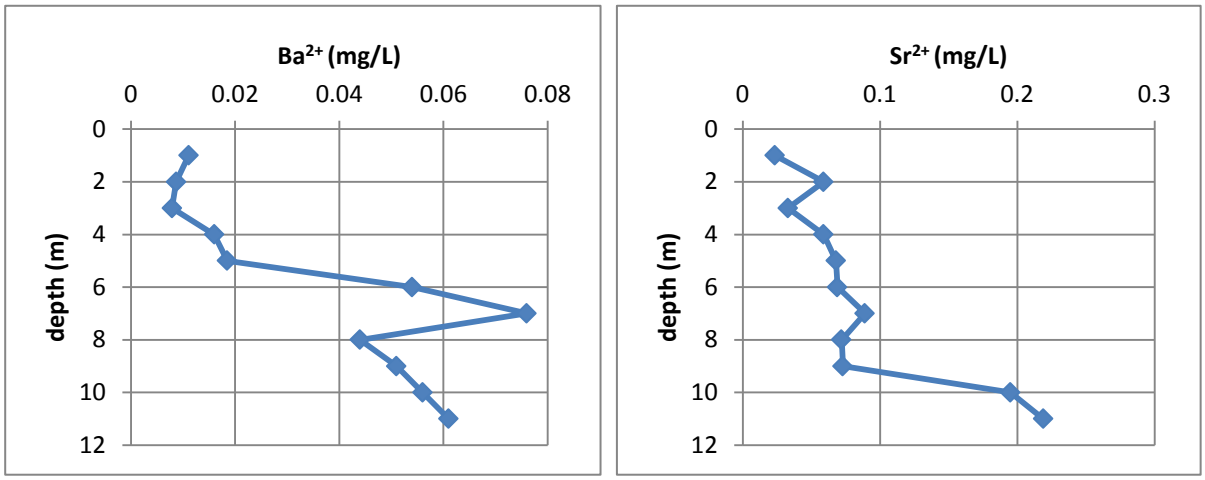

Figure A.11: Cation profiles for WC-70.

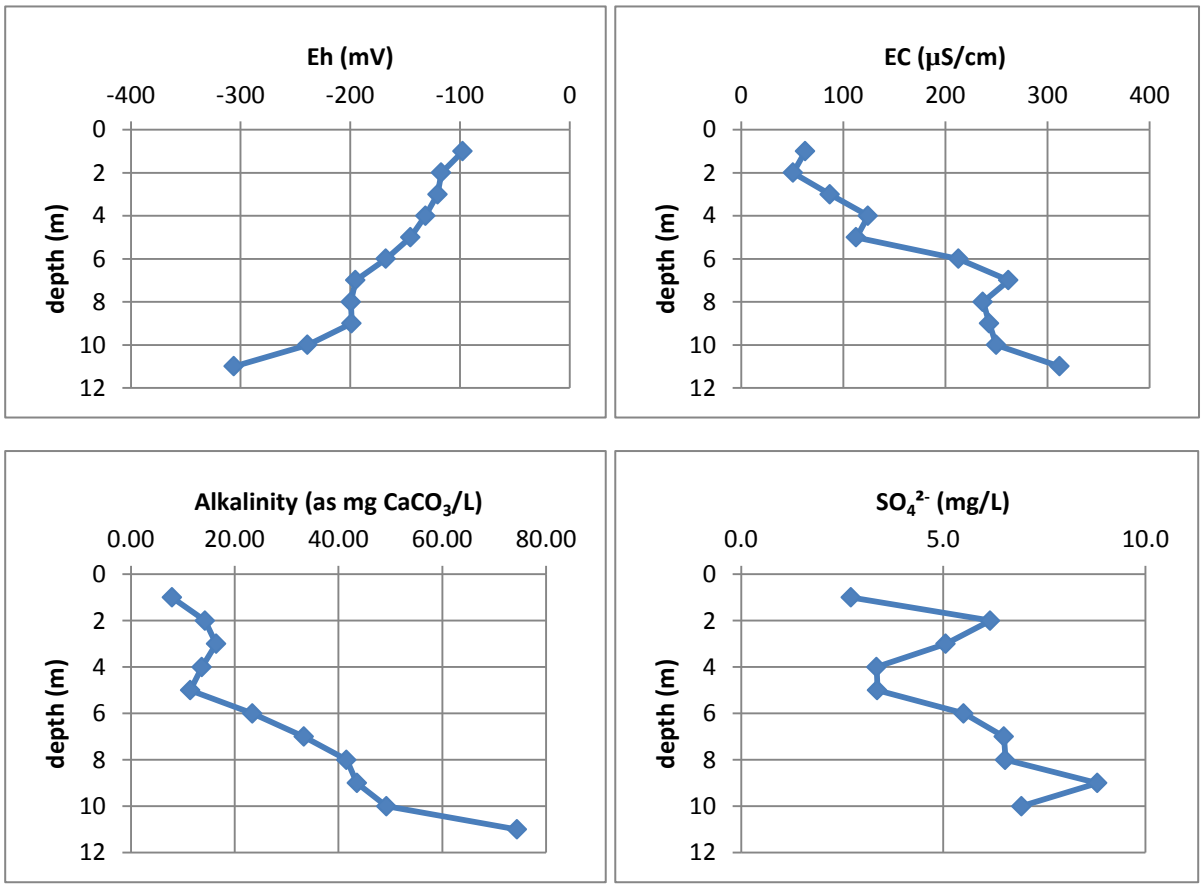

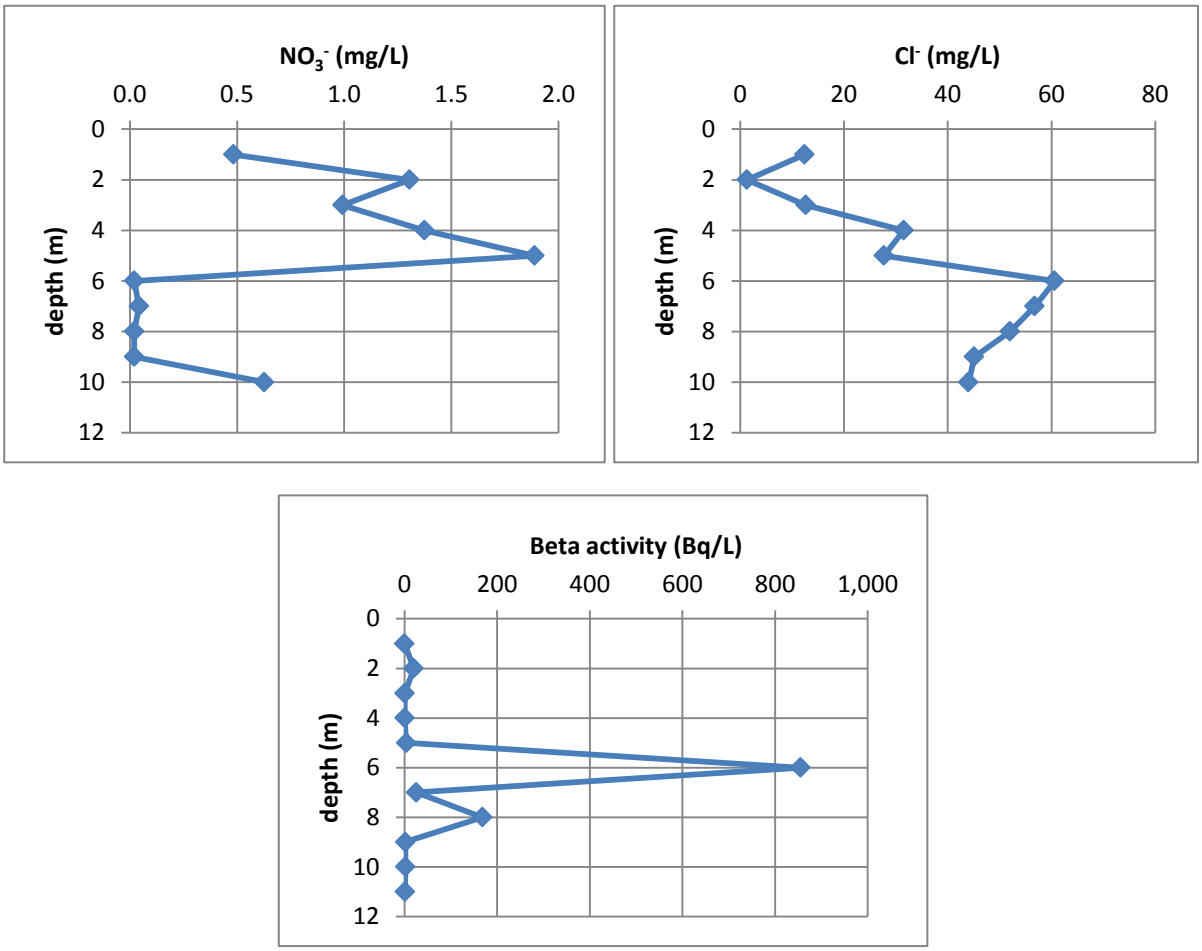

Figure A.12: Groundwater chemistry profiles of anions, *in situ* measurement and beta activity for well WC-68.

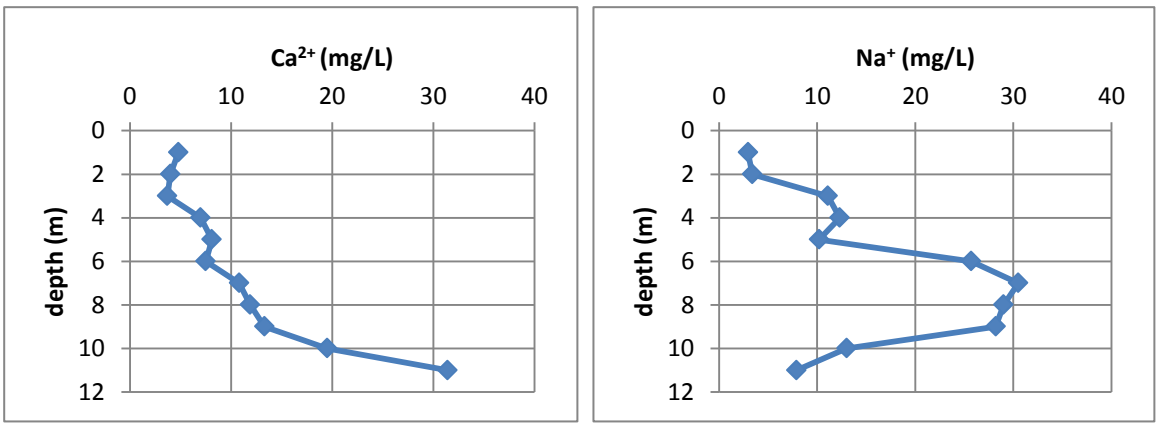

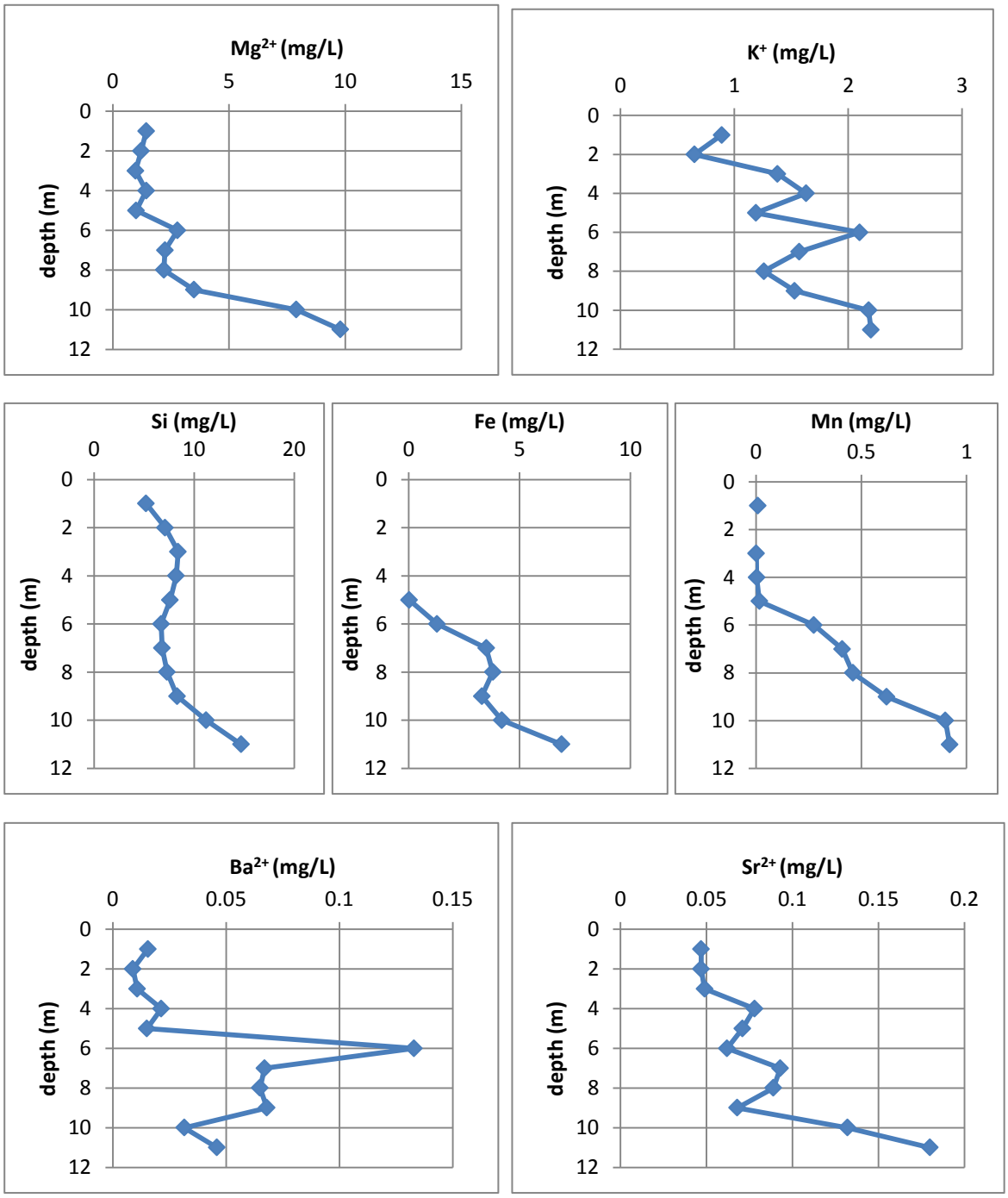

Figure A.13: Cation profiles for WC-68.

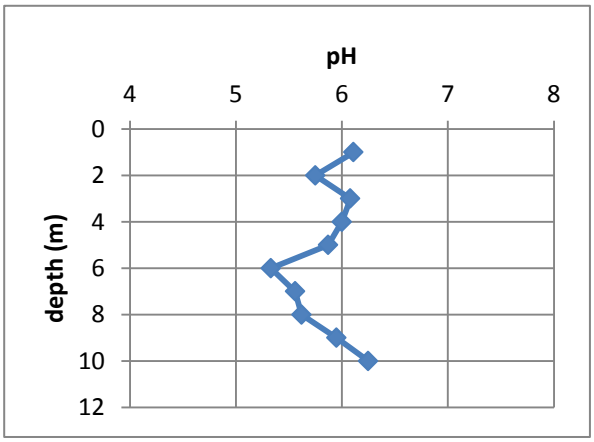
pH
4
5
6
7
8
depth (m)
0
2
4
6
8
10
12

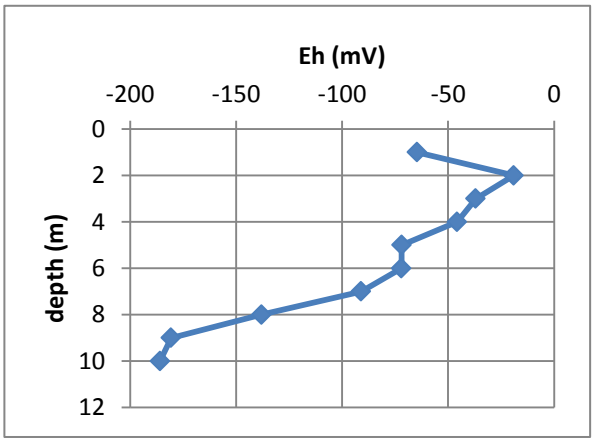
Eh (mV)
-200
-150
-100
-50
0
depth (m)
0
2
4
6
8
10
12

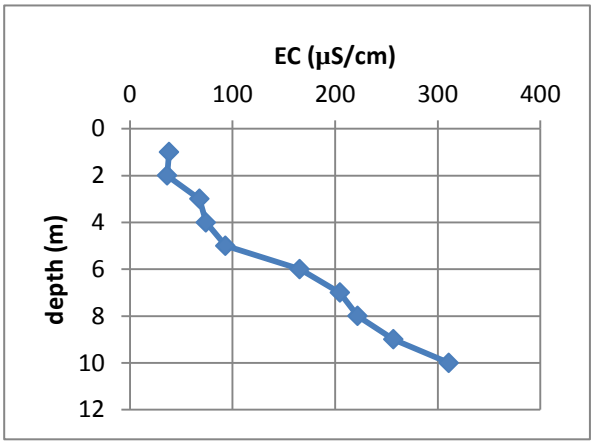
EC (µS/cm)
0
100
200
300
400
depth (m)
0
2
4
6
8
10
12

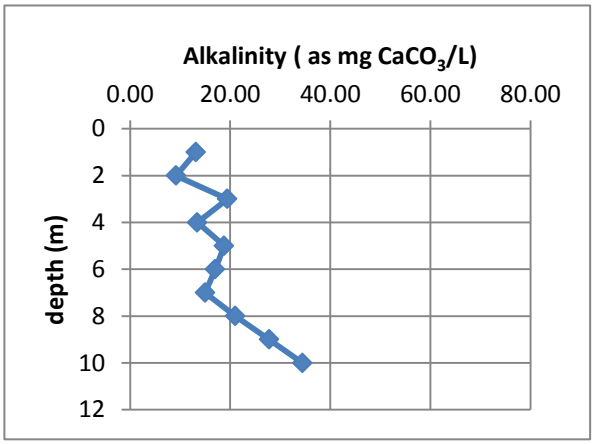
Alkalinity (as mg CaCO3/L)
0.00
20.00
40.00
60.00
80.00
depth (m)
0
2
4
6
8
10
12

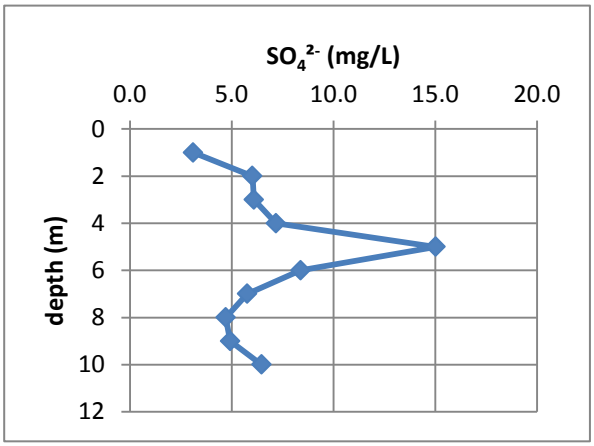
SO4 2- (mg/L)
0.0
5.0
10.0
15.0
20.0
depth (m)
0
2
4
6
8
10
12

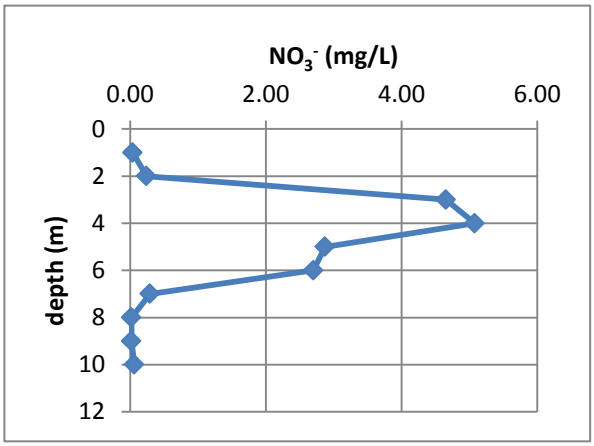
NO3 - (mg/L)
0.00
2.00
4.00
6.00
depth (m)
0
2
4
6
8
10
12

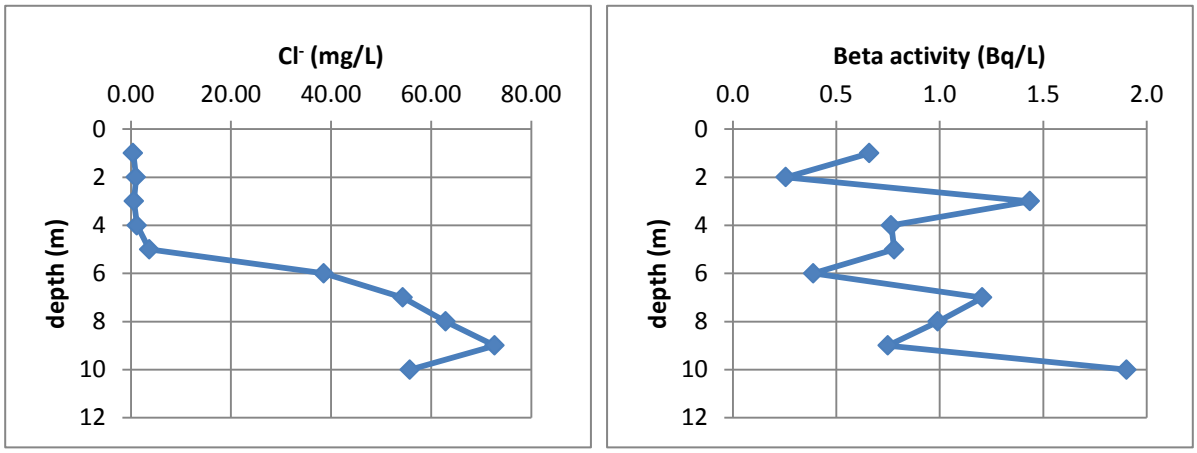

Figure A.14: Groundwater chemistry profiles of anions, *in situ* measurement and beta activity for well WC-65.

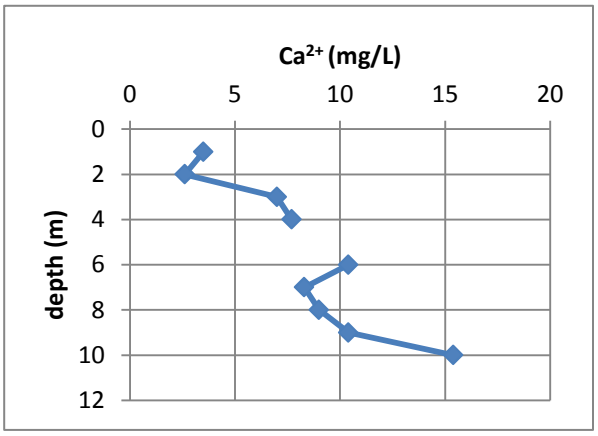
Ca2+ (mg/L)
0
5
10
15
20
depth (m)
0
2
4
6
8
10
12

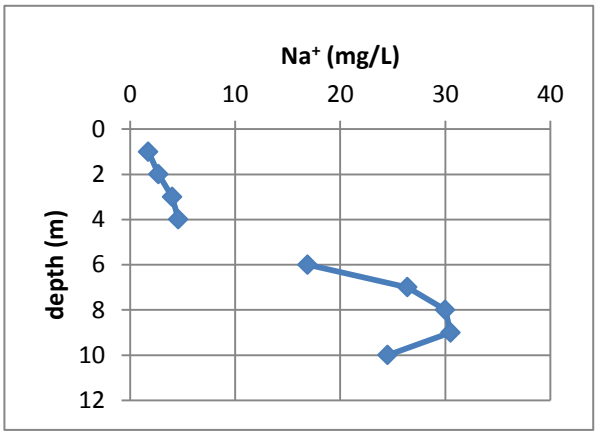
Na+ (mg/L)
0
10
20
30
40
depth (m)
0
2
4
6
8
10
12

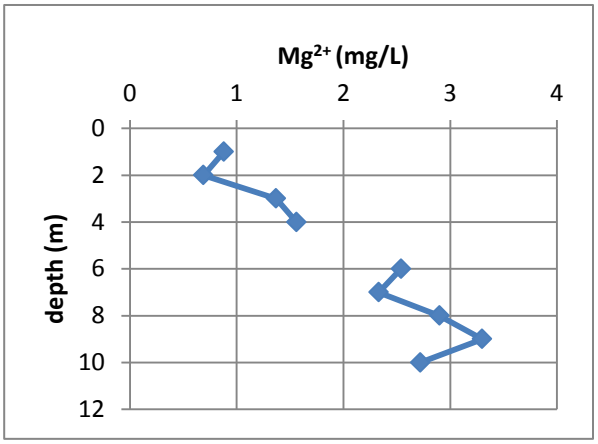
Mg2+ (mg/L)
0
1
2
3
4
depth (m)
0
2
4
6
8
10
12

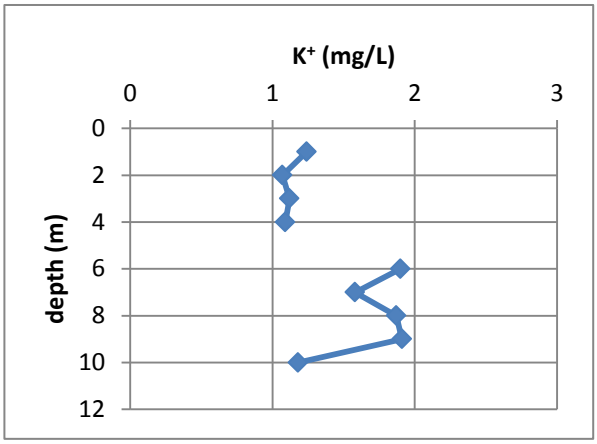
K+ (mg/L)
0
1
2
3
depth (m)
0
2
4
6
8
10
12

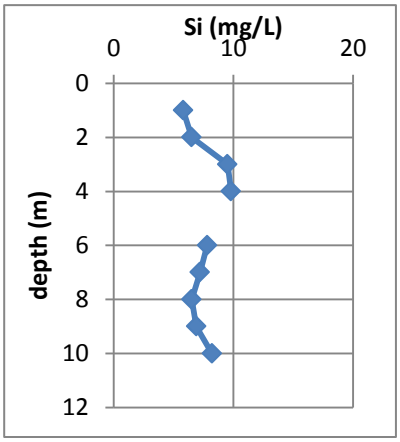
Si (mg/L)
0
10
20
depth (m)
0
2
4
6
8
10
12

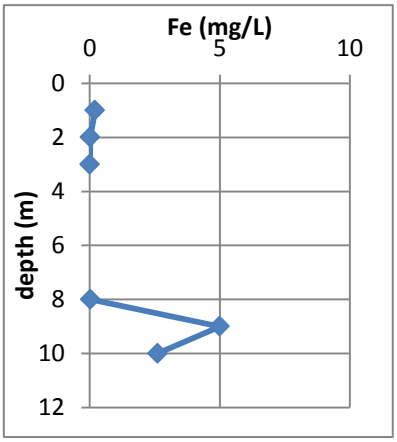
Fe (mg/L)
0
5
10
depth (m)
0
2
4
6
8
10
12

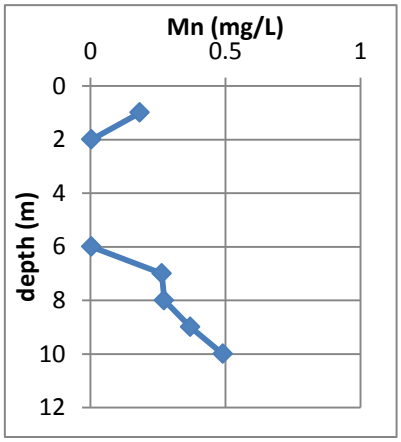
Mn (mg/L)
0
0.5
1
depth (m)
0
2
4
6
8
10
12

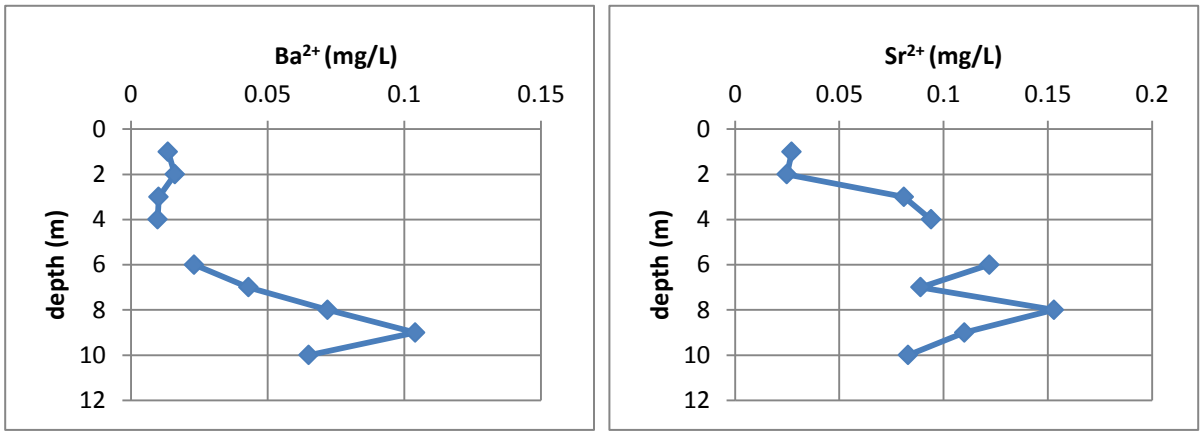

Figure A.15: Cation profiles for WC-65.

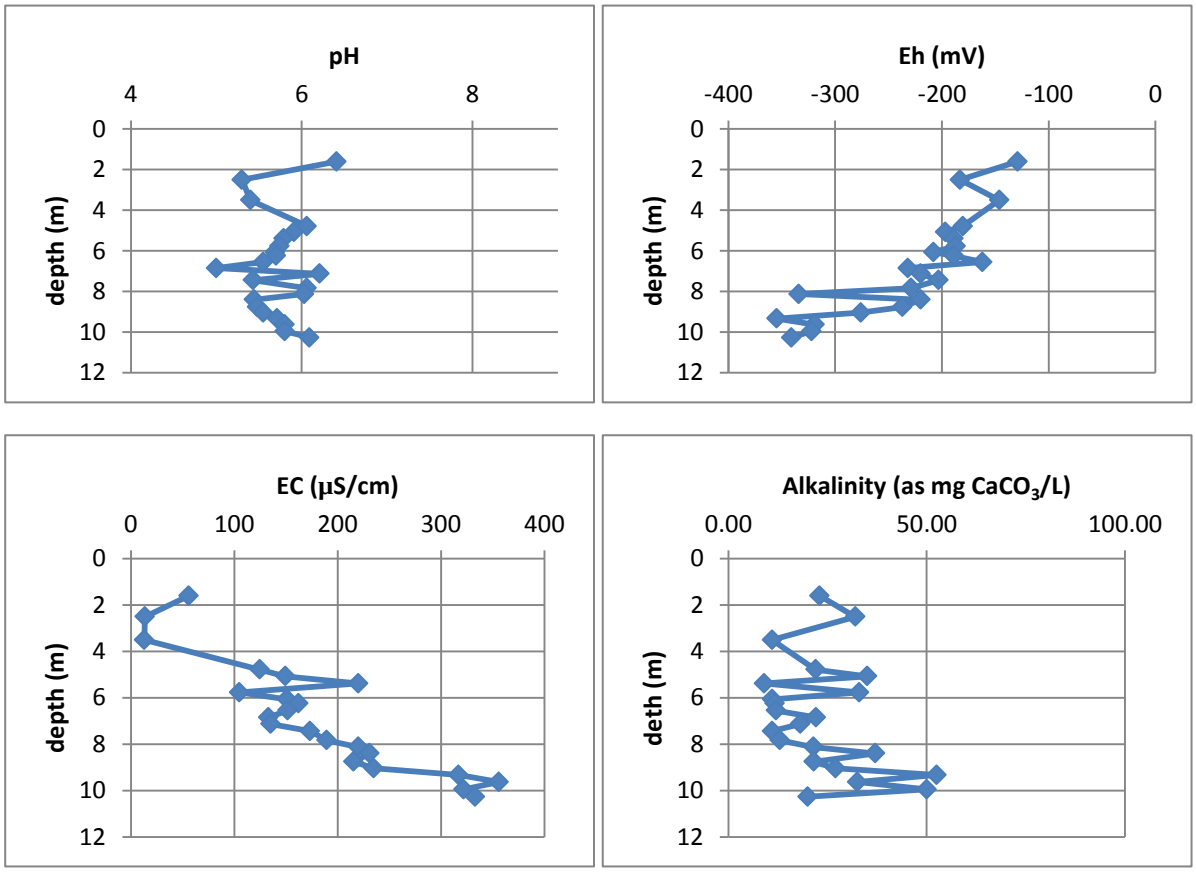

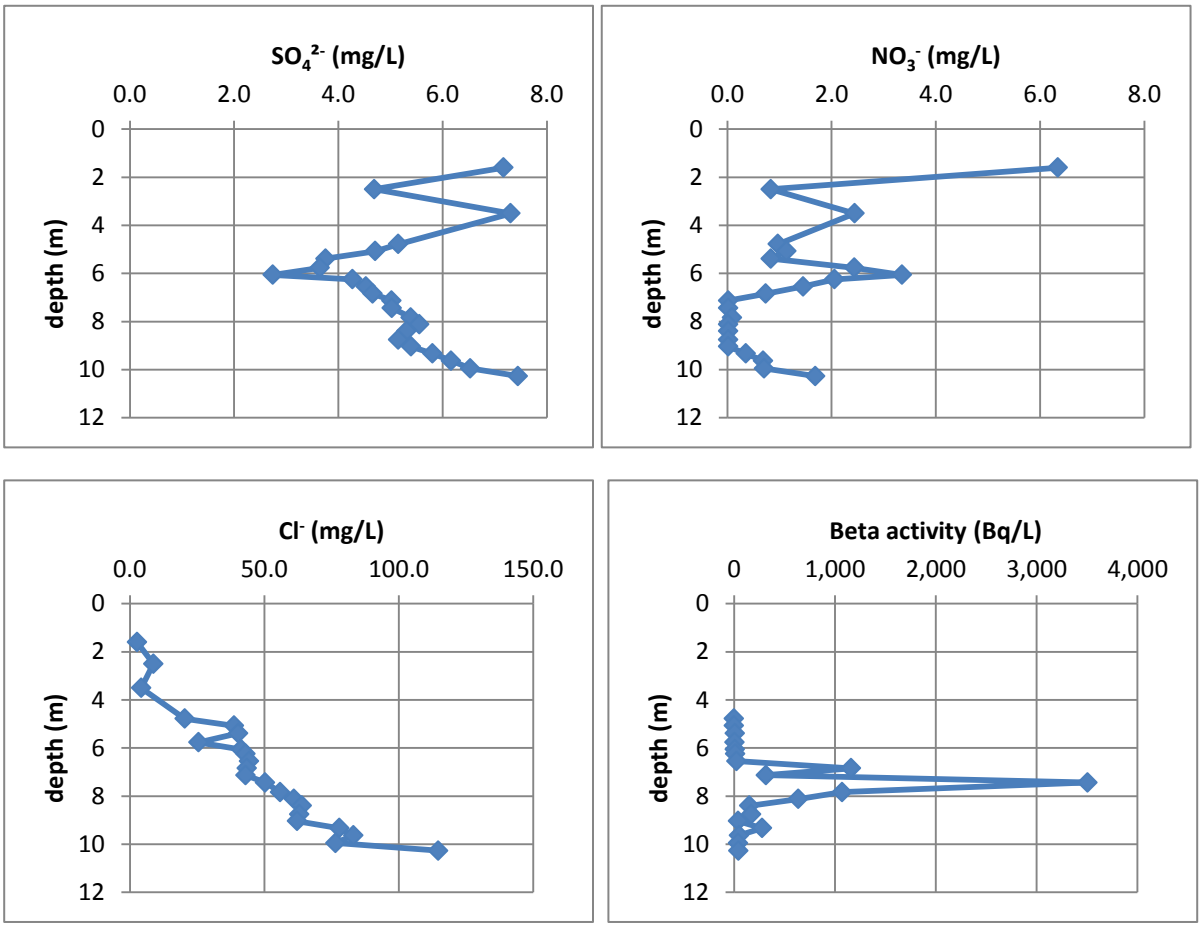

Figure A.16: Groundwater chemistry profiles of anions, *in situ* measurements and beta activity for drive-point piezometer DP-1.

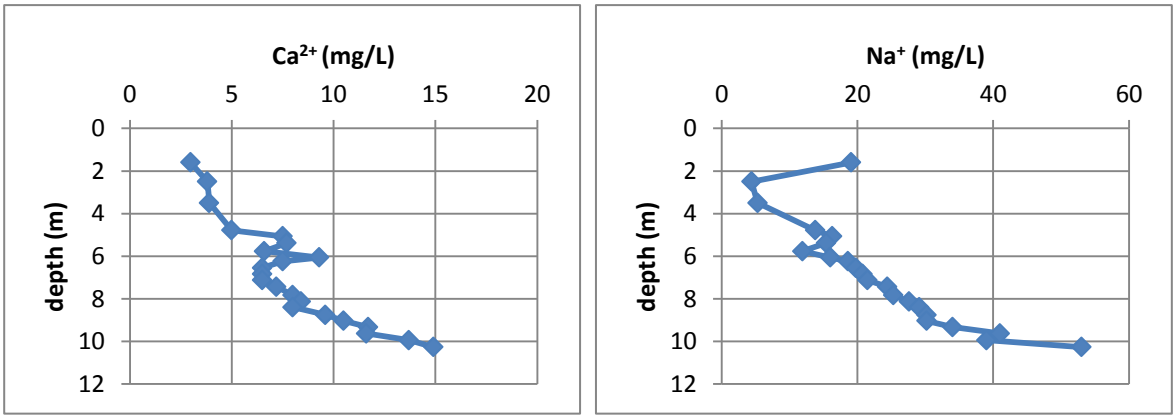

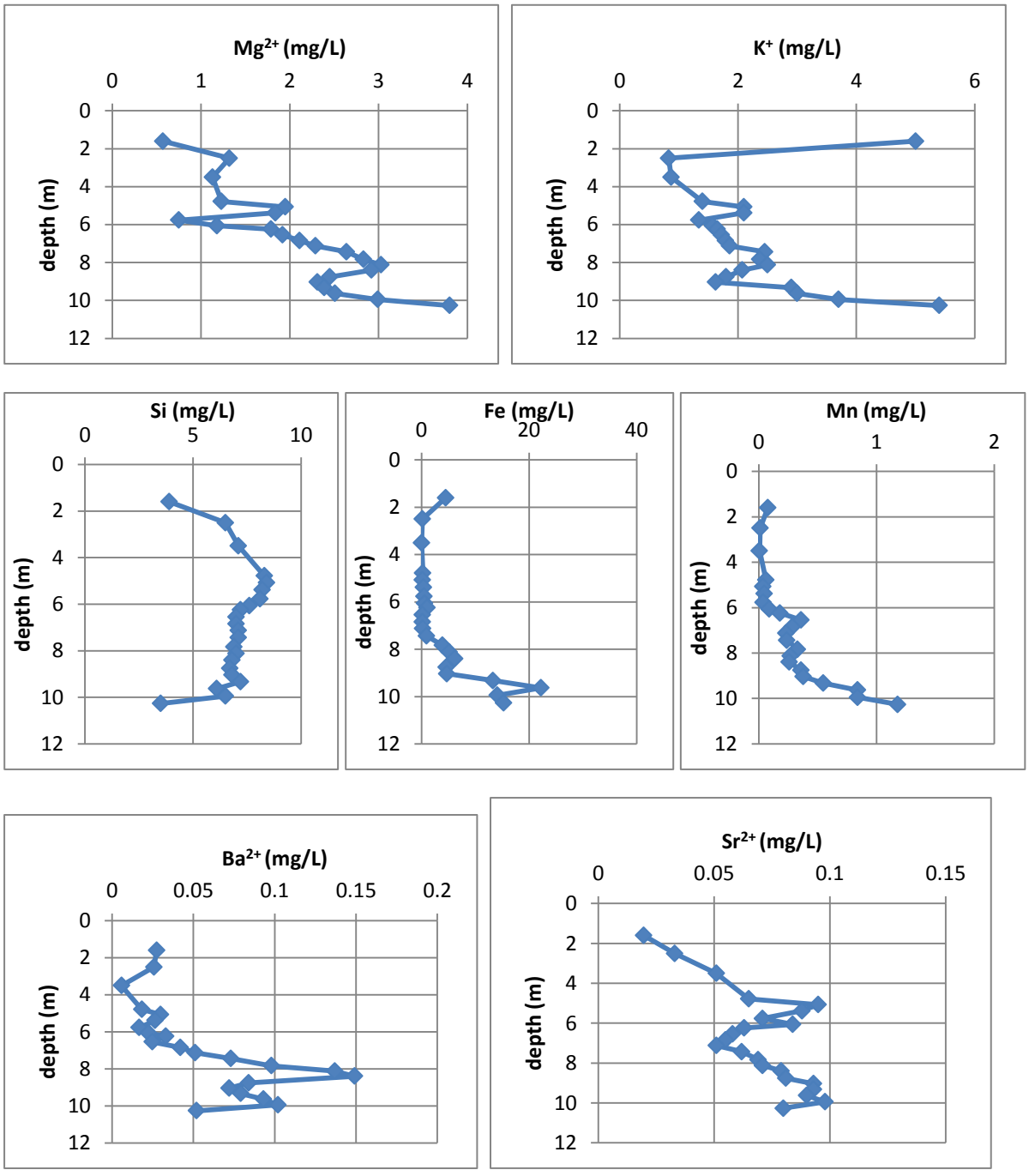

Figure A.17: Cation profiles for DP-1.

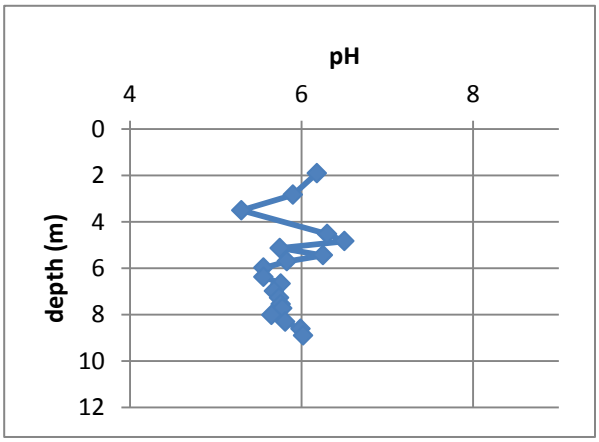
pH
4
6
8
depth (m)
0
2
4
6
8
10
12

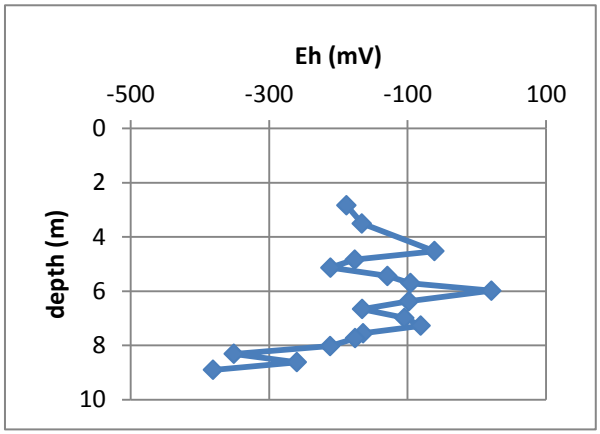
Eh (mV)
-500
-300
-100
100
depth (m)
0
2
4
6
8
10

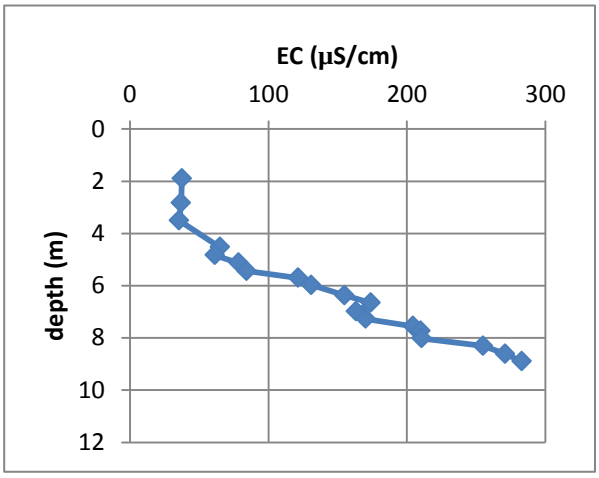
EC (µS/cm)
0
100
200
300
depth (m)
0
2
4
6
8
10
12

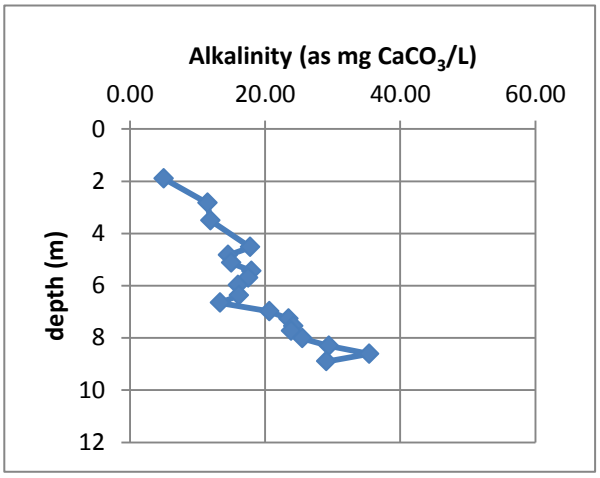
Alkalinity (as mg CaCO3/L)
0.00
20.00
40.00
60.00
depth (m)
0
2
4
6
8
10
12

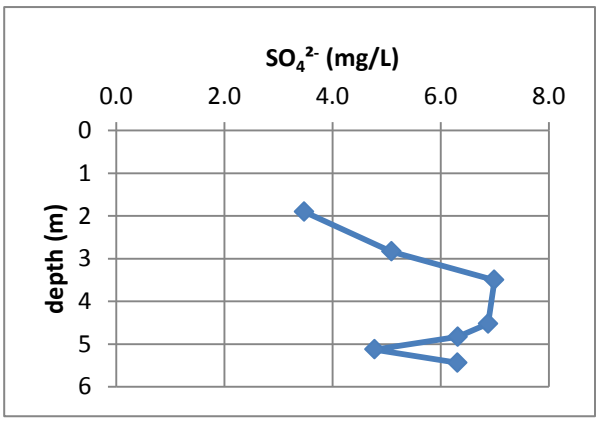
SO4 2- (mg/L)
0.0
2.0
4.0
6.0
8.0
depth (m)
0
1
2
3
4
5
6

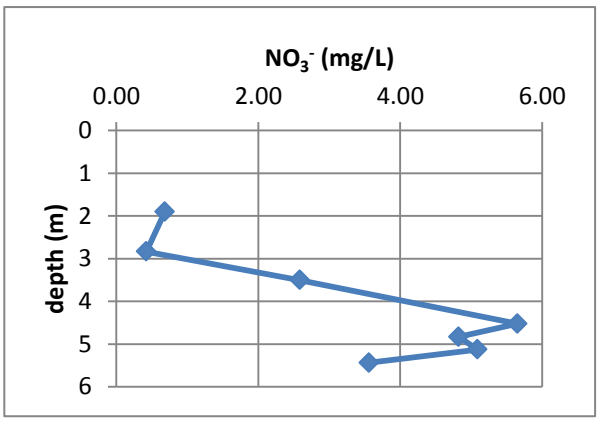
NO3- (mg/L)
0.00
2.00
4.00
6.00
depth (m)
0
1
2
3
4
5
6

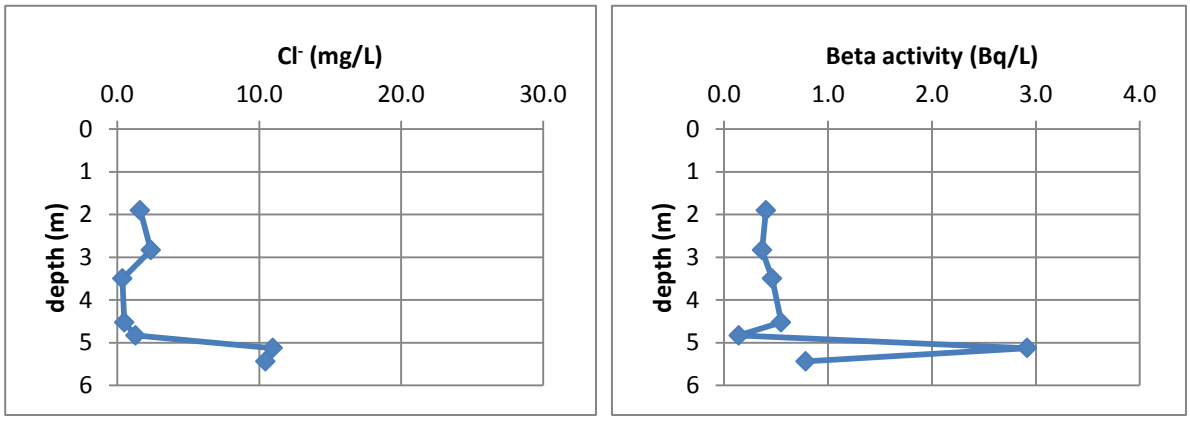

Figure A.18: Groundwater chemistry profiles of anions, *in situ* measurement and beta activity for drive-point piezometer DP-2.

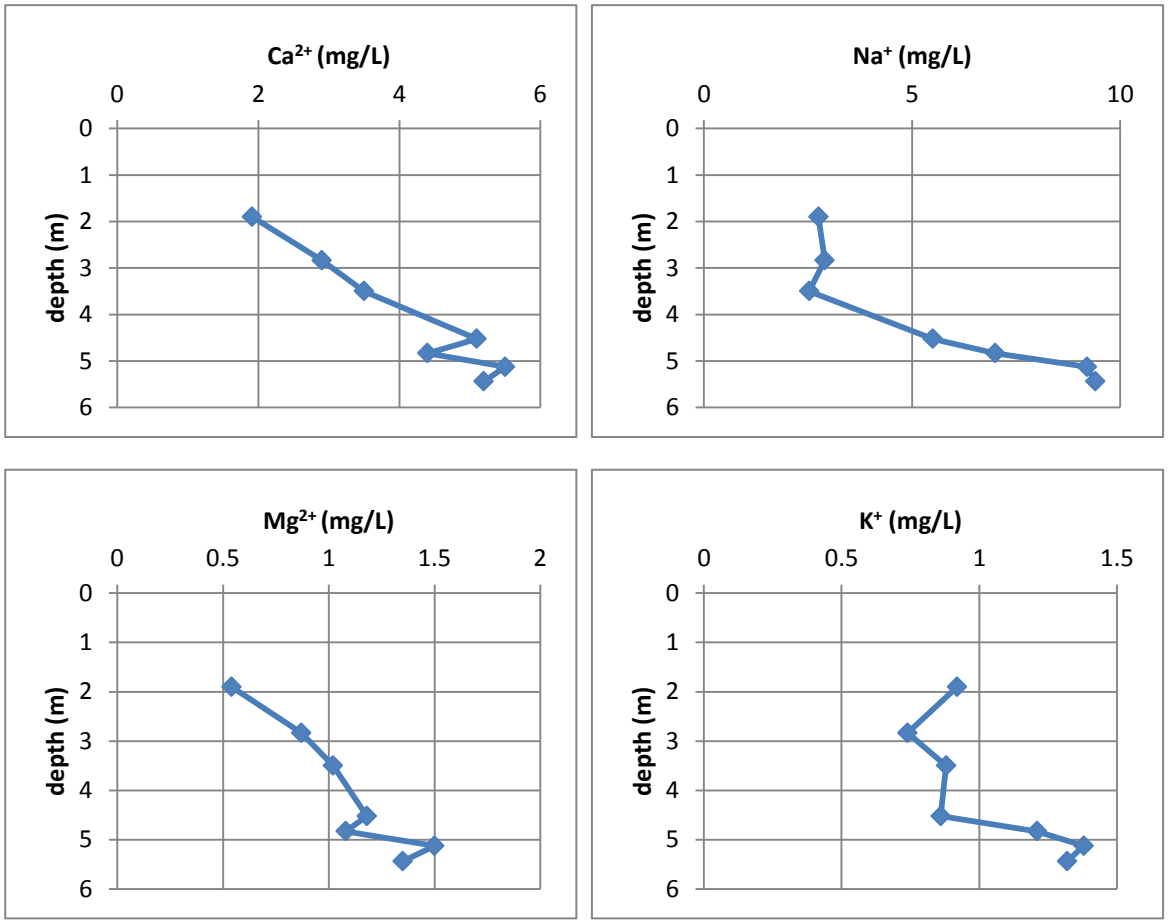

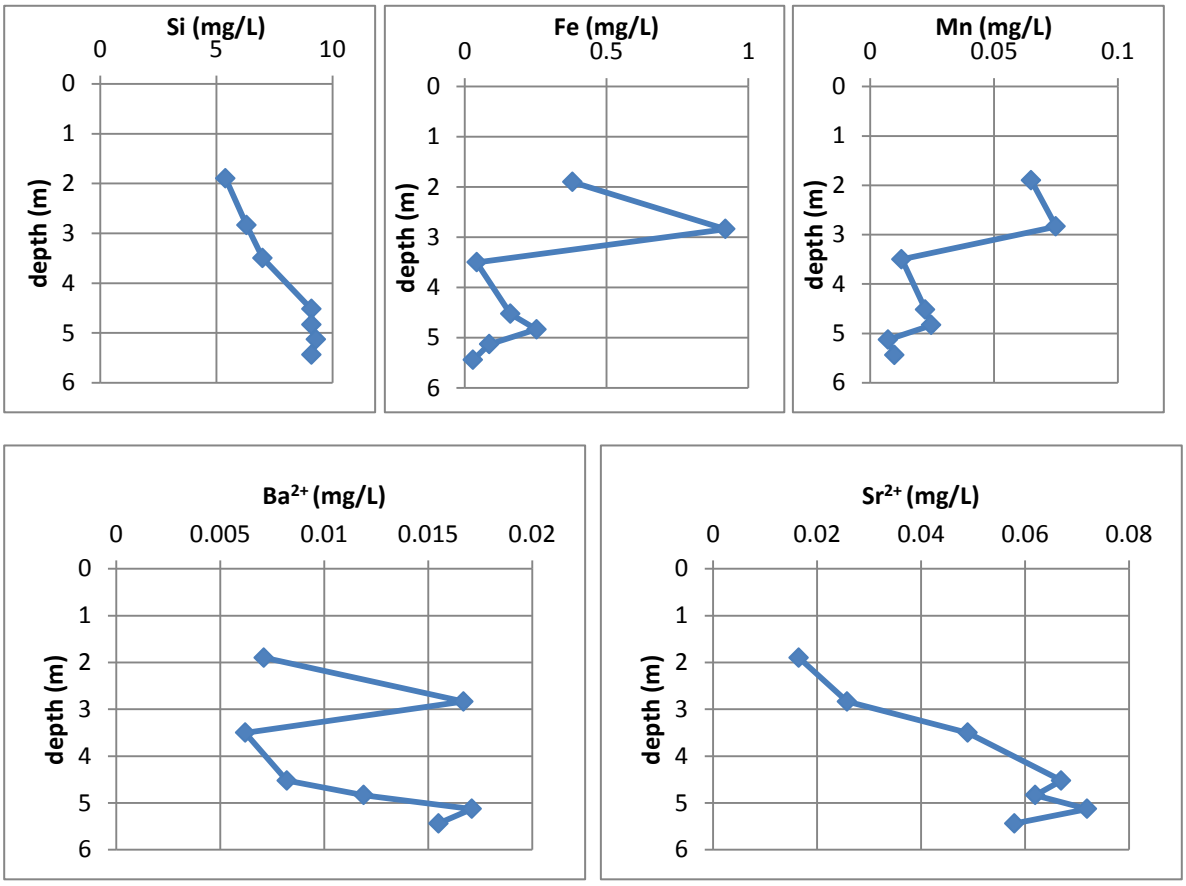

Figure A.19: Cation profiles for DP-2.

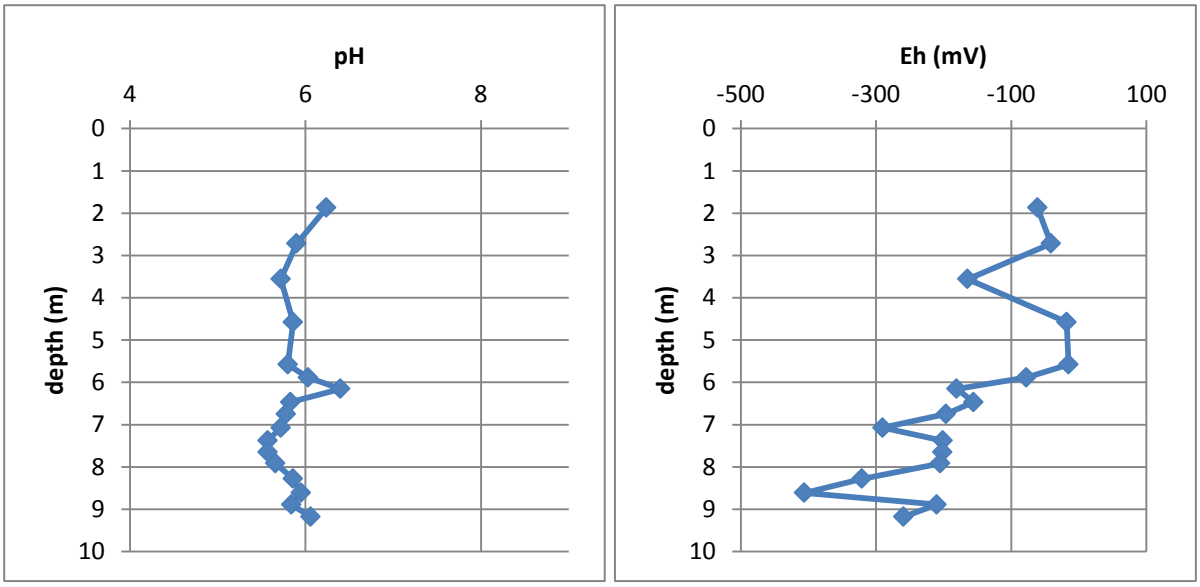

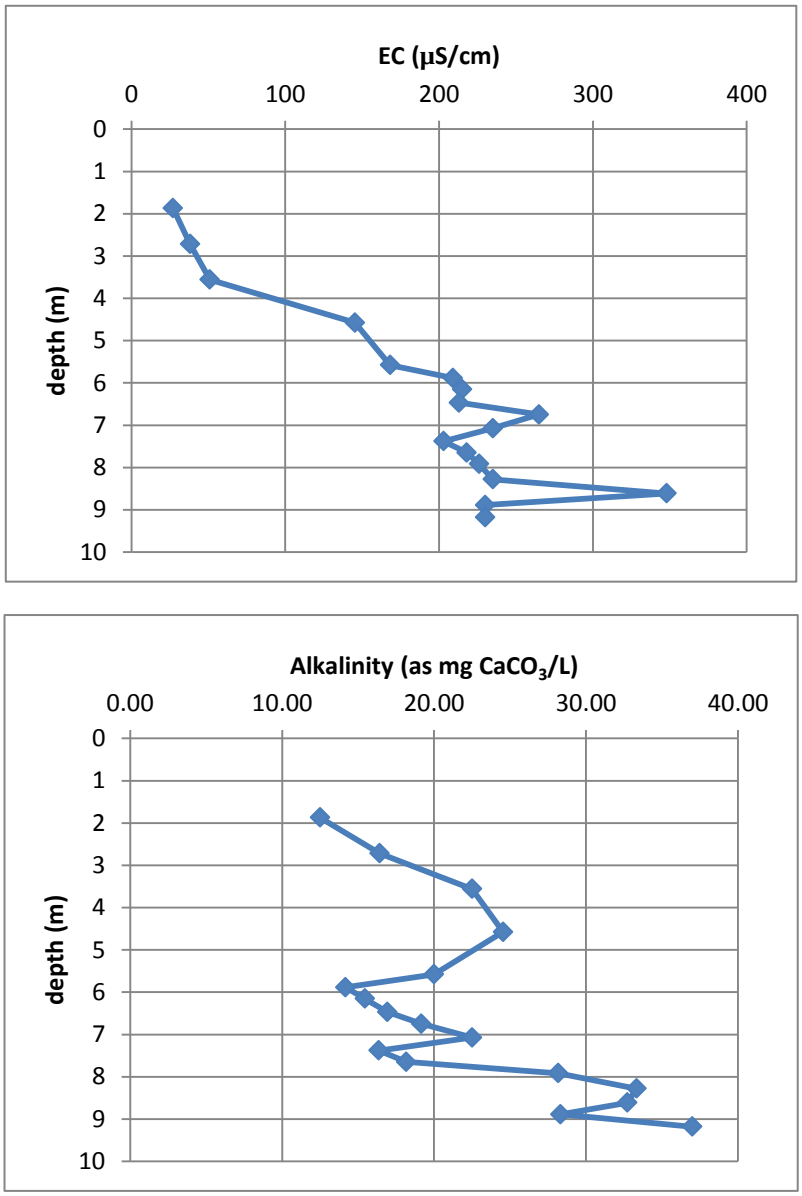

Figure A.20: ***In situ*** **measurement profiles for drive-point piezometer DP-3 (no anion report yet received).**

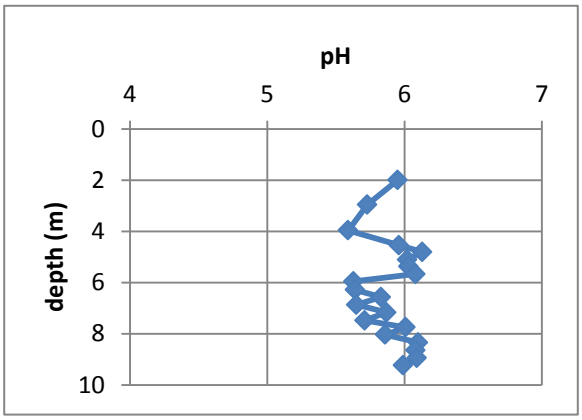
pH
4
5
6
7
0
2
4
6
8
10
depth (m)

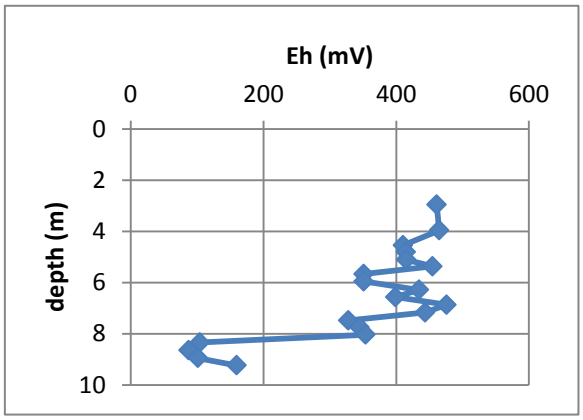
Eh (mV)
0
200
400
600
0
2
4
6
8
10
depth (m)

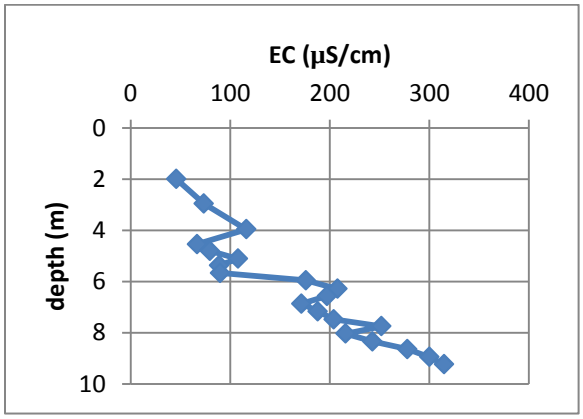
EC (µS/cm)
0
100
200
300
400
0
2
4
6
8
10
depth (m)

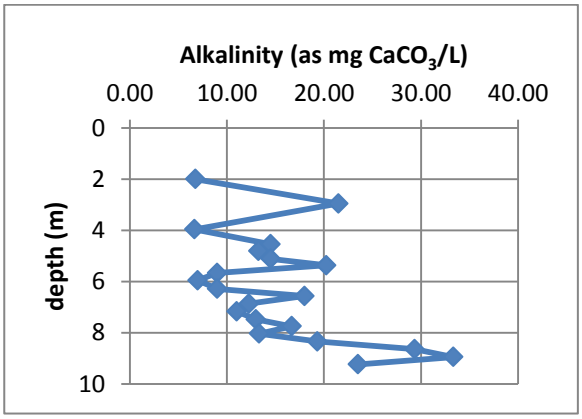
Alkalinity (as mg CaCO3/L)
0.00
10.00
20.00
30.00
40.00
0
2
4
6
8
10
depth (m)

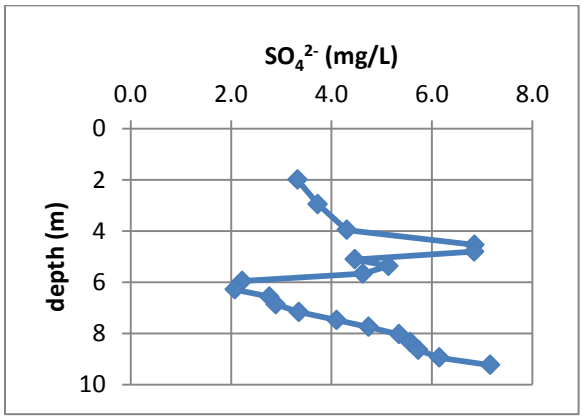
SO4 2- (mg/L)
0.0
2.0
4.0
6.0
8.0
0
2
4
6
8
10
depth (m)

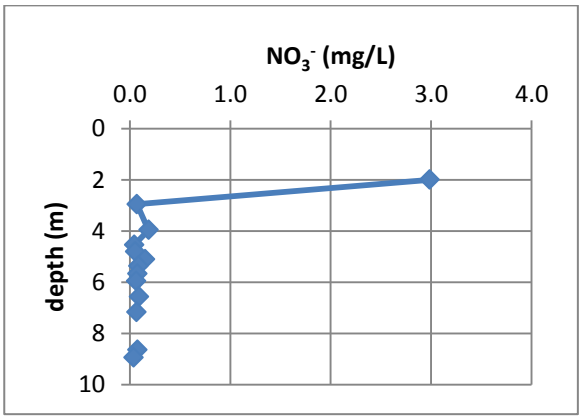
NO3- (mg/L)
0.0
1.0
2.0
3.0
4.0
0
2
4
6
8
10
depth (m)

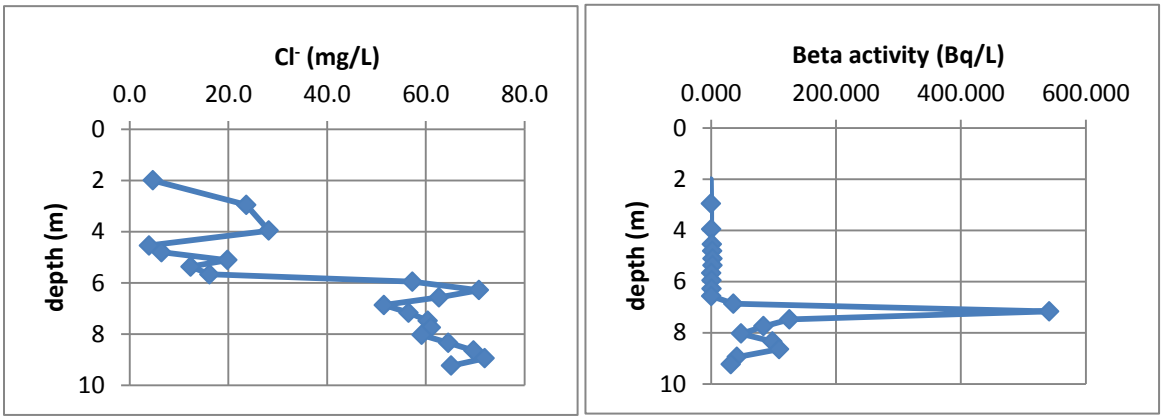

Figure A.21: Groundwater chemistry profiles of anions, *in situ* measurement and beta activity for drive-point piezometer DP-4.

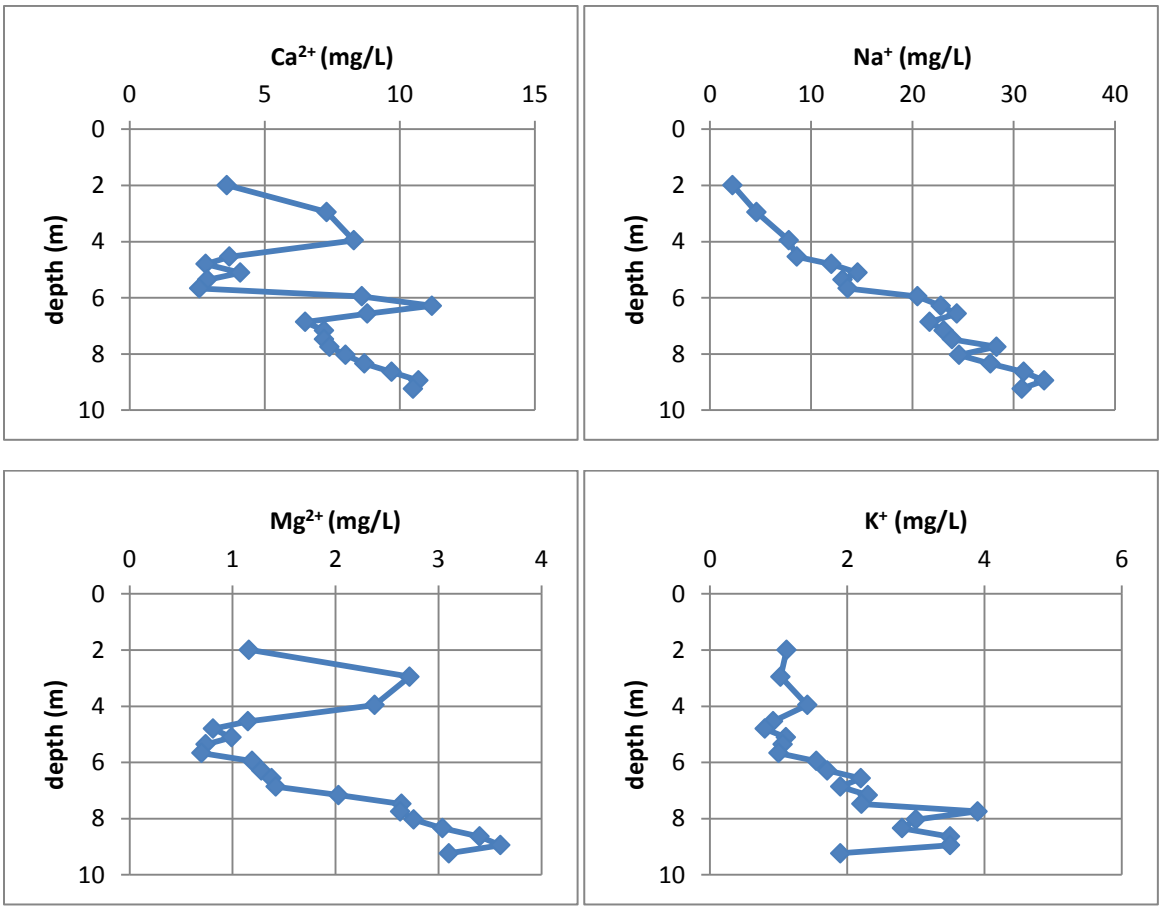

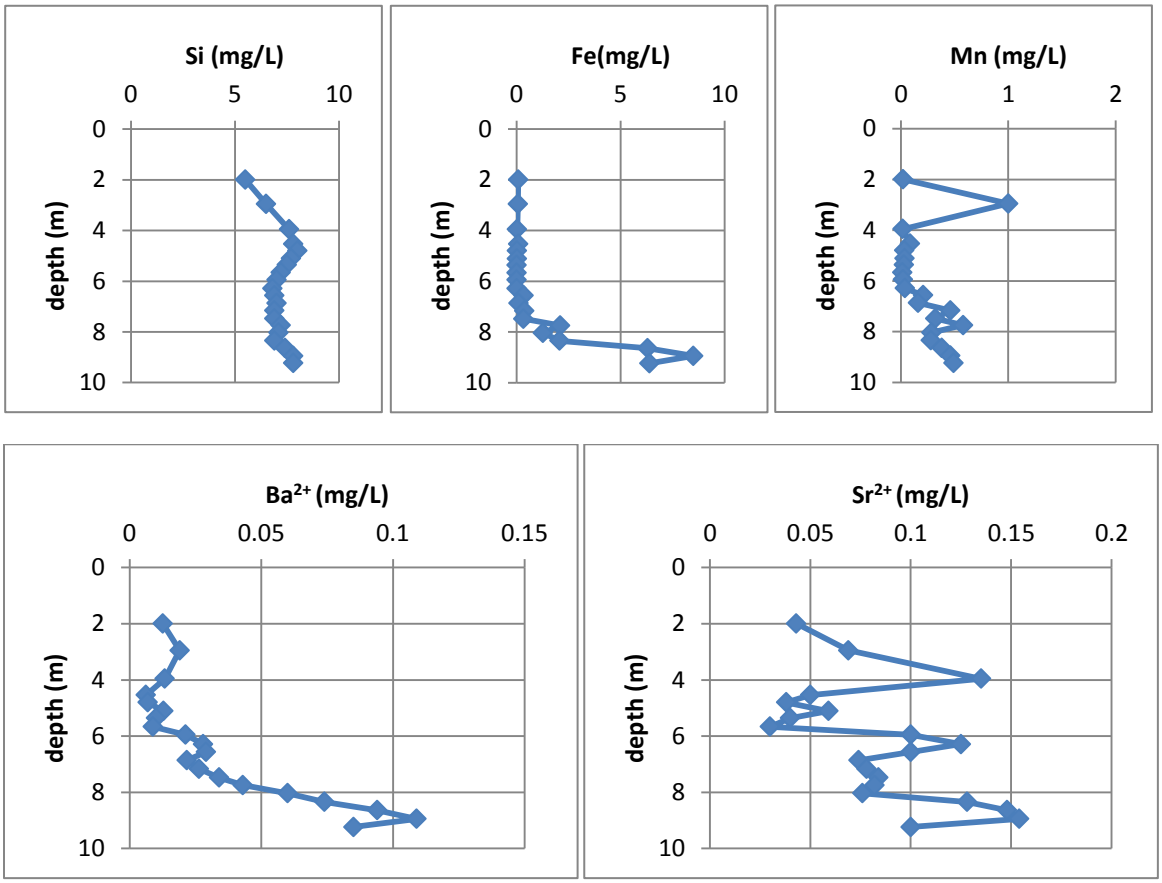

Figure A.22: Cation profiles for drive-point piezometer DP-4.

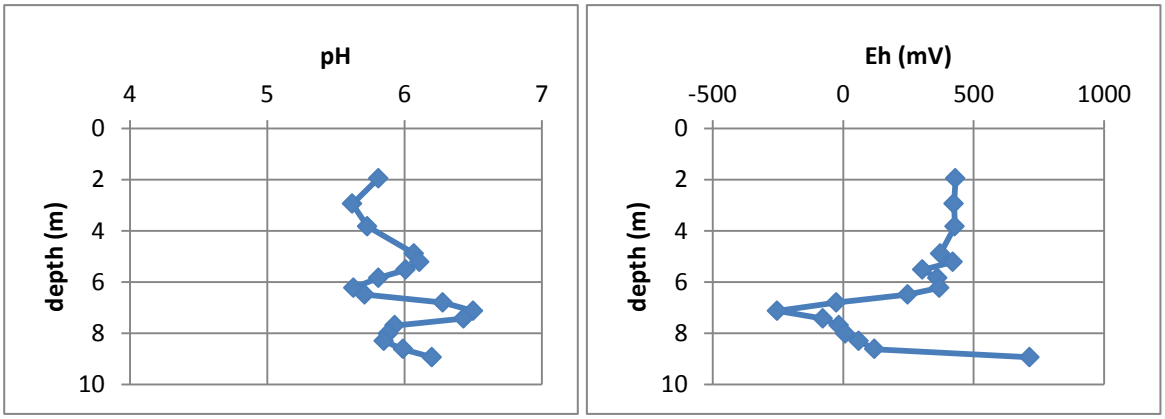

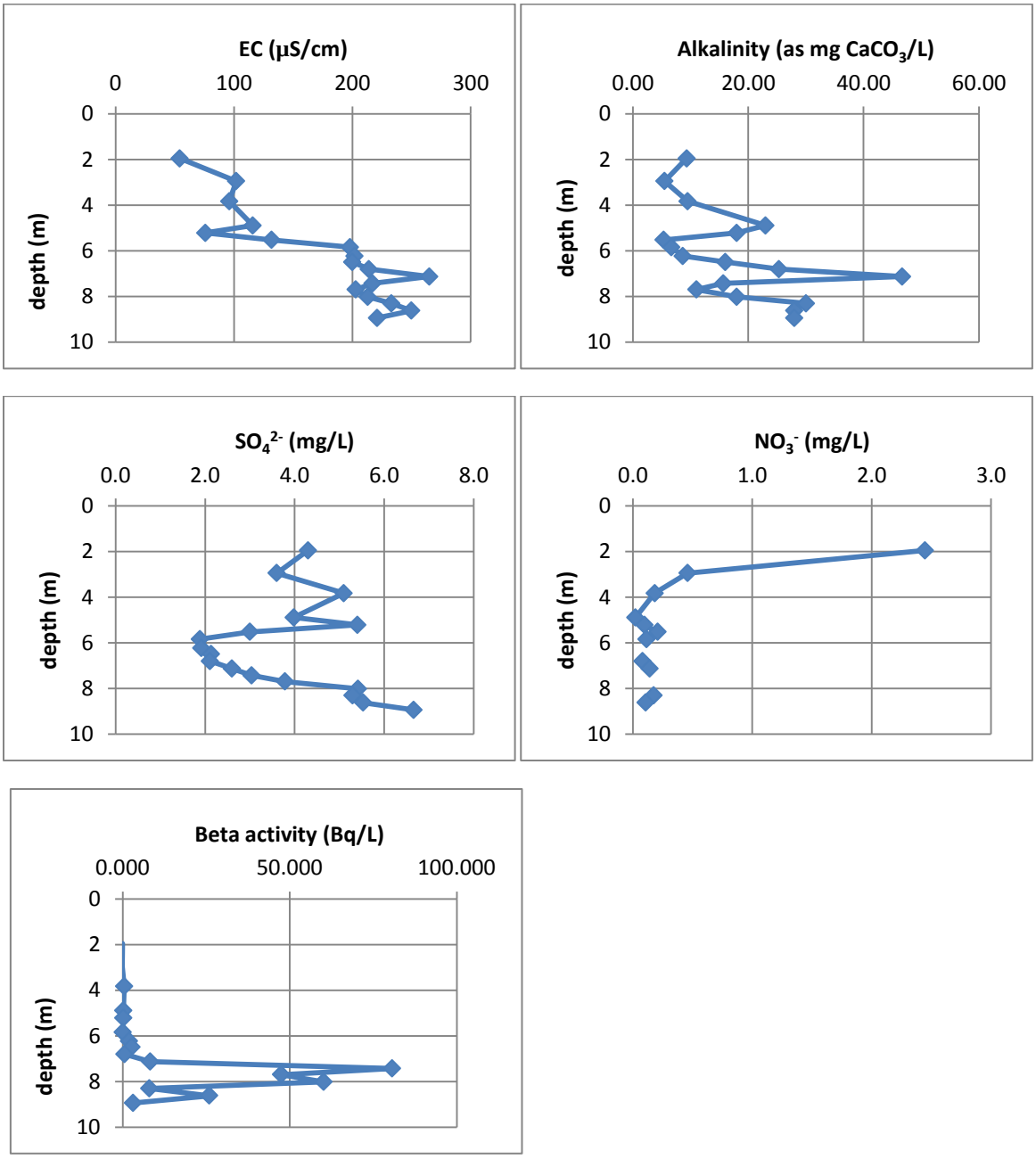

Figure A.23: Groundwater chemistry profiles of anions, *in situ* measurement and beta activity for drive-point piezometer DP-5.

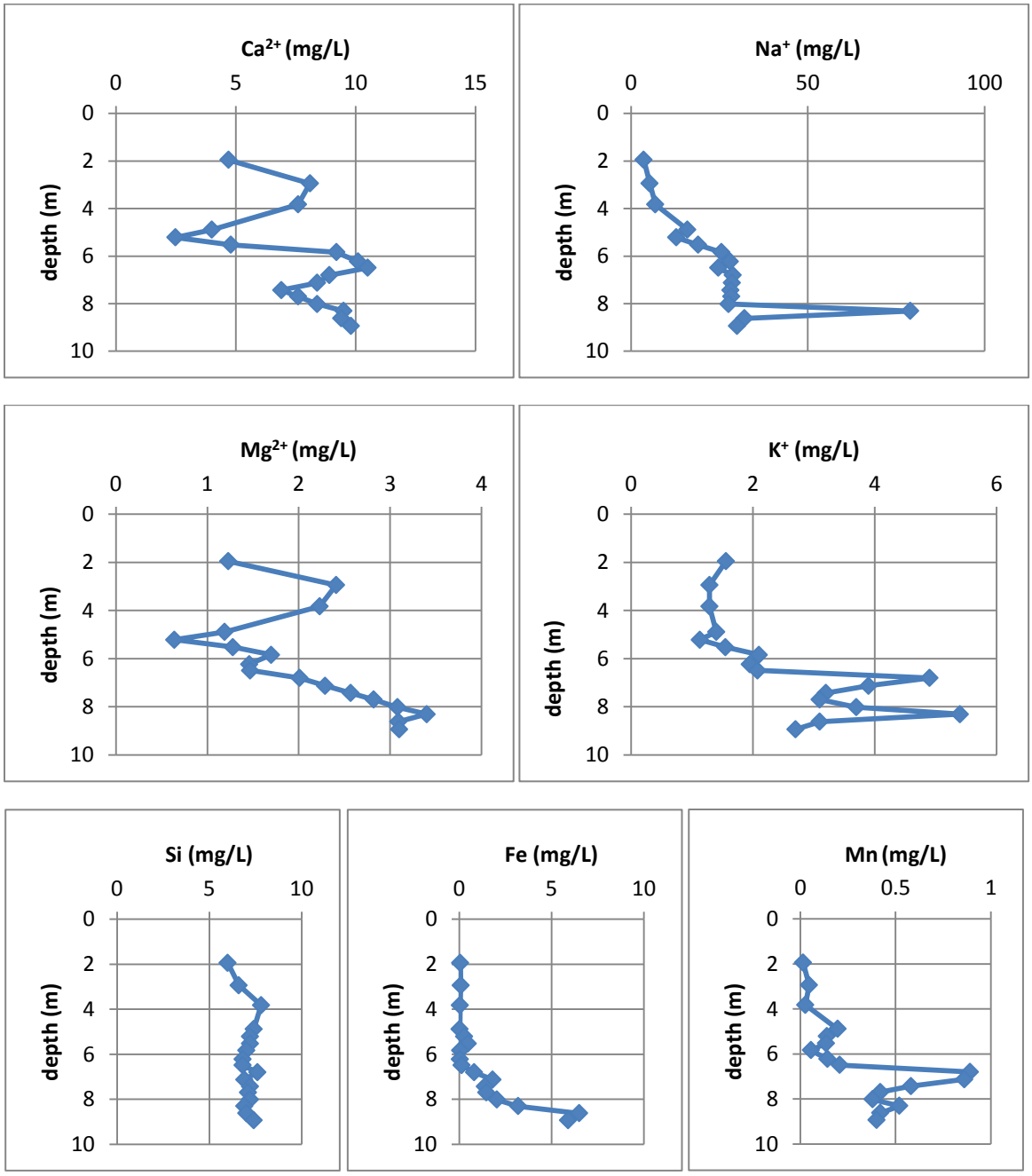
Ca2+ (mg/L)
0
5
10
15
depth (m)
0
2
4
6
8
10
Na+ (mg/L)
0
50
100
depth (m)
0
2
4
6
8
10
Mg2+ (mg/L)
0
1
2
3
4
depth (m)
0
2
4
6
8
10
K+ (mg/L)
0
2
4
6
depth (m)
0
2
4
6
8
10
Si (mg/L)
0
5
10
depth (m)
0
2
4
6
8
10
Fe (mg/L)
0
5
10
depth (m)
0
2
4
6
8
10
Mn (mg/L)
0
0.5
1
depth (m)
0
2
4
6
8
10

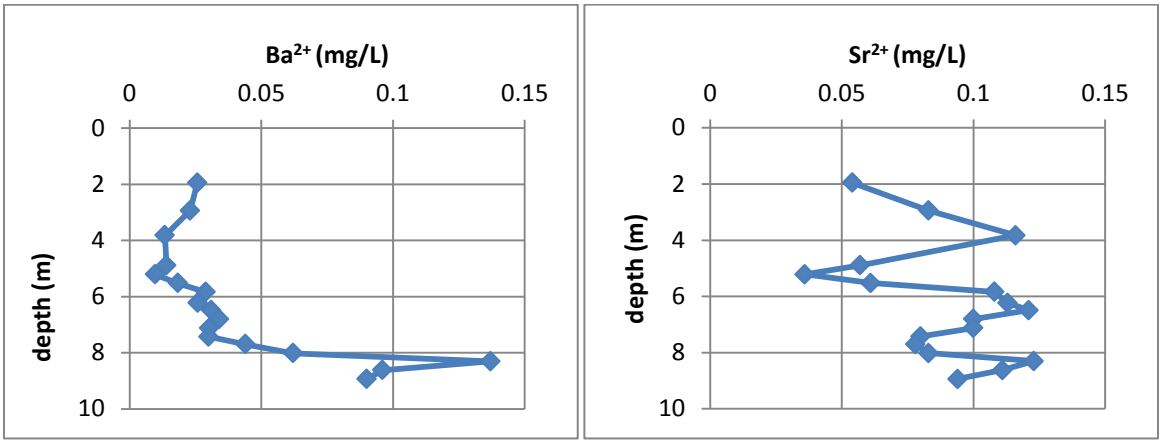

Figure A.24: Cation profiles for drive-point piezometer DP-5.

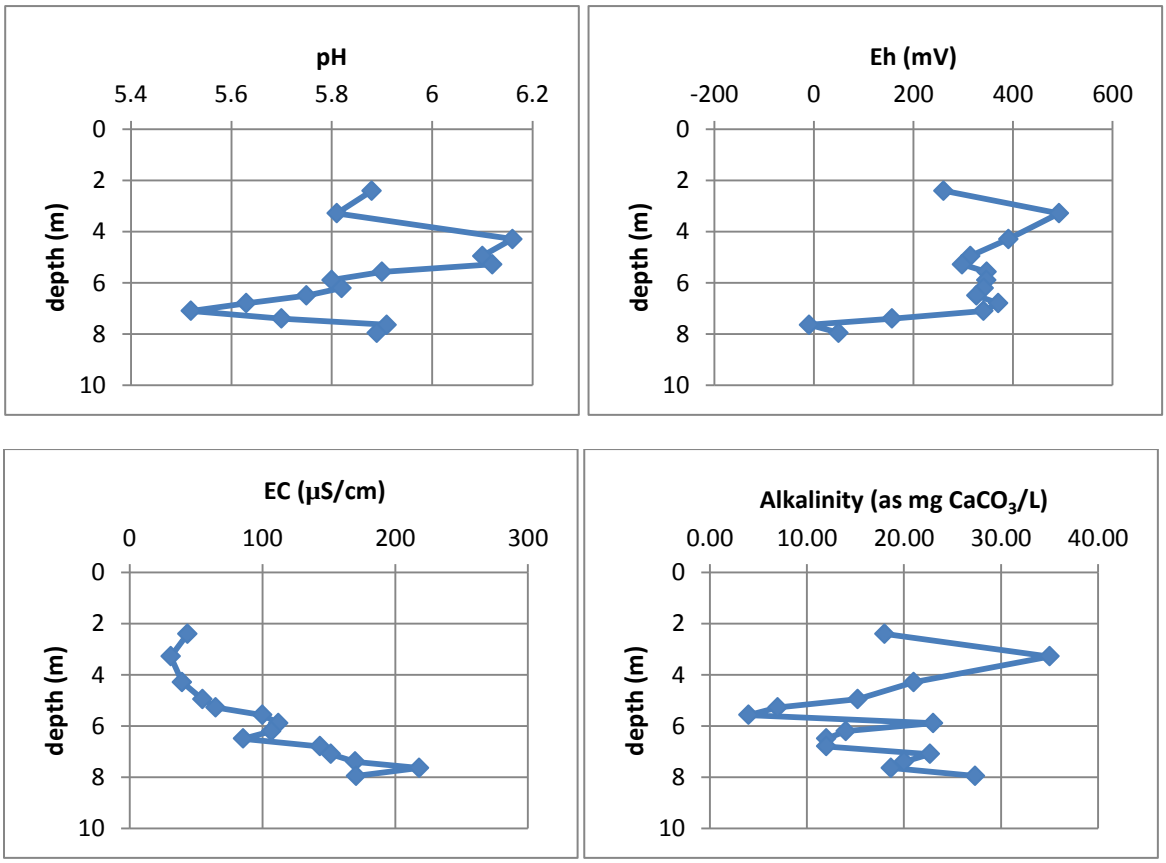

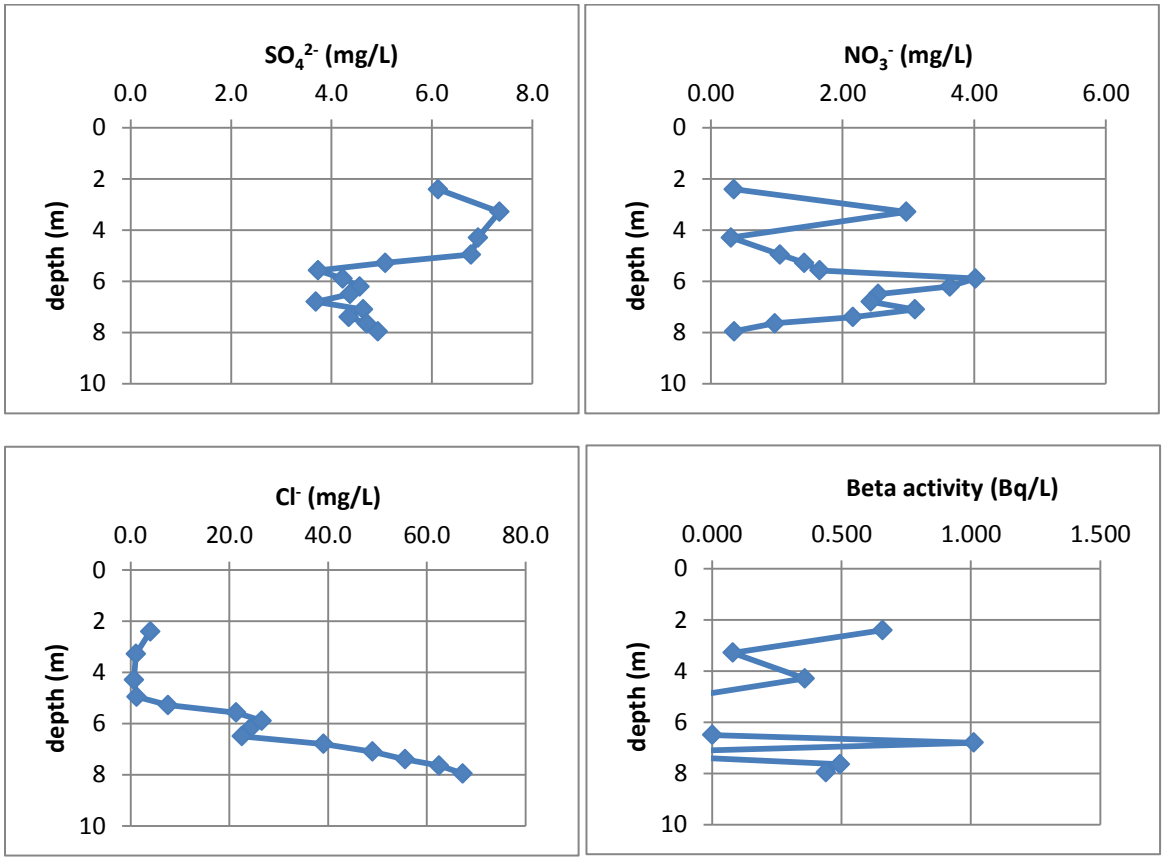

Figure A.25: Groundwater chemistry profiles of anions, *in situ* measurement and beta activity for drive-point piezometer DP-6.

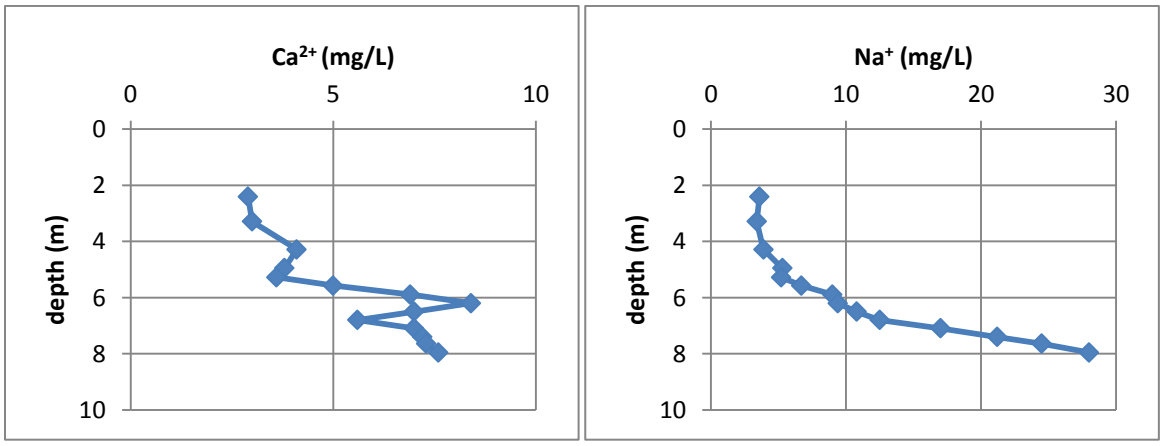

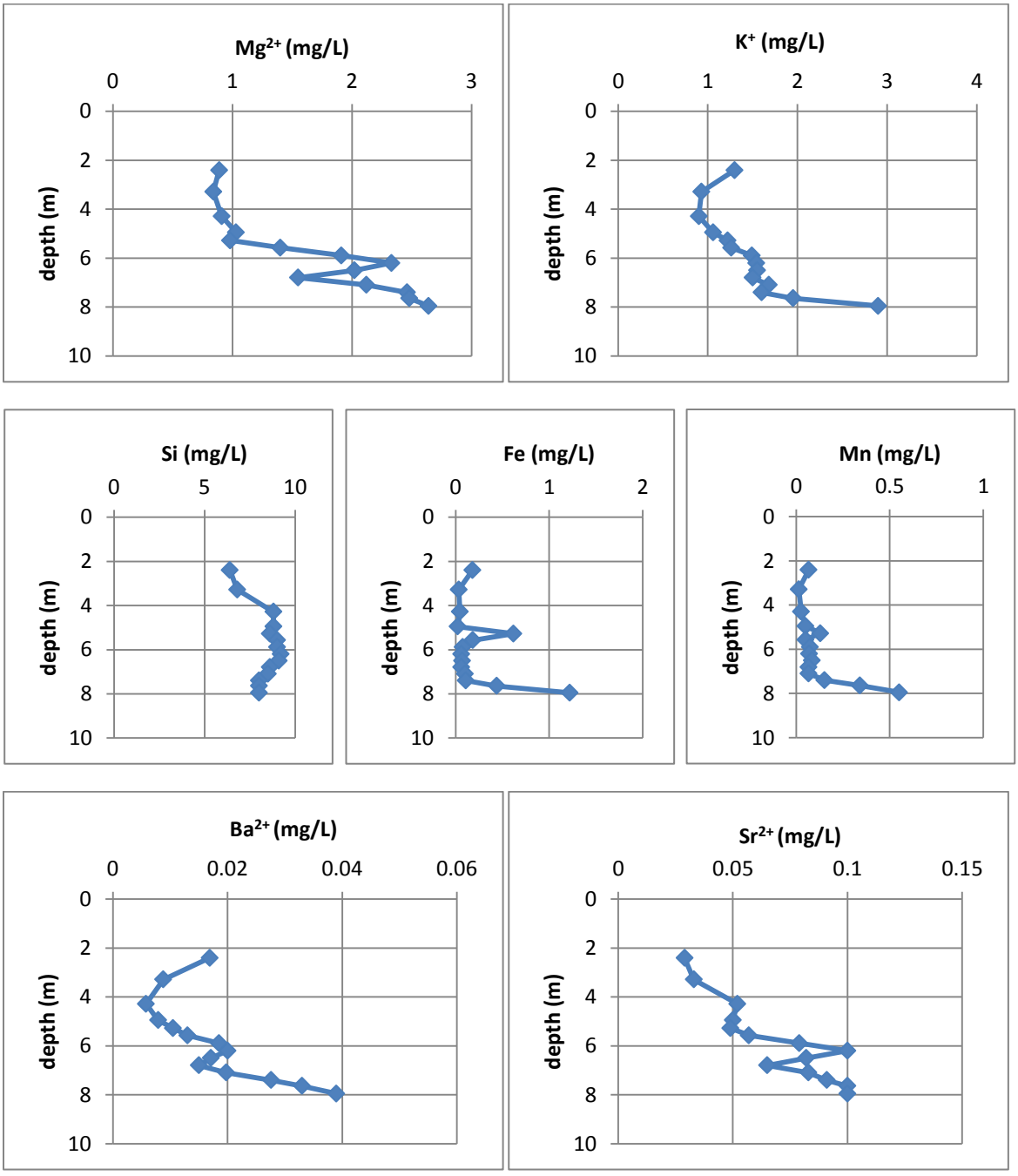

Figure A.26: Cation profiles for drive-point piezometer DP-6.

Bibliography

Amos, R. T., K. U. Mayer, D. W. Blowes, and C. J. Ptacek, 2004. Reactive transport modeling of column experiments for the remediation of acid mine drainage, Environ. Sci. Technol., 38:3131-3138.

Blowes, D.W., Ptacek, C.J., Benner, S.G., McRae, C.W.T., Bennett, T.A., Puls, R.W. 2000. Treatment of inorganic contaminants using permeable reactive barriers. Journal of Contaminant Hydrology 45: 123–137.

Brunner, P. and Simmons, C. T., 2012. HydroGeoSphere: A Fully Integrated, Physically Based Hydrological Model. Ground Water, 50: 170–176. doi: 10.1111/j.1745-6584.2011.00882.

Brunner, P., C. T. Simmons, and P. G. Cook, 2009. Spatial and temporal aspects of the transition from connection to disconnection between rivers, lakes and groundwater, Journal of Hydrology, 376 (1-2), 159-169.

Cai, Z., D. N. Lerner, R. G. McLaren, and R. D. Wilson 2007. Conceptual analysis of zero-valent iron fracture reactive barriers for remediating a trichloroethylene plume in a chalk aquifer, Water Resour. Res. 43 W03436

Cantrell, K. J., P. F. Martin, and J. E. Szecsody 1994. Clinoptilolite as an In-Situ Permeable Barrier to Strontium Migration in Groundwater. Thirty-Third Hanford Symposium on Health and the Environment, November 7-11, 1994, Part 2. pp. 839-850.

Department of Health and Human Services, Centers for Disease Control and Prevention 2005. Radiation Emergencies. Radioisotope Brief Strontium-90 (Sr-90).

Doble, R., Brunner, P., McCallum, J., Cook, P.G. 2011. An Analysis of River Bank Slope and Unsaturated Flow Effects on Bank Storage, Ground Water, 25 APR 2011, doi:10.1111/j.1745-6584.2011.00821.x

Drost, W., Klotz, D., Koch, A., Moser, H., Neumaier, F., Rauert, W. 1968. Point dilution methods of investigating ground water flow by means of radioisotopes. Water Resour. Res. 4 (1): 125–146.

Dyer, A., Chimedtsogzol, A., Campbell, L. and C. Williams 2006. Uptake of caesium and strontium radioisotopes by natural zeolites from Mongolia. In: Microporous and Mesoporous Materials, Volume 95, pages 172-175, 2006.

Elizondo, N.V., Ballesteros, E. and B.I. Kharisov 1999. Cleaning of liquid radioactive wastes using natural zeolites. In: Applied Radiation and Isotopes, Volume 52, pages 27-30, 2000.

Freeze, R.A. and Cherry, J.A. 1979: Groundwater. Hemel Hempstead: Prentice-Hall International. 604 pp.

Frind, E.O., Molson, J.W., Schirmer, M, Guiguer, N. 1999. Dissolution and mass transfer of multiple organics under field conditions: The Borden emplaced source. Water Resour. Res., 35 (3): 683-694.

Fuhrmann, M., Aloysius, D., Zhou, H. 1996. Permeable, subsurface sorbent barrier for ^{90}Sr: Laboratory studies of natural and synthetic materials. Waste Management 15 (7): 485-493.

Grisak, G.E., Merritt, W.F and D.W. Williams 1977. A fluoride borehole dilution apparatus for groundwater velocity measurements. Can. Geotech. J. 14: 554-561.

Hvorslev, M.J. 1951. Time Lag and Soil Permeability in Ground-Water Observations. Bull. No. 36, Waterways Exper. Sta. Corps of Engrs, U.S. Army, Vicksburg, Mississippi, pp. 1-50.

Jackson, R. E., K. J. Inch, R. J. Patterson, K. E. Lyon, T. G. Spoel, W. F. Merritt, and B. A. Risto 1980. Adsorption of radionuclides in a fluvial sand aquifer: Measurements of the distribution coefficients K_d^{Sr} and K_d^{Cs} and identification of mineral adsorbents. Contaminants and Sediments. Vol. I, edited by R. A. Baker, pp. 311-329, Ann Arbor Science, Ann Arbor, Mich., 1980.

Jackson, R. E. and K. J. Inch 1989. The in-situ adsorption of ^{90}Sr in a sand aquifer at the Chalk River Nuclear Laboratories. Journal of Contaminant Hydrology 4 (1989): 27- 50.

Jeen, S.-W., K. U. Mayer, R. W. Gillham, and D. W. Blowes, 2007. Reactive transport modeling of trichloroethene treatment with declining reactivity of iron. Environ. Sci. Technol., 41:1432-1438.

Jurjovec, J., D. W. Blowes, C. J. Ptacek, and K. U. Mayer (2004), Multicomponent reactive transport modeling of acid neutralization reactions in mine tailings, Water Resour. Res., 40, W11202, doi:10.1029/2003WR002233.

Killey, R.W.D. and J.H. Munch 1987. Radiostrontium migration from a 1953-54 liquid release to a sand aquifer. Water Poll. Res. J. Canada 22 (1): 107-128.

Klukas, M.H. and G.L. Moltyaner 1995. Numerical simulations of groundwater flow and solute transport in the Lake 233 Aquifer. Environmental Research Branch, Chalk River Laboratories, Chalk River, AECL. 54 p.

Konikow, L.F and Bredehoeft, J.D. 1992. Ground-water models cannot be validated. Advances in Water Resources 15: 75-83.

Lee, D.R. and Forsyth, R.J. 1983. Water flow through crystalline rock using the borehole dilution technique: method development and preliminary field results at Chalk River. Technical Report Atomic Energy Canada Limited (unpublished).

Lee, D.R. and D.S. Hartwig 2005. Zeolite prevents discharge of strontium -90-contaminated groundwater. Canadian Nuclear Society Waste Management, Decommissioning and Environmental Restoration for Canada's Nuclear Activities: Current Practices and Future Needs Ottawa, Ontario Canada May 8-11, 2005.

Lemieux, J.-M., Sudicky, E.A., Peltier, W.R. and Tarasov, L., 2008. Simulating the impact of glaciations on continental groundwater flow systems II. Model application to the Wisconsinian glaciation over the Canadian landscape, Jour. Geophys. Res., 14pp.

Li, Q., Unger, A.J.A., Sudicky, E.A., Kassenaar, D., Wexler, E.J. and Shikaze, S., 2008. Simulating the multi-seasonal response of a large-scale watershed with a 3D physically-based hydrologic model, Jour. Hydrol., Vol. 357 (3-4), 20pp.

Mayer, K. U., E. O. Frind, and D. W. Blowes, 2002. Multicomponent reactive transport modeling in variably saturated porous media using a generalized formulation for kinetically controlled reactions, Water Resour. Res., 38, 1174, doi: 10:1029/2001WR000862

Molins, S., K. U. Mayer, R. T. Amos, and B. A. Bekins, 2010. Vadose zone attenuation of organic compounds at a crude oil spill site - Interactions between biogeochemical reactions and multicomponent gas transport, J. Contam. Hydrol, 112:15-29.

O'Hara, M.J., Burge, S.R., Grate, J.W., 2009. Automated radioanalytical system for the determination of Sr-90 in environmental water samples by Y-90 Cherenkov radiation counting. Anal. Chem. 81, 1228–1237.

Ogilvi, N. A. 1958. An electrolyrical method of determiningthe filtration velocity of underground waters (in Russian). Bull. Sci.-Tech. Ini. No. 4 (16), Gosgeoltekhizdat, Moscow, 1958.

Osmanlioglu, A. E. 2006. Treatment of radioactive liquid waste by sorption on natural zeolite in Turkey. Journal of Hazardous Materials B137 pages 332-335, 2006.

Pabalan, R. T. and F. P. Bertetti 1999. Experimental and Modeling Study of Ion Exchange Between Aqueous Solutions and the Zeolite Mineral Clinoptilolite Journal of Solution Chemistry, Vol. 28, No. 4, pages 367-398, 1999.

Palmer, J. L. and M. E. Gunter 2001. The effects of time, temperature, and concentration on Sr2+ exchange in clinoptilolite in aqueous solutions. American Mineralogist, Volume 86, pages 431–437, 2001.

Park, Y.-J., E. A. Sudicky, R. G. McLaren, and J. F. Sykes 2004. Analysis of hydraulic and tracer response tests within moderately fractured rock based on a transition probability geostatistical approach, Water Resour. Res. 40 W12404

Pors Nielsen, S., 2004. The biological role of strontium. Bone 35, 583–588.

Price, J.S. ,McLaren, R.G., and D.L. Rudolph 2010. Landscape restoration after oil sands mining: conceptual design and hydrological modelling for fen reconstruction, International Journal of Mining, Reclamation and Environment, Vol. 24, No. 2, 109–123.

Rabideau, A. J., Van Benschoten, J., Patel, A., Bandilla, K. 2005. Performance assessment of a zeolite treatment wall for removing Sr-90 from groundwater. Journal of Contaminant Hydrology, Volume 79, pages 1-24, 2005.

Rozemeijer, J. C., Y. van der Velde, R. G. McLaren, F. C. van Geer, H. P. Broers, and M. F. P. Bierkens (2010), Integrated modeling of groundwater–surface water interactions in a tile-drained agricultural field: The importance of directly measured flow route contributions, Water Resour. Res., 46, W11537, doi:10.1029/2010WR009155

Sale, K.S. 2003. A performance study of permeable reactive barriers concentrating on preferential flow. MSc thesis in Earth Sciences at the University of Waterloo, 2003. 120 p.

Smičiklas, I., Dimović, S., Plećaš, I. 2006. Removal of Cs1+, Sr2+ and Co2+ from aqueous solutions by adsorption on natural clinoptilolite. In: Applied Clay Science, Volume 35, pages 139-144, 2007.

Stumm, W., and J.J. Morgan 1996. Aquatic Chemistry. Chemical Equilibria and Rates in Natural Waters. Third Edition. John Wiley & Sons, Inc. New York. 1022 p.

Therrien, R., McLaren, R.G., Sudicky, E.A. and S.M. Panday 2010. HydroGeoSphere: A Three-dimensional Numerical Model Describing Fully-integrated Subsurface and Surface Flow and Solute Transport. Groundwater Simulations Group, University of Waterloo. 443 p.

Wallace, S. H., Shaw, S., Morris, K., Small, J. S., Fuller, A. J., Burke, I. T. 2012. Effect of groundwater pH and ionic strength on strontium sorption in aquifer sediments: Implications for 90Sr mobility at contaminated nuclear sites. Applied Geochemistry 27 pages 1482

Wilkin, R.T., Puls, R.W. and G.W. Sewell 2002. Lon-Term Performance of Permeable Reactive Barriers using Zero-Valent Iron: Geochemical and Microbiological effects. Groundwater 41 (4): 493-503.

Yin, J., Mayer, K.U., Jeen, S.-W., Lee, D.R. in preparation. Reactive transport modeling of Sr-90 sorption in reactive sandpacks.

Yung, S. P. H. 2010. Remediation of Strontium 90 by granular clinoptilolite: Column experiments. Bachelor of Science thesis, Department of Earth and Environmental Sciences, University of Waterloo.